CENTRO DE INVESTIGACIONES
EN OPTICA, A.C.

Final version. Suggested modifications by Tutorial Committee are included.

"EFFICIENT FLUORESCENT AND PHOSPHORESCENT OLEDs BY SPIN COATING TECHNIQUE AND A NEW ANODE BASED ON CONDUCTIVE PEDOT:PSS"

Thesis to earn the degree of Doctor of Science (Optics)

Presents: Luis-Abraham Lozano-Hernández

Thesis Director: José-Luis Maldonado-Rivera

Vo.Bo Advisor

19/Agosto/2020

León · Guanajuato · México
August 2020

Acknowlegments

I would like to thank to all my family, specially my wife Edith, my parents, my sister.

I would like to thank my thesis advisor, Dr. José-Luis Maldonado, for his example, teaching and orientation.

I would like to thank to CONACYT for my PhD scholarship, Ce-MIE-Sol 207450/27, Fondo sectorial CONACYT SUSTENTABILIDAD ENERGÉTICA, CONACYT (Grant CB-251693) and DGAPA-UNAM (PAPIIT IN 203517).

I want to express my thanks to Prof. Peter Skabara and his group of work, especially to Joe Cameron, Holly Yu, Neil Findlay, Hao Yang, Eman Hussien, Minming Yan and Ahmet Battal, for their hospitality and support during my international research internship in the University of Glasgow in Glasgow, United Kingdom.

ABSTRACT

Fluorescent and phosphorescent Organic Light Emitting Diode (OLED) devices were fabricated by solution process and optimized. From their basic characterization (J-V-L curves, electroluminescence spectra) external quantum efficiency (EQE) was calculated. Two small molecule, carbazole derivatives (CZ-1 and CZ-2), previously reported and used for OLEDs showed very good luminances (~ 4000 cd/m^2) and current densities (< 200 mA/cm^2) resulting in a high EQE (9.5 %). Likewise, fluorescent OLEDs based in the new polymer PF-2F presented an acceptable performance even on a simple architecture with a good EQE (2.6 %), photoluminescence quantum yield (PLQY) about 1 and excellent properties of processability. The influence of its CF_3 group in the optical, chemical, electronic and mechanical properties in OLEDs was determined.

Also, a new family of three fluorescent oligomers (BT-$F3_2$, BT-$F4_2$ and BT-$F5_2$) with excellent properties in solution, high PLQY (~1) and highly luminescent, were used in simple and multilayer OLEDs achieving a very high luminance (29 499 cd/m^2). These oligomers have different chain lengths, which influence the device luminance, efficiency and their lifetime. Lifetime was monitored and the stretched exponential decay (SED) model was used in order to obtain the device half-life (LT50). Also, phosphorescent devices, based on a host/guest system (PVK:$Ir(ppy)_3$), were prepared, the influence of the electron transport layer (ETL) into the electron/hole ratio was analyzed.

By using a new proposed method, a PEDOT:PSS anode was developed and applied in rigid and flexible substrates, with low sheet resistance (40 Ω/□) and acceptable transmittance (> 85%). This new proposed method consists in *volume evaporation*, in which basically the loss of water induces closeness among the conductive fractions of PEDOT. This PEDOT:PSS anode easy of fabricating following an economical procedure could be applied not just in OLEDs but in other optoelectronic devices such as organic photovoltaic cells (OPVs), perovskite solar cells (PeSCs), etc.

INDEX

1 INTRODUCTION 1
1.1 State of the Art 1
1.2 Thesis work 7
2 ORGANIC LIGHT EMMITING DIODES (OLEDs) 10
2.1 OLED 10
2.2 HOMO, LUMO and work function 13
2.3 PLEDs and SMOLEDs 14
2.4 Fluorescence, phosphorescence and TADF 16
2.5 Emissive layers type Host/Guest 19
3 FABRICATION AND CHARACTERIZATION OF OLED DEVICES 22
3.1 Fabrication techniques 22
3.2 OLED devices characterization 25
3.2.1 J-V-L curve 25
3.2.2 Current and Luminous efficiency 26
3.2.3 External Quantum Efficiency (EQE) 27
3.2.4 Degradation and lifetime 30
4 FLEXIBLE DEVICES 34
4.1 PEDOT:PSS anodes 34
4.2 Carbon based anodes 37
4.3 Metal based anodes 38
4.4 Hybrid structure anodes 39
5 EXPERIMENTAL 40
5.1 Anode 40
5.2 Hole Transport Layer 40
5.3 Emissive Layers (EMLs) 40
5.4 Electron transport layer 41
5.5 Electron injection layer 41
5.6 Cathodes 41
5.7 OLEDs Characterization 41
5.8 Anode based on conductive PEDOT:PSS polymer 42

6 RESULTS 44
6.1 Efficient small molecule OLEDs based on carbazole and Thienopyrrolediones derivatives 44
6.1.1 Conclusions 48
6.2 Efficient OLED devices with polymer PF-2F as EML 50
6.2.1 Conclusions 58
6.3 Highly luminescent OLED devices based on 3 novel fluorescent oligomers 60
6.3.1 Conclusions 68
6.4 Efficient Phosphorescent OLED devices by optimizing their ETL 70
6.4.1 Conclusions 73
6.5 Flexible anodes based on conductive PEDOT:PSS and their application in OLED devices 74
6.5.1 Conclusions 85
7 CONCLUSIONS 86
8 Perspectives 88
9 References 90
10 APPENDIX. Additional OLED devices 105

1 INTRODUCTION

1.1 State of the Art

The first organic light emitting diode was manufactured by Tang et. al[1] and its evolution and improvement induced an intensified research on the organic materials area. This first OLED was a very simple device with a double-layer structure of organic thin films, now the devices could vary from the simplest structure up to a multilayer configuration of 10 or even more layers[2,3]. A wide variety of new materials, small molecules and polymers have been developed since the invention of the OLED. Small molecules and polymers, have advantages between them, for example, polymers can be deposited by solution processes due their good solubility and film forming capacity, this is helpful to reduce the costs of this kind of OLED devices (sometimes named polymer OLEDs or PLEDs). On the other hand, small molecules in general present higher efficiencies and their synthesis are quite replicable[4,5].

In order to improve the performance of OLED devices two principal areas are being studied, the first of them is the design of new materials that enhance the spectral emission, current-voltage characteristics and therefore the overall device efficiency. Secondly in order to enhance OLED devices, deposition/fabrication methods are being widely studied[6,7].

The performance of OLED devices is obtained by measuring luminance, current and voltage of operation, electroluminescence spectrum. With these basic characteristics, some others as color coordinates, efficiency (external quantum efficiency, current efficiency and luminous efficiency), lifetimes, can be obtained.

The research in the field of new materials for OLED devices, has resulted in new kind of devices or generations, as fluorescent OLEDs, phosphorescent OLEDs (PHOLEDs) and Thermally Activated Delayed Fluorescence (TADF) OLEDs. The main difference between them is the limit of their efficiency. Fluorescent OLEDs can reach a maximum internal quantum efficiency (IQE) of 25 % while PHOLEDs and TADF OLEDs can reach 100 %.

For example, Naresh *et. al*.[8] have reported a high efficient and stable single-layer OLED based on a new TADF material (CzDBA) with a exceptionally low operating voltage of only 2.9 V at a luminance of 10 000 cd/m^2, and an impressive EQE of 19 % (@ 500 cd/m^2) by using an architecture ITO/PEDOT:PSS/MoO_3/C_{60}/CzDBA/TPBi/Al. Also, they are reporting a half life time of 1880 h with an initial luminance of 1000 cd/m^2.

The maximum efficiencies reported for phosphorescent and TADF materials are quite similar (and higher than fluorescent materials), but no the stability. It is worth of mention that nowadays phosphorescent OLED devices present a higher lifetime compared with fluorescent and TADF based OLEDs, allowing them to be used in industry applications. Even in the last year, the data of the lifetime and stability for TADF OLEDs was still limited. In 2020, the number of reported TADF materials with good stability and lifetime have increased. For instance, Kamata *et. al*.[9] reported record-breaking performances among the existing reported TADF OLED devices, the first one an stable green TADF OLED with an excellent EQE of 19.2 % and a lifetime (LT50) of 24 000 h for an initial luminance of 1000 cd/m^2 (@ 4 V). On the other hand, they also reported a blue OLED with a similar EQE (21.5 %) but a significantly lower lifetime of 1700 h at an initial luminance of only 500 cd/m^2. TADF materials can theoretically capture 100 % excitons without incorporating noble metals (as phosphorescent materials) making them effective emitters for OLEDs and even can be used as host materials simultaneously[10] reasons why TADF is referred to as the 3rd generation OLED emitter technology.

Another really important parameter is the color or bandwidth of emission (for commercial applications white, blue, green and red colors) because the performance change with the bandwidth, for example, the blue bandwidth has the lower performance in general.

The different colors or wavelength of emission is a very important factor in OLEDs research, because most of the current industrial applications uses three or even four primary colors: red, blue, green and sometimes white. It is worth of mention that white OLEDs can be obtained by using the simultaneous emission of the three primary colors (RGB) or by using two complementary blue-orange emissive materials[11].

Performance of OLEDs used on commercial displays is shown in Table 1. As can be seen, red and green OLEDs present a significant higher performance compared with the blue one.

The low lifetime of the blue OLED devices in general is one of the most important subjects of research currently.

Table 1. Device performance of OLEDs used on commercial displays.

	EQE_{max} (%)	η_{max} (cd/A)	LT50 (h)	Type	Ref.
Red	> 20	30	900 000*	Phosphorescent	[12]
Green	> 20	85	400 000*	Phosphorescent	[12]
Blue	24.8	47	20 000*	Phosphorescent	[12]

EQE_{max} = maximum external quantum efficiency, η_{max} = current efficiency, *measured at 1000 cd/m^2, LT50 = time for the luminance to decay to 50 % of the initial luminance.

For white OLEDs, Reineke S. *et. al*.[13] have reported an efficiency of 90 lm/W (@ 1000 cd/m^2) for a real lighting device, with potential 124 lm/W if the light coupling can be further improved. In comparison, technologies as fluorescent tubes produce around 70 lm/W. Also, in the industry, LG chemical has developed OLED panels with 135 lm/W and 40 000 h lifetime at a brightness of 3000 cd/m^2[14].

Also in the area of new materials for OLED devices, new types of flexible substrates to use them instead of rigid ones are being developed, then they need to have similar properties not only flexibility. They must have a high transparence (to allow the extraction of light), low coefficient of thermal expansion (CTE)(how material change with the variation of temperature) and low optical birefringence (refractive index independent of the light polarization)[15].

The ITO conductor is the most commonly used transparent conductive electrode (TCE) material for OLEDs and OPVs devices but is not enough for flexible devices[16], because suffers from the intrinsic brittleness, the high material costs, and the need for the high processing temperature (300 °C)[17]. Then the alternative is the development of new flexible TCEs. There are a wide variety of new TCEs like graphene based[18], polymer based[19], metallic nanowires (NW)[20], hybrids as graphene-metallic NW[21], etc.

And finally, as was mentioned before the second area of great research is the design of new architectures for optimizing the performance of OLED devices. The first of them focus on

adding more and new materials to improve the injection and transport of electrons and holes. The second based on light extraction through different mechanisms as modification of specific surfaces to improve the outcoupling of light[22].

OLEDs are now being commercialized mostly in smartphones and large-screen TVs (55" or bigger). Due to their great advantages as color purity, perfect black (turn each pixel on or off) and low power consumption, its commercialization is every day larger in a market in which LED technology is the most used technology yet. As happened with the LED technology, when the OLED technology matures, the price will fall substantially[23].

As can be seen in Fig. 1, most of the OLED market came from the displays of the smartphones. OLED televisions are the second best market, but because their high cost is really low compared with the market of smartphones. The best OLED devices at lab scale are performing at over 100 lm/W efficiency and at least 30 lm/W at industrial applications[24].

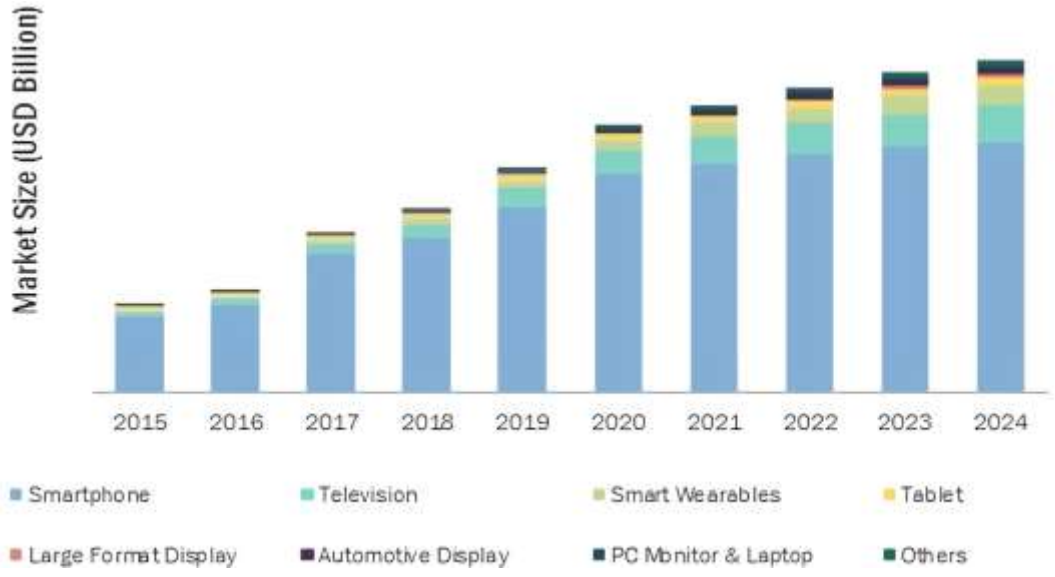

Fig. 1. OLED display panel market, by product, 2015-2024[23].

Another important parameter in OLED devices besides the lifetime is the brightness or luminance. Luminance has a great importance in all kind of OLED devices, because depending on the application the value of this luminance changes. For example, for one OLED TV (LG B9 model 2020) the maximum luminance displayed is around 767 cd/m^2[25]

for the smartphone Samsung Galaxy S20 ultra is 1342 cd/m^2 (Fig. 2)[26]. On the other hand, the lifetime promised by LG for its OLED TV is 100 000 hours[27].

Fig. 2. LG OLED TV (B9 model 2020) with a maximum luminance of 767 cd/m^2 and the Samsung galaxy s20 ultra with a maximum luminance of 1342 cd/m^2.

OLEDs have been applied in other not very well-known areas, some of them creatives as the 7-inch OLED virtual mirror system incorporated in the electric cars Audi e-tron[28], which consisting of small exterior side cameras and a door-mounted interior OLED display (Fig. 3 (a)). Also, LG (LG Chem) has been producing light panels for exterior and interior illumination, for example, in Fig. 3 (b) an OLED light panel for desk is shown[29]. Finally, as an example of a really simple application, Coca Cola embedded flexible OLED lighting panels (with battery enough for 4000 s of light) in limited edition bottles as a part of a new Star Wars film promotion[30].

(a)

(b) (c)

Fig. 3. (a) 7-inch OLED virtual mirror system incorporated in the electric cars Audi e-tron[28], (b) Lg Chem OLED light panel for desk[29] and (c) Coca Cola limited edition bottle with an embedded flexible OLED lighting panels of a new Star Wars film promotion[30].

On the other hand, in the past years, the area of flexible optoelectronics have been of great interest, because of its potential to be applied in flexible displays, flexible OPVs, smart and wearable devices, and others[31–33]. This kind of devices can be flexible and even stretchable, and that properties are really attractive for research and the industry. In this area of flexible optoelectronics, the research is focused in the development of new types of flexible substrates, new transparent conductive electrodes (TCEs) and the design of new architectures for optimizing the device performance[22]. The area of TCEs is maybe the most attractive in this kind of devices, because it can be applied in other devices as organic photovoltaic cells (OPVs) for example. The big challenge is to match the performance of the ITO (sheet resistance/conductivity and transmittance) but with a better mechanic properties since ITO crack in flexible substrates[34]. This is being developed by the use of alternative materials such as conductive polymers (as PEDOT:PSS conductive), carbon based materials (graphene, carbon nanotubes, etc), metal nanowires (MNWs), metal mesh and even hybrid materials based on the combination (of two or more) of the mentioned before. In general, conductive polymer based anode (as conductive PEDOT:PSS) present a lower cost that the others, but a lower conductivity (high sheet resistance) too. On the other hand, metal based anodes (MNWs, metal mesh) present a higher conductivity, comparable with the ITO (10

Ω/□) but with a higher manufacturing cost. Finally, hybrid anodes present a very good sheet resistance (even lower than ITO) a similar transmittance but most expensive and difficult fabrication.

Currently, new flexible OLED devices have been releasing in the industry, but they are few and even have some early troubles[35]. For example, Huawei has presented the new smartphone Huawei Mate X with a foldable OLED display[36] and LG a new rollable OLED smart TV 8K[37], both of them at a high cost because this kind of technology is new and difficult to produce in massive quantities (Fig. 4).

Fig. 4. Foldable OLED device Huawei Mate X and rollable OLED LG smart TV 8K.

1.2 Thesis work

- While there is a common belief that efficient OLED devices must have a complicated and multilayer structure, a closer examination proves that not necessarily this is the only way to reach good efficiencies. In this thesis is shown that the design of materials and the adequate optimization of the OLED devices (based on their energy levels) can lead to efficient OLED devices by using simple architectures.
- In similar way, reported free ITO anodes for optoelectronic devices have been using even 3 or more different material in order to reach values of sheet resistance and transmittance similar to ITO. In this work by the use of only conductive PEDOT:PSS (PH1000), is proposing a new simple, cheap, easy-fabrication method with sheet

resistance and transmittance quite similar to ITO that can be applied not only in rigid substrates but also in plastic ones.

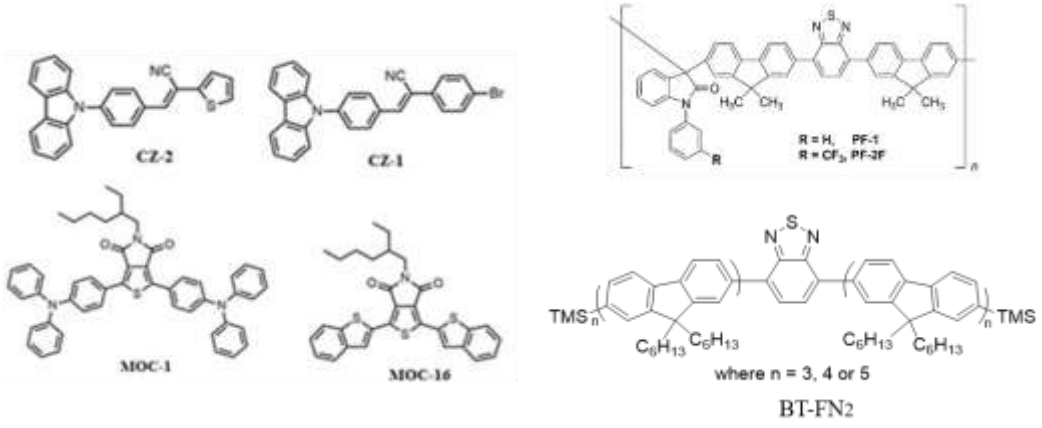

Fig. 5. Materials used as EMLs in the OLED devices fabricated in this thesis work.

Efficient OLED devices based on fluorescent and phosphorescent materials were fabricated. Fluorescent devices were based on new polymer and small molecule materials. The first of them, a group of four previously reported small molecules[38] synthesized in the research Group of Optical Properties of Materials at the Optical Research Center (GPOM-CIO) group, **CZ-1**, **CZ-2**, **MOC-1** and **MOC-16**, which were deposited by spin coating technique, were fully optimized and characterized. EQE for these OLED devices was calculated, by using the basic characterization: J-V-L curves and the electroluminescence spectra.

Also, OLED devices based on a new fluorescent material (**PF-2F**) synthesized in the Materials Research Institute (UNAM)[39] based on a reported polymer (PF-1)[6] but with a CF_3 group added were made and optimized, in order to see the influence of this trifluoromethyl group in the electroluminescence and the efficiency of the devices.

The other three are a family of three oligomers (**BT-F3$_2$**, **BT-F4$_2$** and **BT-F5$_2$**) synthesized in the Peter Skabara research group (University of Glasgow) which are highly luminescent, present a PLQY about 1 and can be deposited by spin coating technique. For this family of molecules, simple and multilayer architectures were used. In order to analyze the influence of their structures (specifically their length) in the performance and stability, EQE calculations and their lifetime measurements were made. Also, phosphorescent OLED devices were made, by using $Ir(ppy)_3$ as guest material and PVK as host, in order to optimize the ETL (TPBi specifically) which is really crucial in this kind of devices.

Finally, an anode was developed by using a cheap and simplified method based on conductive PEDOT:PSS (PH1000) only. The principle is based on that the conductivity of this PEDOT:PSS can be enhanced if the conductive fractions (PEDOT) is separated from the non-conductive fractions (PSS). This anode reach excellent values of transmittance (85 %) and sheet resistance (40 Ω/□). Furthermore, a difference of most of the reported anodes in literature, we are only using one deposit of PEDOT:PSS (by spin coating) and one post-treatment which make it a fast, easy and cheap way to obtain a functional anode. Furthermore, this anode can be deposited on glass or even plastic substrates as common as acetate.

2 ORGANIC LIGHT EMMITING DIODES (OLEDs)

2.1 OLED

An Organic light emitting diode (OLED) is composed by one or more layers of organic material that are between an anode and a cathode, all of them stacked on a glass or plastic substrate (Fig. 6). In the simplest case only one layer of organic material working as emissive layer (EML) between one anode with a high transmittance, to allow the emission of the device, and one cathode with a high reflectivity to favor the emission by the side of the anode.

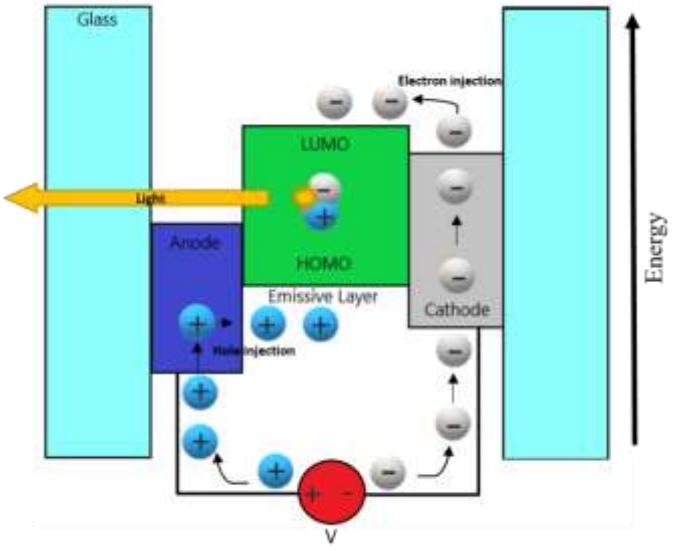

Fig. 6. Simplest OLED device with a single organic layer as EML between two electrodes: anode and cathode.

Normally the number of layers improve the efficiency of the devices, by using specific materials making specific functions. In OLED devices, electrons are injected from the cathode to the EML and holes are injected from the anode to the EML. For example:

Electrode: anode and cathode. In the most basic OLED device, one layer of emissive material is sandwiched between two electrodes. Indium Tin Oxide (ITO) is the most used material because its high work function, good conductivity (10-12 Ohms/square), high transmittance in the visible region (>90 %), among others. There are various treatments to improve both

the work function and surface conditions in the ITO, as the UV and O_2 plasma treatment[40]. In the UV treatment, the ITO is treated in a N_2-O_2 ambient environment which improve the driving voltage and prevent the formation of dark spots in the devices, improving in this way the lifetime. The O_2 plasma treatment has the capability of remove organic contaminations from surfaces. Also, O_2 plasma works creating chemical functional groups (as amine, carboxyl, carbonyl and hydroxyl) and remove hydrocarbon contaminants in the surface which leads to an hydrophilic surface, this helps to enhance the bonding or adhesion of the layers that will be deposited. On the other hand, decrease the energy barrier of the cathode improves the efficiency of the device. Aluminum (Al) is the most used cathode because of its low work function, which is in general the most reactive layer in presence of oxygen or water. To protect the EML, in OLED devices, two-layer cathode materials are usually used. Low work function materials as Ca, Mg, CsF and LiF are deposited before the deposition of the "top cathode", this layer is known sometimes as cathode EIL. Compounds as the LiF, are insulators, and for this reason they must be deposited to a thickness of a few nanometers which allows an appropiate small electron injection layer. The use of this bilayer cathode leads to the Vacuum Level Shift, this is the formation of electric double layer where the injection barrier height is lowered and then the injection from cathode to organic layer is improved[41].

Hole injection layer (HIL). This layer has the function of improve the injection of holes (or electrones extraction) from the anode to the EML or the HTL. The potential barrier for hole injection from anode to organic layer is reduced by introducing this layer. The HOMO level of the HIL should be between the HOMO layer of Hole Transport Layer (HTL) (or EML in its absence) and the work function of the anode. The most used material for this HIL is the polymer polyethylenedioxythiophene poly-styrene sulfonate (PEDOT:PSS) due its relatively high conductivity and its good transmittance in the visible region[42]. This polymer is a water dispersed polyelectrolyte emulsion with good film-forming properties for it deposition by wet methods. The ratio of PEDOT and PSS control the conductivity of the material, even in the right ratio PEDOT:PSS can be used directly as anode. Also, is worth of mention that PEDOT:PSS has a few disadvantages as a high acidity that corrodes the ITO electrode and absorbs moisture, both sources of degradation[43].

EML. The most important layer in the OLED device is the EML. The conjugated π electron system provides the electronic conduction in organic materials, this is, the alternate single and double bonds between carbon atoms. The electrical properties of the conjugated materials is related to the degree of π-conjugation. In a polymer with high grade of conjugation, the electron delocalization increases and also the mobility of electrons through the system[14].

Electron injection layer (EIL). This layer has the function of improve the injection of electrons from the cathode to the EML or to the ETL. This layer also presents a relatively high mobility of holes compared with the mobility of electrons in organic materials. Some materials commonly used for this kind of layer are: LiF, Mg, MgO_x, etc and they used to have optimized thickness of 0.3-10 nm[14].

Electron transport layer (ETL). Located between cathode and the EML, has the function of improve the transport of electrons from the cathode to the emissive layer. The ETL used depends on the OLED design, mostly of the adjacent energy levels but also mobility must be of the same order of the HTL for the recombination occur at the emissive layer. Some commonly used ETLs are Alq_3 (Tris-(8-hydroxyquinoline) aluminum), TPBi (22',2"-(1,3,5-benzenetriyl)-tris-[1-phenyl-1-H-benzimidazole]), BCP (2,9-dimethyl-4,7-diphenyl-1,10-phenanthroline), etc. TPBi for example, a typical ETL, poses a high HOMO level of 6.2 eV and then TPBi is also working as Hole Block Layer (HBL) too[44].

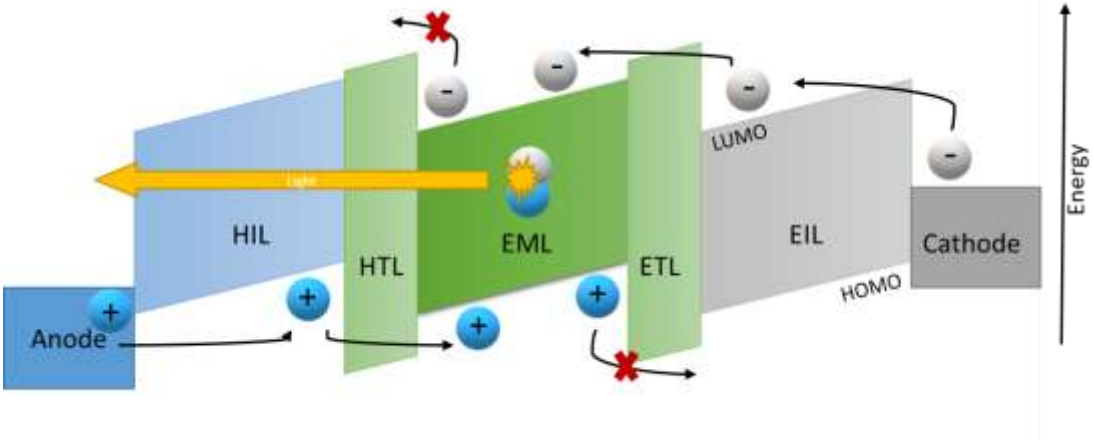

Fig. 7. Multilayer OLED device.

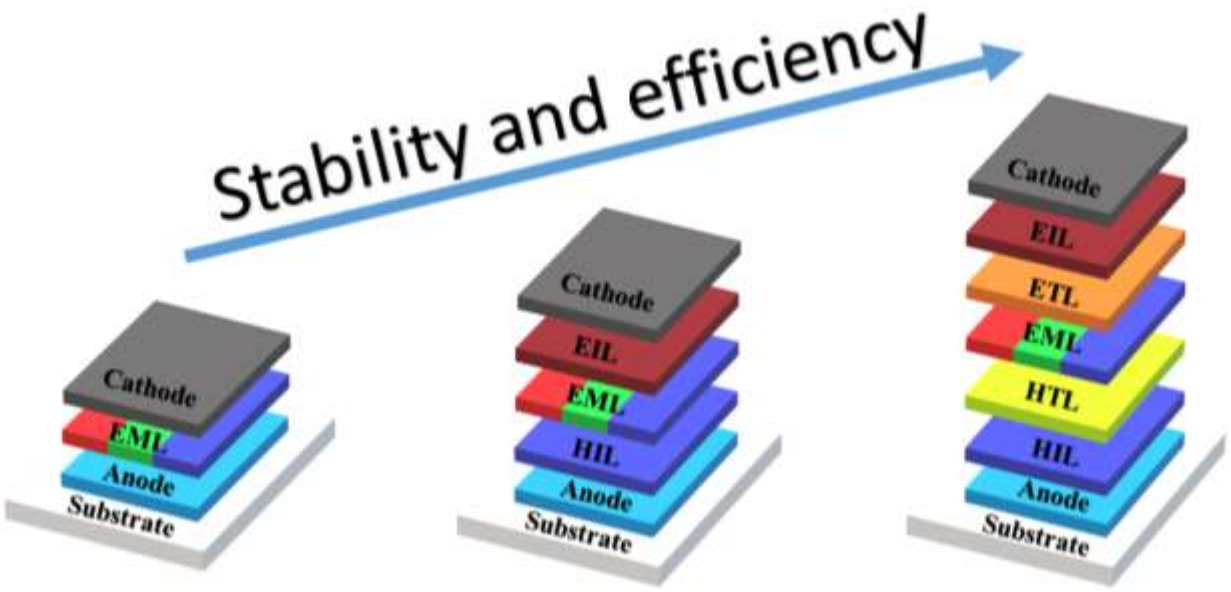

Fig. 8. Structure of OLEDs from single layer to multilayered.

Exist different methods, techniques and architectures to make an OLED, with various and new materials, and not only with one or two layer, even with 10 layers or more[2,3].

2.2 HOMO, LUMO and work function

HOMO (highest occupied molecule orbital) is for the organic semiconductor which is the valence band for the inorganic semiconductors. In the same way LUMO (lowest un-occupied molecule orbital) is for the organic semiconductor which is the conduction band for inorganic semiconductors. The difference of energy between this HOMO-LUMO levels is known as the band gap. The band gap (E_g) has a great importance in OLED devices, because it is responsible of the emission color. The energy of one photon in the visible (350-750 nm) is around 3.1 – 1.8 eV, then the band gap for the EMLs must be in this range.

On the other hand, the electrodes have the work function which is defined the minimum energy that must be given to one electron to release it from the surface of one specific material. All, work function, HOMO and LUMO levels, have a great importance in the OLED devices because the energy levels of the layers must be coupled. This is, choose an

HOMO level between the HOMO level of the HTL and the anode's work function in order to the optimum injection of holes from the anode to the HTL. Similar for the injection of electrons, the LUMO level of the EIL must be between the cathode's work function and the LUMO level of the ETL for the adequate injection of electrons from the cathode to the ETL. Finally, the difference between HOMO level between EML and the HTL must be low (the same for the LUMO levels between EML and ETL).

2.3 PLEDs and SMOLEDs

OLEDs might be mentioned as small molecule organic light emitting diode (SMOLED) or polymer organic light emitting diode (PLED). Unlike polymers that form films with low roughness (RMS) by using spin-coating technique (or another wet technique), organic molecules of low molecular weight, usually form films with many defects and high roughness (RMS), further, in several cases they do not have good solubility to be used under wet methods. SMOLEDs fabricated by wet techniques are being investigated widely due that a high processability (as polymers) by wet methods are attractive to make OLEDs in large area, may be light, flexible, self-emitters, have low power consumption, high speed video rate, intense colors, high contrast and possess a potential low cost compared with evaporation methods[45]. On the other hand, small molecules having a well-defined molecular structure that provides greater reproducibility in their synthesis, besides in general posses a higher purity than polymers[46]. The use of a large number of layers to increase the device performance usually increase the manufacture time and the costs, that is why OLED devices with the minimum number of layers are of great importance i.e. the research of new and efficient materials have a big rol in the actual research field[3].

Polymers may be classified as non-conjugated or conjugated, this last characterized by a backbone chain of alternating double and single bonds. Conjugated polymers (such as MEH PPV, Super Yellow, PVK, etc), formed by carbons with hybridization sp^2, possess high mobility of electrons and holes because their delocalized π-electrons system which benefits its use as EML in OLED devices. On the other hand, some non-conjugated polymers have been designed to maximize device performance in host-guest blend type used as EML. This

is, functional units are bound to the non-conjugated polymer and then used as a host material. Finally, guest materials are doped in low quantities into the host material. One example of this non-conjugated polymers is poly-vinylcarbazole (PVCz). Otherwise, some typical examples of conjugated polymers are poly-phenylenvinylene (PPV), poly-p-phenylene (PPP) and polyfluorene (PF)[47].

On the other hand, for SMOLEDs (such as Alq_3, MADN, DBP, etc.) the introduction of soluble groups to existing structures is one of the most significant technologies for OLED devices. The introduction of this kind of groups offers advantages as lower fabrication costs due it can be used another methods different of evaporation. This versatility is of great importance because these technologies move towards industry production and the scalability is necessary[48].

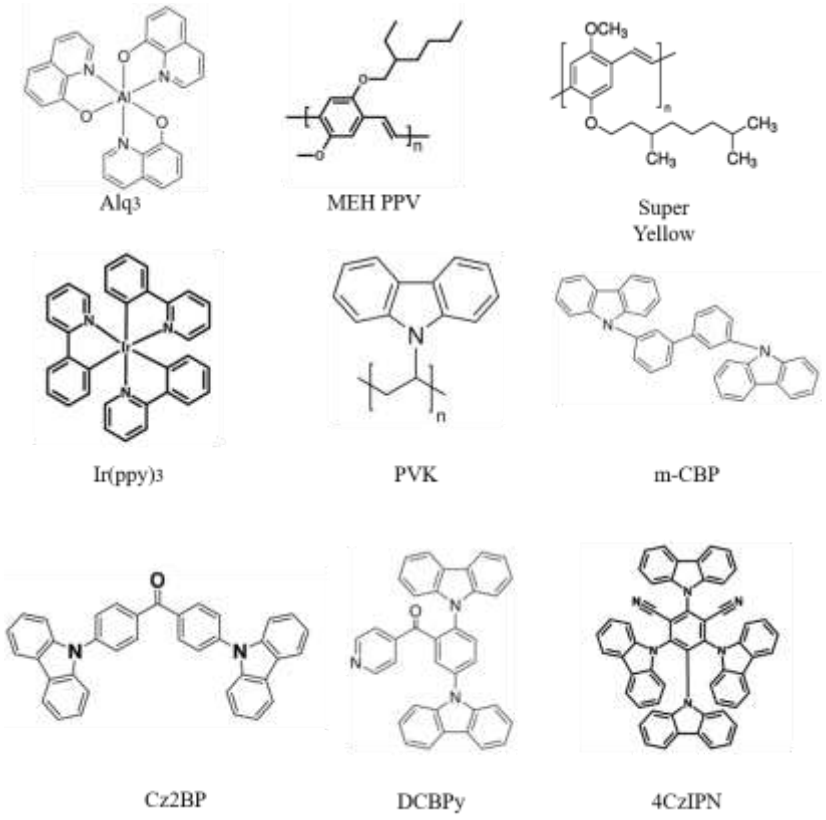

Fig. 9. Typical commercial materials used for OLED devices.

2.4 Fluorescence, phosphorescence and TADF

The photoluminescence (PL) is the emission of light due to transitions of electrons from molecular orbitals of higher energy to those of lower energy known as ground energetic state. Such transitions are referred to as relaxations. The electrons that are in the closer layers at the core are less energetic than those that are not so close. When some atoms are exposed to light of some specific wavelength, a photon will make that an electron in a ground energetic state becomes in an electron with high energy, also named excited electron. For each kind of electron the difference between orbitals is quantized and the electrons only can move in trough them by winning or losing an specific quantity of energy, which is known as electronic transition. When the electron decays at its ground state (or a lower energy level) release the extra energy via radiative route (photon) or as heat via non-radiative. This photon is the light that can be seen by our eyes, which wavelength is dependent of the type of atom that was excited[7].

In the case of the OLED devices, the excitation of the molecules used as EML occur through injection of holes and electrons from the electrodes, which are excited from a ground state to one excited state .Of course, the correct injection is dependent of the optimum alignment of the HOMO-LUMO levels of their layers and the work function of the electrodes.

The total energy emitted as photons (called electroluminescence in OLEDs) is always lower than the total energy injected and the difference between them is dissipated in form of heat by vibrations. Most of the cases, the wavelength of this light is higher than the wavelength of the absorbed (or injected), and then, has a lower energy.

The PL has 3 fundamental steps: absorption (injection for OLEDs), non-radiative decay and radiative decay. Furthermore, electronic excitation can occur to two electronic states known as electronic state singlet S_1 and electronic state triplet T_1.

Now, depending of the mechanisms of decay and the emission of light on EML, OLED devices can be categorized by 3 types or generations: fluorescence (1^{st} generation),

phosphorescence (2nd generation) and thermally activated delayed fluorescence (TADF) (3rd generation).

PL occurs when a molecule or atom returns to it ground state (S_0) after being electronically excited (singlet state S_1), which can be expressed as

$$S_0 + h\nu_{ext} \rightarrow S_1 \quad (1)$$

On the other hand, we can express the fluorescence as

$$S_1 \rightarrow S_0 + h\nu_{em} + heat \quad (2)$$

$h\nu$ is the one photon energy, h is the Planck's constant and ν is the frecuency of the light. A luminescent molecule in the excited state S_1, can return to its ground state by different paths, the first of them is the non-radiative decay in which the energy is dissipated in heat form and the second one is the emission of one photon. Also, in the specific case of fluorescent materials can be excited to a triplet state (T_1), but its only path to return at a ground state is dissipating heat. Fluorescent materials can not have radiative decay from a triplet state. As is shown in Fig. 10, from the spin statistic it is known that only 25 % of the excitons (or excited states) formed are of the singlet type, while triplet type excitons represents the 75 %. So, a fluorescent type OLED can have a maximum internal efficiency of only 25 % [7]. On the other hand phosphorescent materials with a heavy metal center (such as ruthenium, rhodium, osmium, iridium, platinum and gold) can have radiative decay from both, singlet and triplet states, enabled by the strong spin-orbital coupling (SOC) effect or heavy metal effect, which allow them reach a theoretical maximum internal efficiency of 100 %.

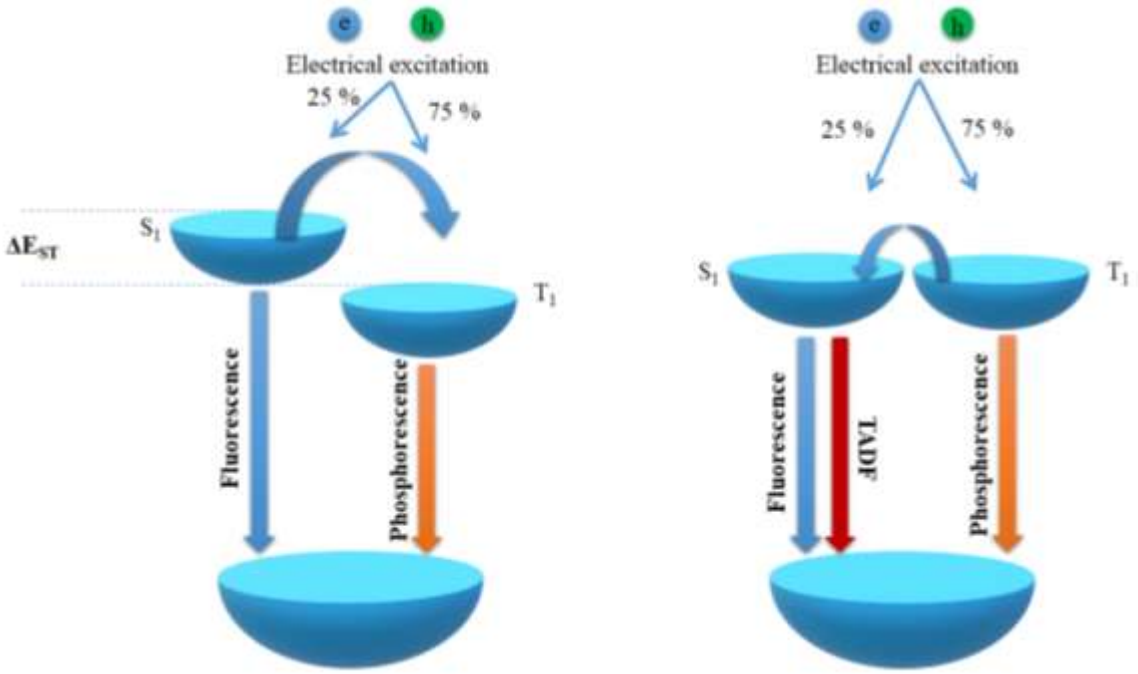

Fig. 10. Light generation in (a) fluorescent and phosphorescence-based OLEDs and (b) TADF based OLEDs.

TADF is the name given to materials (such as Cz2BP, DCBPy, 4CzIPN, etc.) that have a mechanism of fluorescence relying on a specific molecular design where the first excited singlet state (S_1) can be thermally repopulated by RISC (reverse intersystem crossing) from the first excited triplet state (T_1). Only when the energy difference between the triplet and the singlet-excited states (ΔE_{ST}) is small enough, this process is possible (Fig. 10 (b)). In most fluorescent molecules the ΔE_{ST} is in the range of 0.5–1.0 eV, because of this, TADF can not be possible[49]. Then, by this mechanism, the non-radiative triplet states can repopulate the singlet state and participate to light emission, enabling OLEDs reach an internal quantum efficiency of 100 %[50].

In Fig. 11 devices structure of a phosphorescent OLED is shown. The lifetime of the emissive excited state in a phosphorescent complex, as iridium for example, is quite long compared with fluorescent materials (microseconds and nanoseconds, respectively). In the case of phosphorescent materials, iridium (III) complexes are the most promising due its facile chemical modifications, tunable photophysical properties and good stability. In general for the EML deposition, phosphorescent complex are doped in host materials at low concentrations, aiming to avoid efficiency loss caused by triplet-triplet annihilation (TTA).

TTA is the process of energy transfer from one triplet excited state to another, after which the excitons decays non-radiatively to the ground state.

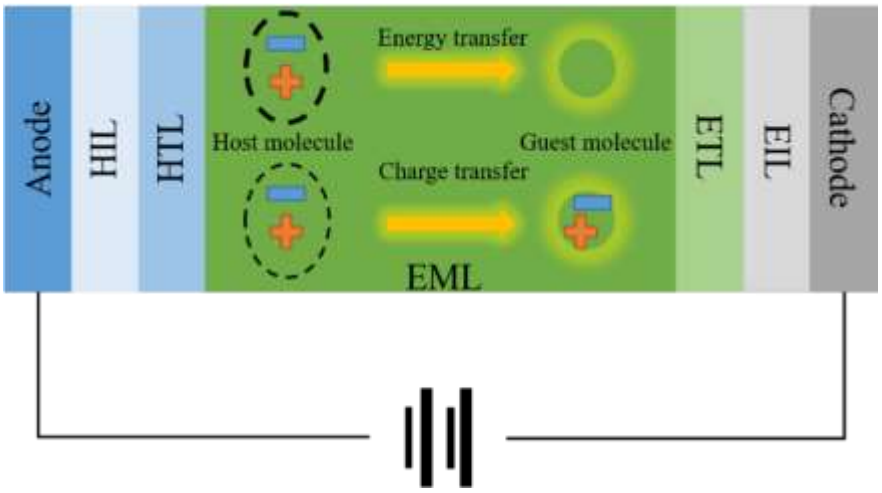

Fig. 11. Device structure of an OLED with two different excitation mechanisms in the EML.

2.5 Emissive layers type Host/Guest

Host/guest systems are an alternative for molecules which have properties of emission but can not be deposited as films by itself. In general, a low quantity of the guest material (6-10 %)[51], also named dye, is dispersed on a host material to obtain an EML with mechanical properties of the host but with the emission properties of the dye.

Host molecules (such as PVK, CBP, m-CBP, mCP, etc.) have important functions in the performance of the EML, depending of the material used as host and the quantity used of dye the performance could be or not better. The parameters that are tuned by this relationship is PLQY, suppression of concentration of quenching, PL spectra and basically the performance of the OLED devices (voltage, current, luminance, efficiency, EL spectra)[52].

As was mentioned before, in the Jablonski diagram, there are different paths of energy transfer. In order to achieve efficient OLEDs, by host/guest system, the singlet formed on the host must transfer to the guest by Förster energy transfer (FRET) and the triplets must transfer its energy by Dexter energy transfer (electron exchange)[3] as is shown in Fig. 12.

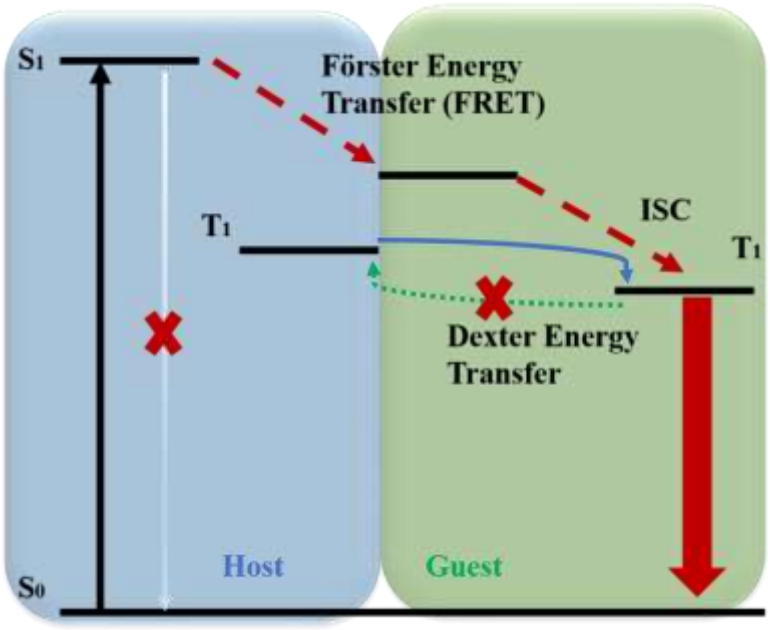

Fig. 12. Host/guest energy transfer system.

FRET is the energy transfer from one excited chromophore to another nearby, by dipole-dipole interactions. On the other hand, Dexter energy transfer sometimes known as short-range transfer is quite similar to FRET but differs in distance range (FRET is 10-100 Å and Dexter is < 10 Å) and mechanism. Dexter energy transfer is basically an exchange of energy but with electron exchange between two molecules or two parts of a molecule.

Furthermore, in host/guest system excitons can also be directly formed on the guest molecules if appropriate dopant is chosen according to the energy levels i.e. the efficiencies can be significantly increased.

Anyway, efficiency in this kind of systems do not depend only on the energy level distribution between the host and the guest materials but also on the energy transferring capability. For example, in Fig. 13 the CF3BNO material favors the electron injection into the host rather than in the guest, resulting on the formation of excitons on the host and hence favoring energy transfer from the host to guest leading to a higher efficiency and performance compared with the cases when BNO and $Ir(ppy)_3$ are used as guest[3].

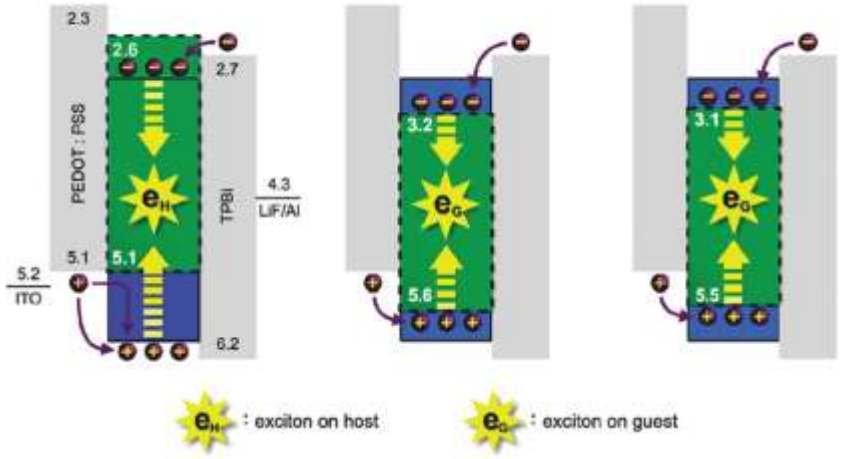

(a) (b) (c)

Fig. 13. Energy level diagram of 3 different guests: (a) CF_3BNO, (b) BNO and (c) $Ir(ppy)_3$ used on a CBP host[3].

3 FABRICATION AND CHARACTERIZATION OF OLED DEVICES

3.1 Fabrication techniques

As was mentioned before, there are two ways to make OLED devices: solution process (also called wet methods) and evaporation. Wet methods have advantages as scalability, easy manufacture and there are cheaper and easier than evaporation.

One of the most used techniques for thin films deposition is spin coating technique. By this technique thin films of micrometer and nanometer can be prepared. A substrate is mounted on a chuck, the solution of organic material is deposited on the substrate and then rotates. Centrifugal force drives the liquid radically outward. The main causes for the film deposition on the substrate are the viscous force, surface tension and finally evaporation of residual solvent as can be seen in Fig. 14(a). By spin coating technique a fine, thin and uniform layer can be produced. The disadvantage of this technique is that is too difficult produce a layer of high quality and large area. The thickness by spin coating technique is defined by different parameters such as the viscosity of solution, the angular speed and the rate of evaporation[53].

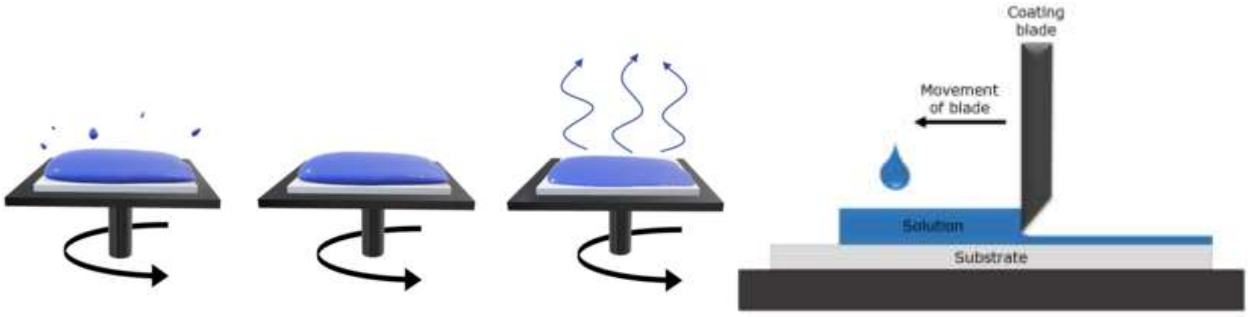

(a) (b)

Fig. 14. Schematic illustration of the (a) spin coating and (b) Doctor blade techniques[54].

Another technique for thin films deposit by solution is Doctor blade, in this technique, basically a coating knife is used to apply a solution over the surface of one substrate. A defined quantity of solution is applied directly on the surface, or when the viscosity is too low, in the gap between the surface and the blade. In the next step, the knife is moved along the substrate with a defined velocity, while a defined value of temperature (depending of the solvent used) is applied in the substrate. A wet thin film is left behind the knife, which dries due to the evaporation of the solvent Fig. 14 (b).

Also, a modified and more precise technique based on Doctor blade was developed: slot die coating. This technique is the promising fabrication scheme for large-area OLED panels because it provides scalability and uniform films. It is capable of deposit a wide range of materials, with low and high viscosity, and a wide range of thickness, from 20 nm to 150 μm[55] [56].

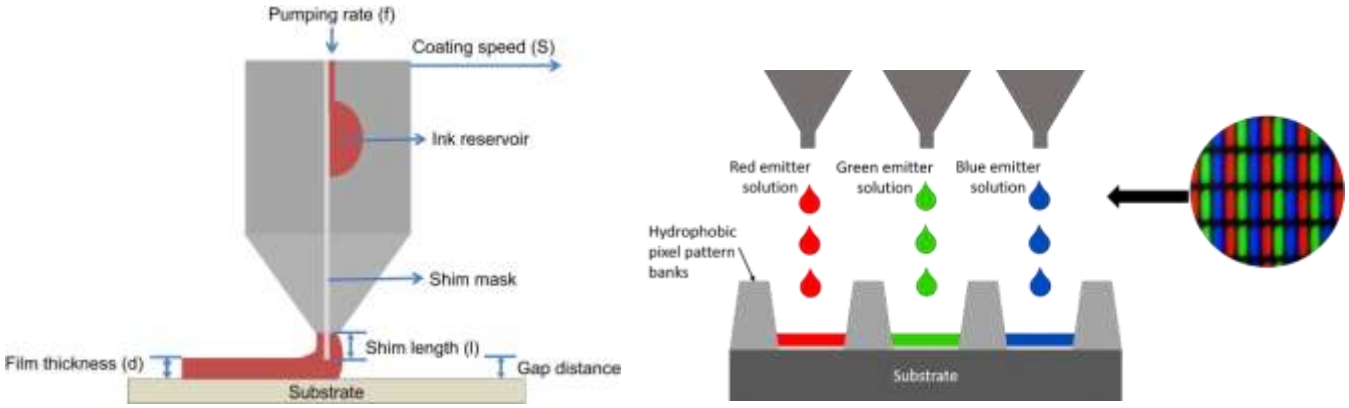

(a) (b)

Fig. 15. Schematic illustration of (a) the slot die technique and (b) Inkjet printing (IJP).

More expensive and top quality techniques were developed too, Inkjet printing (IJP) is one of these. The integration of multiple organic layers to fabricate red, green and blue emitters for color displays is possible by this technique. IJP is able to carry out material deposition and pattering at the same time, and require really small amounts of functional materials. This materials are deposited in solution in little drops on defined surface areas, in the desire shape. One of the major advantages of this process is that the waste of materials is minimum and that decreases the production costs. Other advantage of IJP technology is there does not need contact, so the substrate defects does not exists. OLED devices need accuracy of organic layer thicknesses since it directly affects color uniformity and brightness.

Physical vapor deposition (PVD) is a technique based on the heating the material until evaporation (thermal evaporation). This thermal evaporation has place when an electric resistance is heater to melt the material and raise its vapor. This is done by using a high vacuum. PVD can generate smoother surfaces, compared with wet methods as spin coating, slot die, etc. In Fig. 16 physical vapor deposition mechanism is showed. A controlled current

is applied trough the crucible, heating the material to its evaporation point and then the material is deposited on the substrate. Depending on the current applied, deposition rate i.e. thickness can be controlled. Deposition by evaporation is widely used in the deposit of small molecules and in the deposit of cathodes as Al, Ag, etc. The process of evaporation has the advantage that multilayer OLED can be made easily, but with a big consume of energy and resources. Besides of this significant advantages in the control of thickness and the speed of deposition, also the films deposited are horizontally oriented at intramolecular level. This horizontal molecular orientation has significant effects on the electrical and optical properties of OLED devices, at the point that in general the devices fabricated by vapor deposition present a better performance that its analogue ones fabricated by solution process[57]. This is because by vapor deposition the π-orbital overlap is favored which is beneficial for charge and energy transfer. Also, molecular orientation enhance the radiation direction and then the extraction of light from the OLED device[58]. On the other hand, the cost of this method is high compared with any other based on solution deposition and scalability is a big problem.

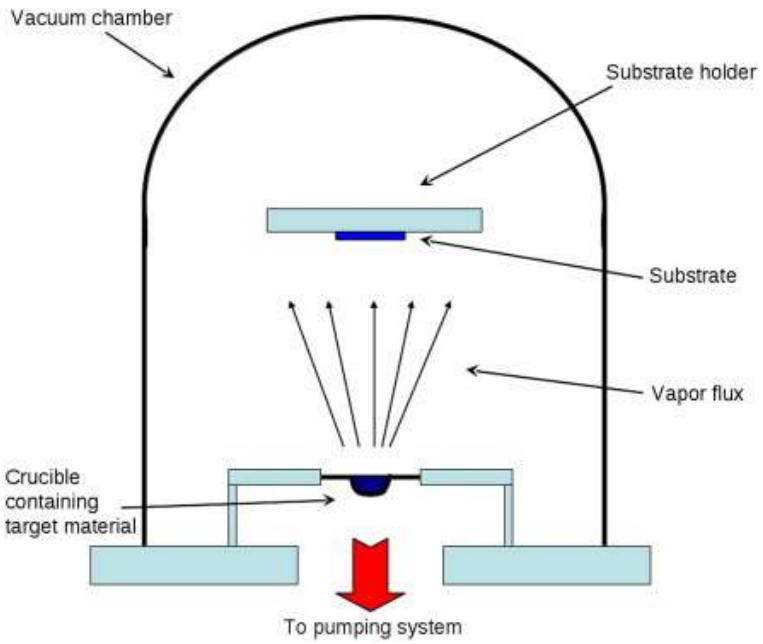

Fig. 16. Schematic illustration of one vacuum chamber. A current is applied trough the crucible, heating the material to its evaporation point and then the material is deposited on the substrate.

3.2 OLED devices characterization

3.2.1 J-V-L curve

Current density vs voltage (J-V) curve is one of the most important characteristics, easier and used techniques in OLED devices. This curve, obtained by using a power supply, represents the relationship between the current per unit area through the circuit, device or material and the correspondent voltage.

The fundamental characterization of OLED devices includes not only the measurement of the J-V curve, also the intensity of the emitted light. This measurement of emitted light, better known as luminance, can be performed by using a calibrated photodiode and will complete the characterization for the J-V-L curve.

Emitted light by OLED devices is quantified in terms of photometric measurements as is the luminance. For this, we will define the photopic vision as the visual perception produced with daylight levels, this is because the correct interpretation of color is based on the eye cones which are sensitives to the light. The spectral sensitivity of the human eye is described by the photopic efficiency function K(λ) shown in the Fig. 18 (with values between 380 and 780 nm, this is the visible range) and standardized by the CIE (Commission Internationale de l'Éclairage) which is the international authority in light, illumination, color and space of color[59].

An OLED device has a luminance L (cd/m^2) coming from its EML. If the device is considered as a lambertian source (radiance uniform in all its surface), the power P_{in} detected by the photodiode located at a distance S_{sd} is given by (Fig. 17)

$$\boldsymbol{P_{in} = \frac{L}{C_v} \iint \frac{\cos\theta_s \cos\theta_d}{S_{sd}^2} dA_s dA_d} \tag{3}$$

C_v is the photopic response, θ_d and θ_s are the angles between the beam of light and the normal line to the surfaces A_d and A_s respectively. Furthermore, as the OLED emission is not monochromatic, the photopic response is given by

$$\boldsymbol{C_v = K_m \int_{380}^{770} \phi(\lambda) K(\lambda) d\lambda} \tag{4}$$

Where $\phi(\lambda)$ is the OLED normalized emission spectra, K_m (683 lm/W) is the conversion factor from watts to lumens.

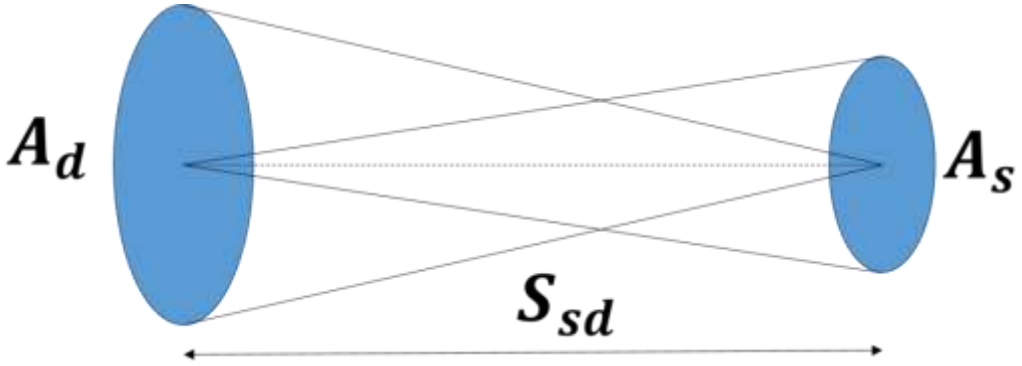

Fig. 17. Schematic illustration of the emission area (A_s) of an OLED and the photodiode detection area (A_d). Also geometrical parameters for luminance calculation are included.

Finally, in order to obtain the luminance, $\cos\theta_{s,d} \sim 1$ is assumed due to the fact that $S_{sd}^2 \gg dA_s, dA_d$. Then

$$\boldsymbol{L \approx P_{in} \frac{C_v S_{sd}^2}{A_d A_s} = \frac{V_{out} C_v S_{sd}^2}{R A_d A_s}} \tag{5}$$

Where V_{out} and R are the photodiode output voltage and the responsivity (V/W) respectively[60].

3.2.2 Current and Luminous efficiency

Current efficiency is another important and usually reported performance value for OLED devices, and is defined as the intensity of light emitted per current consumed, and can be expressed as

$$\boldsymbol{\eta_j = \frac{L}{J}\left[\frac{cd}{A}\right]} \tag{6}$$

Where L is the luminance of the device and J is the current density applied.

Also, luminous efficiency is sometimes reported, and is defined as the ratio of luminous flux and the electric power consumed P, this is[61]

$$\boldsymbol{\eta_p = \frac{F}{P} = \frac{L\pi}{JV}} \tag{7}$$

3.2.3 External Quantum Efficiency (EQE)

External quantum efficiency is the most important factor in the performance of OLED devices. But, the measurement of EQE is not easy to measure precisely because is difficult detect all of the photons emitted from the devices. An integrated sphere is necessary to detect the number of emitted photons and it is not cheap. On the other hand, it is possible calculate the EQE assuming a perfectly diffusive electroluminescent emission surface. Under this assumption, the EQE can be calculated from the classical measured parameters as luminance, electroluminescence spectra and current.

The internal quantum efficiency (IQE) of an OLED device is defined as the number of photons produced by the device per the number of injected electrons in the device, this is

$$\mathbf{IQE} = \boldsymbol{\gamma} \times \boldsymbol{\eta}_{\mathbf{s}} \times \boldsymbol{\phi}_{\mathbf{f}} \tag{8}$$

where γ is a fraction of the injected charges that produces excitons and is known as charge balance factor, η_s is the fraction of singlet excitons called excitons singlet efficiency and ϕ_f is the fraction of energy produced by the material and is called fluorescence quantum yield (FLQY). The external quantum efficiency (EQE) is related with the IQE in the next way:

$$\mathbf{EQE} = \mathbf{R}_{\mathbf{e}} \times \mathbf{IQE} \tag{9}$$

where R_e is the efficiency of extraction (number of extracted photons from the device on the number of generated photons in itself). In other words, EQE is the number of emitted photons outside of the device (N_p) between the number of injected electrons (N_e)

$$\mathbf{EQE} = \frac{\mathbf{N}_{\mathbf{p}}}{\mathbf{N}_{\mathbf{e}}} \tag{10}$$

N_p can be obtained from the measured luminance and EL spectrum. The energy of one photon at a defined wavelength λ (nm) is

$$\boldsymbol{E_p(\lambda)} = \frac{\boldsymbol{hc}}{\boldsymbol{\lambda}}[\mathbf{J}] \tag{11}$$

where h is Planck's constant and c is the velocity of light. Now, the power of a luminous flux of 1 lumen at a wavelength λ (nm) in the visible range is

$$\mathbf{P}(\boldsymbol{\lambda}) = \frac{\mathbf{1}}{\mathbf{683} * \mathbf{K}(\boldsymbol{\lambda})} \ [\mathbf{W}] \tag{12}$$

where K(λ) is the CIE standard photopic efficiency function (Fig. 18).

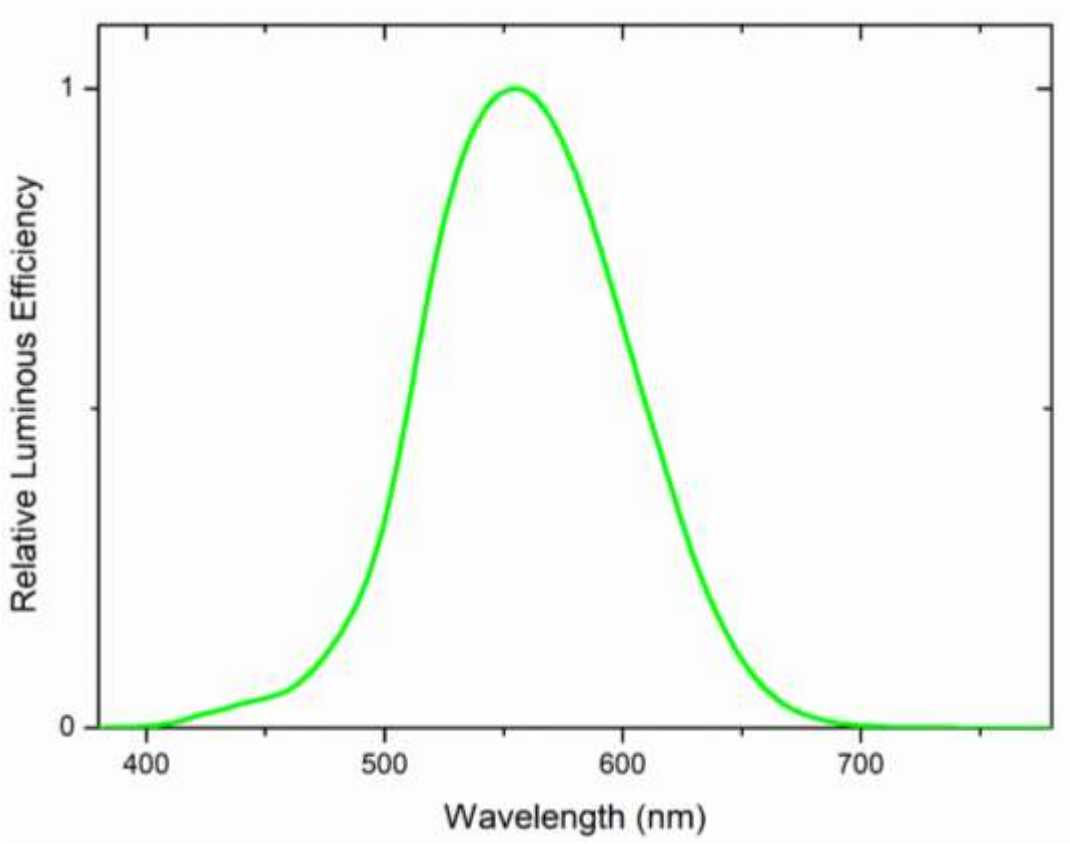

Fig. 18. Commission Internationale de l´Éclairage standard photopic efficiency function.

The number of photons with a luminous flux of 1 lumen at a wavelength λ (nm) is defined as

$$\boldsymbol{N_p(\lambda)} = \frac{\boldsymbol{P(\lambda)}}{\boldsymbol{E_p(\lambda)}} = \frac{\boldsymbol{\lambda}}{\mathbf{683} * \boldsymbol{K(\lambda)} * \boldsymbol{hc}} \ [\boldsymbol{s^{-1}}] \tag{13}$$

If we assume a perfectly diffusive EL spectra emission surface with a luminance of L (λ) (cd/m^2) at λ, the luminous flux is

$$\boldsymbol{\phi(\lambda)} = \boldsymbol{\pi} * \boldsymbol{L(\lambda)} \ [\mathbf{lm}] \tag{14}$$

Therefore, the number of photons with luminance L (λ) (cd/m^2) is

$$\boldsymbol{N_p(\lambda) = \pi * \frac{L(\lambda) * \lambda}{683 * K(\lambda) * hc}\ [s^{-1}]} \tag{15}$$

The total number of emitted photons in the visible wavelength range is

$$\boldsymbol{N_p = \int_{380}^{780} N_p(\lambda) d\lambda} \tag{16}$$

and, L (λ) is related to the total luminance L (cd/m^2) by

$$\boldsymbol{L = \int_{380}^{780} L(\lambda) d\lambda = A \int_{380}^{780} I(\lambda) * K(\lambda) d\lambda} \tag{17}$$

where I (λ) is the relative EL intensity at each wavelength and is obtained by measuring the EL spectra. A is a constant, which can be obtained by

$$\boldsymbol{A = \frac{L}{\int_{380}^{780} I(\lambda) * K(\lambda) d\lambda}} \tag{18}$$

and by using the last equation for luminance, we obtain that

$$\boldsymbol{L(\lambda) = A * I(\lambda) * K(\lambda)} \tag{19}$$

From this equation the number of emitted photons in the visible wavelength can now be written as

$$\boldsymbol{N_p = \pi * A \int_{380}^{780} \frac{I(\lambda) * \lambda}{683 * hc} d\lambda} \tag{20}$$

By using the experimentally obtained luminance and the values of the normalized EL spectrum, the values of the constant A and N_p can be obtained.

N_e is related to current I_e (A) flowing into the OLED device.

$$\boldsymbol{N_e = \frac{I_e}{e}\ [s^{-1}]} \tag{21}$$

e being the charge of an electron. With the values N_p and N_e, the EQE can be obtained from its equation. When an integrated sphere is not used, the photons of the back and the sides of the device are not detected, this yields an error from the true value of the EQE. Then, the estimated value by using this method is approximate, because the value of EQE is lower than the real.

3.2.4 Degradation and lifetime

The degradation in OLED devices is one of the most important issues in the research community and the industry. There exist different factors of degradation in OLED devices grouped in two major mechanisms: external and internal. The first of them, while an electric field is applied organic semiconductors are unstable in ambient conditions. Water vapor and oxygen are the responsible of degradation in ambient conditions. Dark spots have their origin in particles defects that preexist on the substrate and after the deposit of the organic layers and the cathode, derives in a pin-hole formation in the cathode providing a chance to oxygen and moisture to infiltrate through[62]. Dark sports appear and grow at specific sites in the surface as well as at the edges of the cathode and they can be seen as non-emissive areas in the OLED as is shown in Fig. 19 (a). Cathodes with low work function, as the majority used for OLEDs, make possible the electrochemical reduction of water leading to the formation of hydrogen gas around the dark spots. Because this gas, bubbles are created raising up the cathode giving also new spaces for the entry of additional water vapor. In the specific case of the oxygen, the dark spot is due the oxidation of the electrode at the cathode/organic interface. Oxygen also act on the organic layer which under applied bias results in a decreased efficiency around the dark spots and the cathode edges. This oxidation has a direct effect in the luminescence efficiency and in the morphology of the organic material[63].

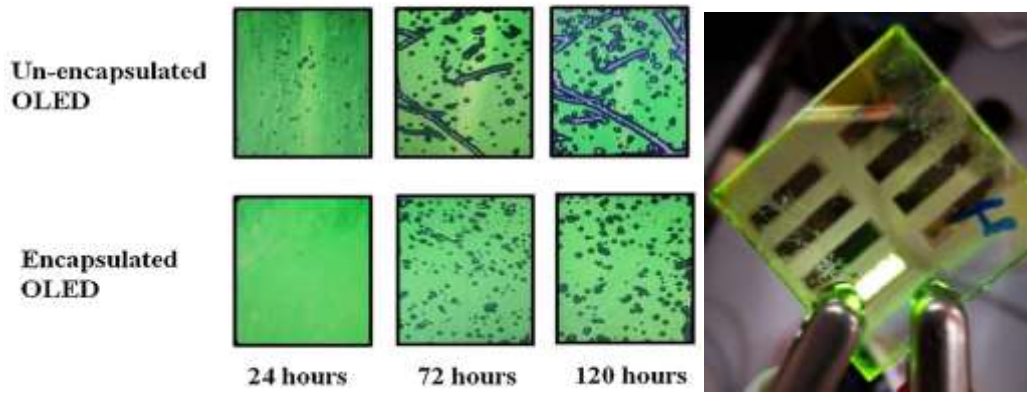

(a) (b)

Fig. 19. (a)Optical images of un-encapsulated and encapsulated OLED at different times(under a current density of 10 mA/cm^2)[24] (b) un-encapsulated phosphorescent OLED with degradation due Ca/Al cathode.

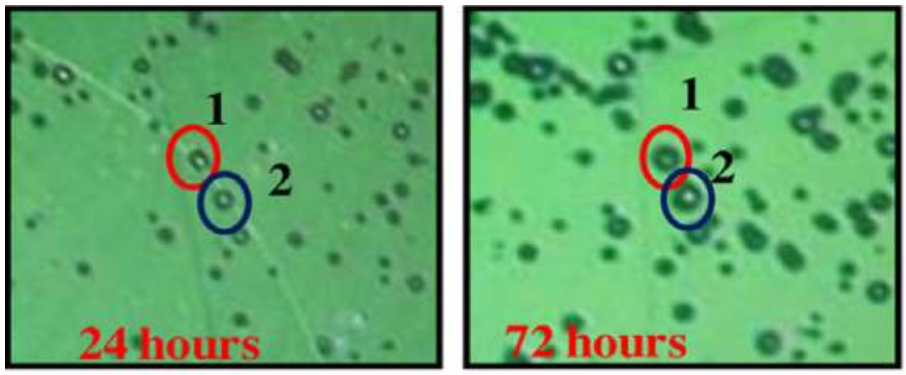

(a) (b)

Fig. 20. Dark spot expansion (a) after 24 h and (b) after 72 h[24].

The other external mechanism of degradation is because the operation of the device. This is, the luminance decreases in the time while a current is applied and accelerates the expansion of the dark spots. Also, the additional entrance of water vapor will accelerate the growth rate of dark spots. It is worth of mention that when the current stops applying then also the expansion in the dark sports. The first reason of this is the thermal stability of organic layers determined by its glass transition temperature (T_g). When the device temperature increases while the operation over the transition temperature, the material crystallizes and degrades the device. This is the reason why, materials with high T_g are preferred. Another reason of the degradation while the device is in operation is the bulk trap states which are formed in the form of non-luminescent centers inside the EML. When this trap states are formed, the voltage operation increase. Interface deterioration is other mechanism of degradation while the device is in operation, any deterioration of any interface will lead to an interface degradation. In general, OLEDs based on small molecules are more sensitive to this kind of degradation because their bigger number of layers compared with POLEDs (polymer OLEDs). The anode degradation is another important mechanism. For example, ITO the most used anode has the problem of diffusion of indium and also diffusion of oxygen that form non-radiative centers in the organic layers and increases the operation voltage respectively. Finally, the operation of any OLED device generates a significant amount of heat due the resistance of organic layers and the non-radiative decay of excited states that becomes a source of degradation. It is worth of mention that the heat has influence and increases the

number of excitons dissociated. All this external and internal mechanism of degradation affect and limit the lifetime of the OLED devices.

In general, to obtain the lifetime of the OLED devices, a number of measurements are taken with which the lifetime is calculated. This lifetime calculation can be made by different methods, as stretched exponential decay (SED)[64,65]. This model, works well to find the lifetime and its behavior, but it does not have a real physical explanation. The SED model describes a decaying behavior,

$$\frac{L}{L_0} = \exp[-\left(\frac{t}{\tau}\right)^{\beta}] \tag{22}$$

The measurements can be defined by two ways, by defining the initial luminance (L_0) or the current density applied. If L_0 is defined, a current density must be applied to produce the emission. On the other hand, if the current density is defined (constant), this will produce a defined luminance. This is, a constant current density is applied to the OLED device along a defined period of time (t), in which luminance (L) measurements will be made. With this luminance, a fit based on the SED model will be made in order to obtain the expected behavior in the time of our OLED device, without run the device overall its lifetime.

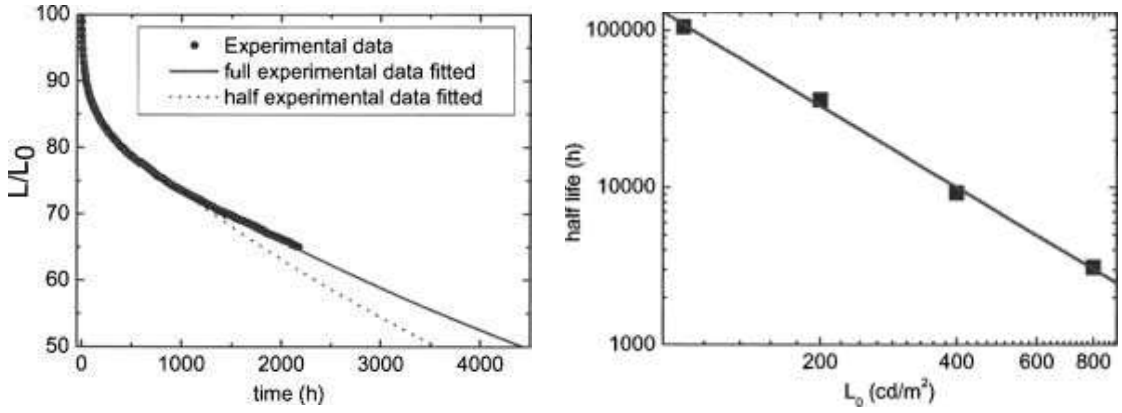

(a) (b)

Fig. 21. (a) Typical L-t curve, showing the experimental data, with the fit and (b) estimated LTs for different luminances by using the SED model[64]

Depending on the number of measurements and the interval of time, the model will be more or less accurate. For example, in Fig. 21 (a) the fitted model with all the experimental data

obtained and when only the half of it is shown. As expected, when all the experimental data is used, the fit is more accurate.

Now, from the SED model the lifetimes (LTs) for different luminances (at least 3) also can be obtained by using the equation

$$\boldsymbol{L_0^n t_{1/2} = const} \tag{23}$$

Where n is the acceleration coefficient, $t_{1/2}$ is LT50 or half-life. Also, a fit that describes the half-life dependence on the luminance can be obtained as is shown in Fig. 21 (b). As can be expected, this model shows how at a higher luminance emitted by the OLED device its lifetime is proportionally reduced.

4 FLEXIBLE DEVICES

4.1 PEDOT:PSS anodes

The development of organic conducting materials has been in continuous advance in organic solar cells, organic light emitting devices, stretchable electronics, and bioelectronics, for that reason it is often desirable in these applications that the electrodes be flexible, highly conductive, stable, and solution processable[16].

Transparent conductive electrodes (TCEs) can be characterized and compared by measuring their sheet resistance (R_{sheet}) and optical transmittance in the visual range (typically at 550 nm, the maximum human sensitivity).

With a low sheet resistance (10 Ω/□) and a transmittance of 93 % in the visible range, indium tin oxide (ITO) is the conductive metal most used in transparent conductive films (TCFs). But, ITO has some disadvantages as the high cost due to scarcity of indium, the poor chemical stability under basic or acid conditions, its relatively high refractive index (which produce power lost to the total internal reflection at the interface with the glass and the organic films), its restricted deposition condition and its poor mechanical robustness (unsuitable for applications in flexible devices). Also, has a highly brittle nature that leading cracking easily if is exposed at moderate mechanical stress, which difficult its use in flexible, stretchable and bendable devices[18,66].

There are a wide variety of emerging materials that could be a replacement of ITO anodes, for example, conductive PEDOT:PSS, carbon nanotube, metal grid, graphene and metal nanowire. Among them, conductive PEDOT:PSS (PH1000) is one of the most studied materials as replacement for ITO because it enables cost-effective flexible devices as well as roll-to-roll mass production[67].

Along with the conductive PEDOT:PSS, another kind of materials are being used and tested as an option for ITO-free anodes. Classically, ITO free anodes are categorized into three groups: carbon based, metal based and hybrid structured.

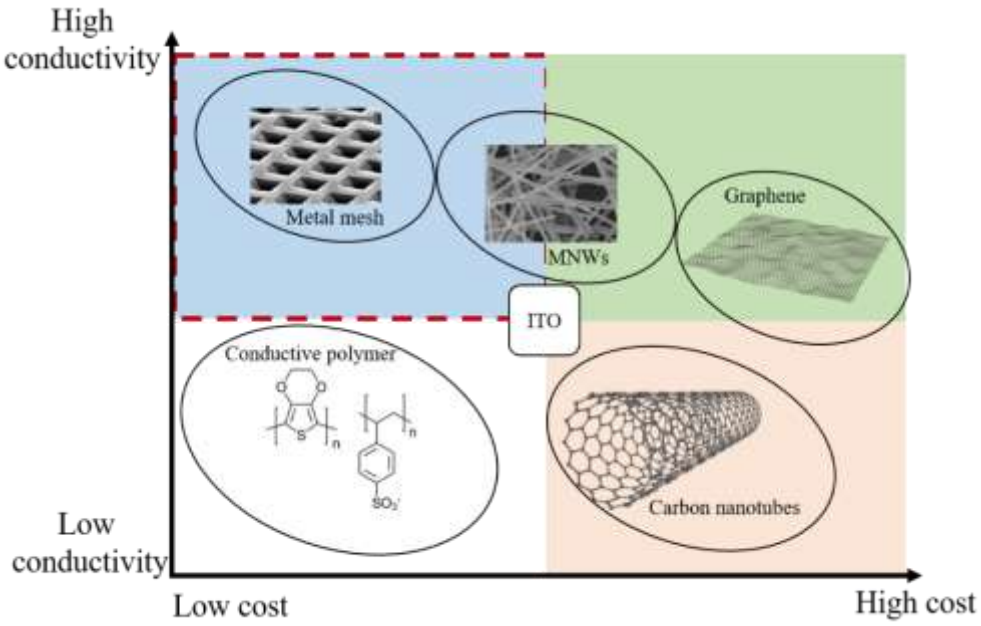

Fig. 22. Comparison of performance-fabrication cost between ITO and ITO free anodes based on metal mesh, metal nanowires (MNWs), conductive polymers, graphene and carbon nanotubes.

Conductive polymers, as PEDOT:PSS, are used in their doped state to take advantage of their conductivities and the flexibility present in their films. From its general chemical structure (Fig. 23), it can be seen that conducting PEDOT can be electrostatically bound to the PSS polyanion[68]. PEDOT itself is an insoluble material but when is synthesized in the presence of PSS becomes a water-soluble dispersion and the most commonly polymer used for this kind of application[69]. PEDOT:PSS typically has a conductivity of 0.1-1 S/cm, but by applying a treatment with certain additives such as dimethyl sulfoxide (DMSO), sorbitol and ethylene glycol (EG) shows a conductivity increase to nearly 1000 S/cm (or improves the sheet resistance from 10^4 to 10^2 Ω/□)[70]. It is worth to mention that there exists different grades of PEDOT:PSS i.e. commercial names. For example, the PEDOT:PSS used as HIL, known as Al 4083, has a PEDOT:PSS ratio of 1:6, a solid content of 1.3-1.7 %. On the other hand there exists PEDOT:PSS for conductive electrodes as PH500, PH510, PH1000, with PEDOT:PSS ratios of 1:2.5, 1:25, 1:2.5 and solid content of 1.0-1.4, 1.5-1.9, 1.0-1.3 % respectively.

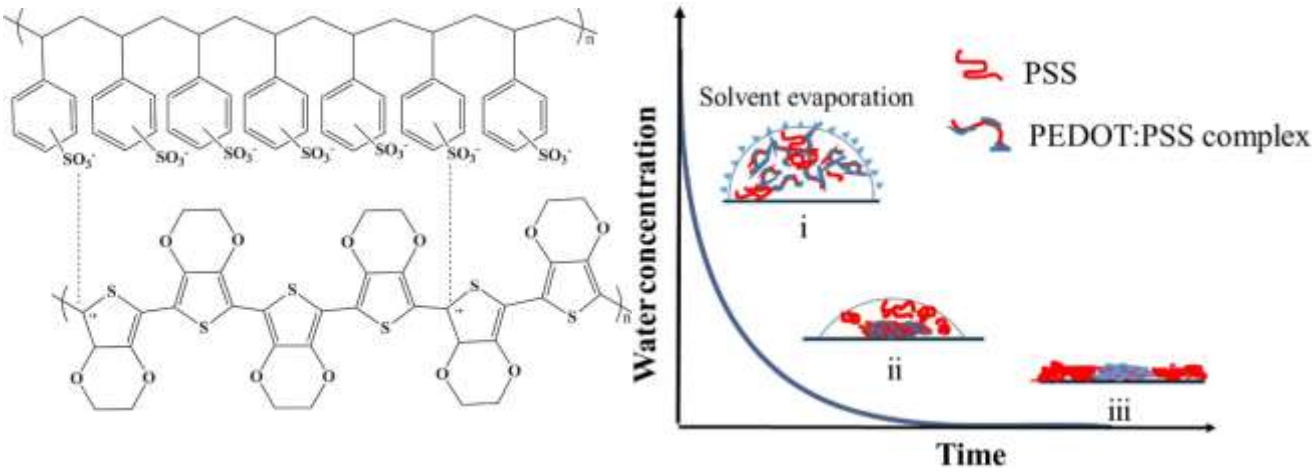

(a) (b)

Fig. 24. (a) Chemical structure of PEDOT:PSS[71] and (b) Phase separation in a slow-drying PEDOT:PSS droplet. i) Droplet of PEDOT:PSS with DMSO is cast on substrate ii) water is evaporating and PSS is dissolved in DMSO iii) Completely dried, PEDOT and PSS occupy different regions on the substrate[70].

The origin of this conductivity enhancement is sometimes under debate, because, it is commonly proposed that the increase in conductivity is associated with the phase separation between the insulating PSS and the conducting PEDOT. Treatment of PEDOT:PSS films with sulfuric acids or co-solvents can remarkably improves the conductivity by separating PEDOT from PSS and inducing morphological changes of films. In the case of treatment with sulfuric acid, the conductivity of PEDOT:PSS is significantly improved but strong-acids may pose safety issues and potential health risk. Then, a treatment free of strong-acid will be always preferable to obtain PEDOT:PSS anodes[72]. For instance, Bjorn *et. al.*[73] fabricated a PEDOT:PSS anode by depositing four layers of PEDOT:PSS using an oxygen plasma treatment and finally applying some post treatment to the film, the resulting anode reach a sheet resistance of 36 Ω/□ and a transmittance of 73 %.

4.2 Carbon based anodes

In this group conducting polymers (as conductive PEDOT:PSS), graphene and carbon nanotubes are included. Graphene is known for its great mechanical strength, very high carrier mobility, excellent optical transparency and very low thickness.

Carbon nanotubes have been used not only as electrode for OLED devices, also as HTL and even have been added to the active layers of organic photovoltaic cells (OPVs) to enhance its efficiency. Carbon nanotubes have good properties as good chemical stability, mechanical flexibility, relatively high conductivity and high transmittance. Furthermore, the fabrication method of carbon nanotubes can be done even by a simple brush-painting method[74].

Graphene first report was by Novoselov *et. al*.[75] in 2004, and since then the research of this material has been intense. Graphene films can be deposited by several methods as mechanical exfoliation, reduction of graphene oxide (rGO), CVD, and more. For instance, Jia et. al.[76] developed an graphene oxide/graphene anode and it was used in highly efficient and flexible OLEDs that reached a current efficiency of 82 cd/A.

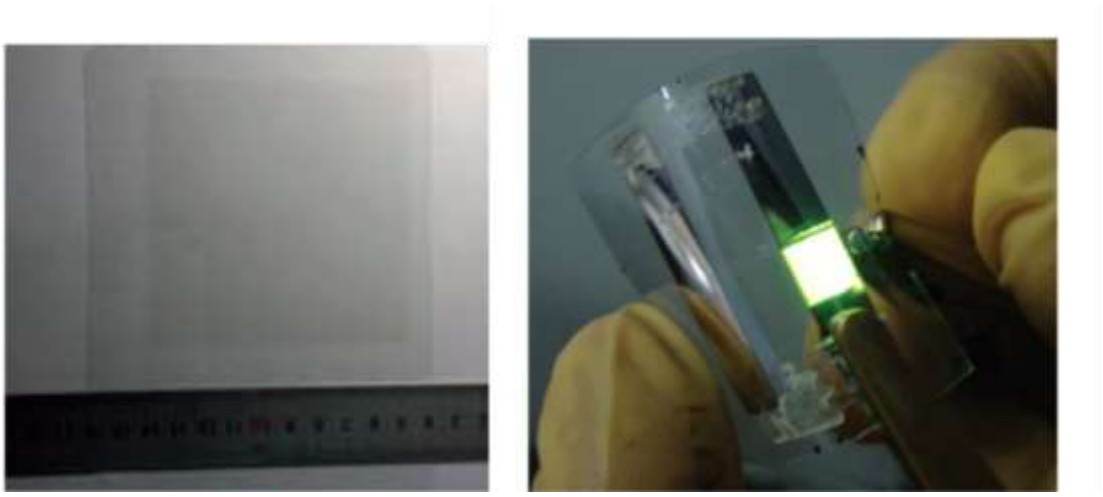

(a) (b)

Fig. 25. (a) Graphene oxide/Graphene anode and (b) flexible OLED by using this anode[76].

Graphene has a wide versatility, even has been used as both anode and cathode in polymer solar cells[77], and can be combined with other materials in order to obtain a better performance (hybrid anodes). For instance, Liu et. al.[78] reported a composite anode based

on conductive PEDOT:PSS and graphene oxide (GO) obtaining a sheet resistance of 73 Ω/□ and a transmittance of 85 % by optimizing the PEDOT:PSS and GO ratio (Fig. 25).

4.3 Metal based anodes

This group is made up for nanostructured films, metal nanowires (MNWs) and metal mesh (also known as metal nanogrids). Metal mesh can be applied with a very interconnected metal network as is shown in the Fig. 26 but also, can be used as a part in a hybrid structure in order to improve its properties. By the variation of line width, depth and spacement, metal mesh can control its properties of transmittance and conductivity.

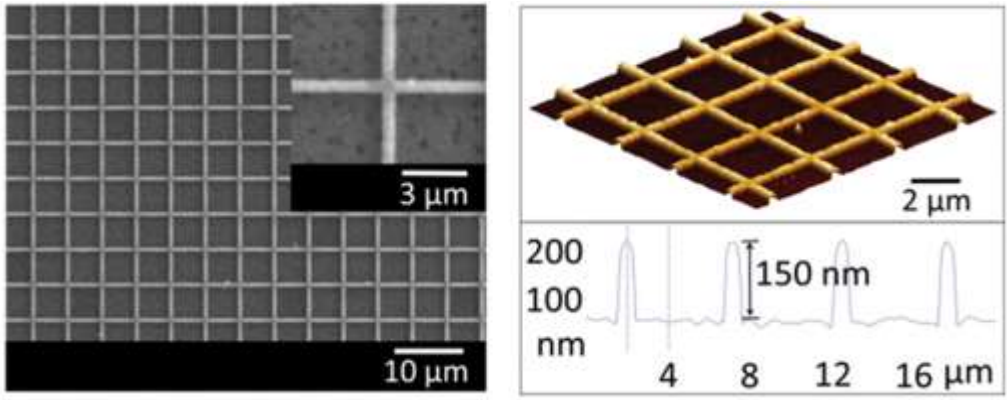

(a) (b)

Fig. 26. (a) SEM and (b) AFM images of metal mesh[79].

In Fig. 27 (a) a 3D-arrayed Ni nanostructure reported by Kim *et. al*.[80] is shown. It was fabricated by lithography in which they also had control of its height.

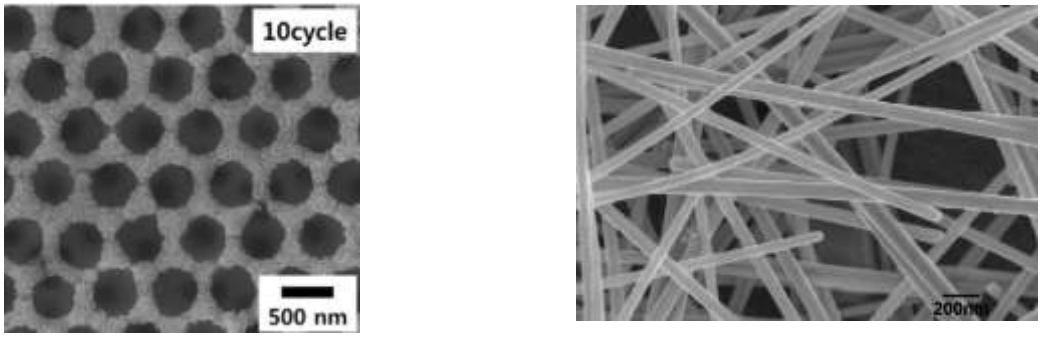

(a) (b)

Fig. 27. SEM images of (a) surface of 3Lyr inverse-opal Ni nanostructure[80] and (b) commercial silver nanowires (AgNWs)[81].

Metal nanowires have excellent properties as good conductivity, high transmittance and mechanical flexibility. Its deposit to form films can be by brush painting, spin coating, drop casting, spray coating, slot die, etc. On the other hand, NWs films in general have issues with its surface roughness, tends to have a rough surface[82]. In Fig. 27 (b) commercial silver nanowires are shown. The NWs presented in the image have a diameter of 70 nm and a length of about 50 μm.

4.4 Hybrid structure anodes

Finally, this group is a combination of conducting polymer, carbon and metal based anodes. Organic semiconductors are inherently complementary to graphene, because these π-conjugated materials can be synthesized with specific properties at the molecular level. However, offer only moderate carrier mobility and are susceptible to degradation. On the other hand, materials as graphene (carbon based) have limited processability, low structural tenability and absence of bandgap. Combining these two materials, conducting polymer and graphene, in a single device the resultant one will generate a bigger effect than the sum of their individual strengths. For example, in this specific case of one conducting polymer with graphene, the chemical similarity (carbon sp^2 networks) and the dimensional redistribution are improved by the presence of both materials in bulk. In the same way, hybrid anodes with even 3 or more different materials have been reported, for instance, Yun et. al.[83] made an anode (applied on OLED devices) based on a multilayer structure AgNWs/IZO/PEDOT:PSS with a sheet resistances even lower than ITO of only 5.9 Ω/□ and a transmittance of 86 %. Conductivity, transmittance and mechanical properties of hybrid anodes can be controlled with the variation of thickness for each layer to modulate different requirements for different applications.

5 EXPERIMENTAL

BT-F3$_2$, **BT-F4$_2$**, **BT-F5$_2$** oligomers and TPBi derivatives (3-COOK and OA67) were synthesized by the group of professor Peter Skabara in the University of Glasgow. Also, the OLED devices in which these compounds were used also were fabricated in Skabara's labs and may present slight experimental variations specified in this section.

5.1 Anode

OLED devices were fabricated on glass substrates coated with indium-tin oxide (ITO). The glass substrates were cleaned with soap, acetone and ethanol in a sonicator, and after a plasma-oxygen treatment was applied for 10 min.

In the specific case of phosphorescent OLEDs and OLEDs based on the 3 new small molecules **BT-F32**, **BT-F42** and **BT-F52**, we used pre-patterned ITO substrates cleaned in an ultrasonic bath 5 min on deionized water, 5 min in ethanol and 5 min in acetone. After the ultrasonic baths, oxygen plasma was applied by 5 min.

5.2 Hole Transport Layer

30-40 nm of Poly(2,3-dihydrothieno-1, 4-dioxin)-poly(styrenesulfonate), known as PEDOT:PSS (CLEVIOS P VP AL 4083), was deposited as hole transport layer by spin-coating. 120 ℃ for 20 min was applied as annealing treatment to remove the residual solvent, which in the case of PEDOT:PSS is water.

On phosphorescent OLED devices and OLEDs based on **BT-F3$_2$**, **BT-F4$_2$** and **BT-F5$_2$**, PEDOT:PSS (Heraeus AL 4083) was spin-coated, followed by an annealing treatment at 120 ℃ for 20 min.

5.3 Emissive Layers (EMLs)

All the EMLs here presented were deposited also by spin-coating technique, inside of a glove box with a controlled nitrogen atmosphere. **CZ-2**, **MOC-1** and **MOC-16** were dissolved in chlorobenzene at a concentration of 36 mg/mL, while **CZ-1**, at the same concentration, in a mixture of chlorobenzene and chloroform (20 wt %) in order to change the polarity of the

used solution, this is because **CZ-1** is not easily dissolved in pure chlorobenzene in comparison to **CZ-2**[45]. These EMLs received thermal annealing at 80 °C for 20 min. A concentration of 6 mg/mL for **PF-2F** on chlorobenzene was used because is easily dissolve it in. After the **PF-2F** deposition, a thermal annealing was applied at 80°C for 30 min to evaporate the residual chlorobenzene of the film.

A concentration of 6.6 mg/mL of **PVK** + 10 % of **Ir(ppy)$_3$** (0.6 mg) in THF was used for phosphorescent EMLs (**PVK:Ir(ppy)$_3$**). After the deposition by spin coating technique, a thermal annealing of 150 °C (30 minutes) was applied.

In the case of OLEDs based on the 3 new oligomers **BT-F3$_2$**, **BT-F4$_2$** and **BT-F5$_2$** the optimum concentration used for the three materials was 20 mg/mL in toluene. Annealing at different temperatures were applied by 20 minutes, being 40 °C the optimum one.

5.4 Electron transport layer

TPBi was used as ETL. Solutions were prepared by using methanol with a concentration of 3-5 mg/mL. This layer was deposited by spin coating technique and the optimum thickness depends directly of each OLED device.

5.5 Electron injection layer

PFN polymer and LiF were used as EIL. PFN was deposited by spin coating technique, with a thickness less than 10 nm. On the other hand, LiF was deposited by vacuum evaporation at a rate of 0.01 nm/s with a final thickness of only 1 nm.

5.6 Cathodes

Aluminum and the bilayer calcium/aluminum were deposited by vacuum evaporation and used as cathodes, the second one was used only for the devices with **BT-F3$_2$**, **BT-F4$_2$** and **BT-F5$_2$** as EMLs. Typically thickness of 100 or 150 nm were used for Al, and 40 nm were deposited for Ca. Rate of 1 A/s was used for deposit. Devices with calcium were always tested inside glovebox to protect them of a fast degradation.

5.7 OLEDs Characterization

Current density versus voltage (J-V) plots and luminance efficiency versus voltage (L-V curves) were measured simultaneously by using a power supply (Keithley 2400, Cleveland, Ohio) with an in-house-designed and calibrated detection system[45]. J-V plots were recorded by direct processing of data acquired from the used Keithley 2400 power supply. Luminous density was estimated through the voltage delivered by a photodiode located at a fixed distance from the OLED (emission area = 0.25 × 0.25 cm^2). Photodiode (GaAsP: G1117) calibration was performed by measuring the luminance of commercial LEDs at different wavelengths and considering the geometrical parameters involved in the detection system. Signal was quantified by a highly sensitive lux meter and correlated with the photodiode voltage response. Data acquisition routines were automated by using LabVIEW software specially designed for this purpose[6]. EL spectra were measured by using an Ocean optics USB2000 + spectrometer. Morphological and film thickness measurements were obtained by atomic force microscopy (AFM) (Nanosurf, easyscan2: Liestal, Switzerland).

In the specific case of phosphorescent OLEDs and OLEDs based on the 3 new oligomers **BT-F3$_2$**, **BT-F4$_2$** and **BT-F5$_2$**, J-V-L curves and lifetimes were measured inside the glovebox with a light-tight box attached. A Keithley Semiconductor Characterization (SCS) 4200 was used to bias the OLEDs. Luminances were obtained by using a Macom L203 photometer with a calibrated silicon photodetector and a photopic filter[48]. For lifetimes, luminance was measured each minute trough an interval of time, applying in all moment a current density of 20 mA/cm^2. EL spectra were measured by using an Ocean optics USB2000 + spectrometer within an integrating sphere.

5.8 Anode based on conductive PEDOT:PSS polymer

For PEDOT:PSS anodes fabrication, specific quantities of the PEDOT:PSS dispersion (Clevios PH1000) were evaporated on a hot plate to have 70 and 80 % volume solutions, with continuous heating (160 °C) and stirring by marking the initial volume in a vial and the specific final value required. After each specific volume (solvent) evaporation, the solution stayed at continuous stirring to assure a correct quality. Oxygen-plasma treatment was applied in glass and plastic substrates (acetate) by 10 min. Then, the dispersion of conductive PEDOT:PSS concentrated at 70 and 80 % were deposited at different rpm. Annealing treatment was applied by 30 min, at 120 °C and 100 °C for rigid and flexible substrates

respectively. After the annealing treatment, DMSO was deposited by drop casting on PEDOT:PSS film, and immediately a temperature of 80 °C was applied for 2 h. In both cases, after the cleaning of glass and acetate, a plasma oxygen treatment was applied for 10 minutes. The thickness and roughness of these anodes were measured by AFM (Nanosurf, easyscan2: Liestal, Switzerland). Sheet resistances were measured by 4 points technique (Keithley 2400) and transmittances were measured on a spectrophotometer.

6 RESULTS

6.1 Efficient small molecule OLEDs based on carbazole and Thienopyrrolediones derivatives

Four previously reported small molecules (Fig. 28)[38] used as EML and the OLED devices were optimized by using a simple architecture (ITO/PEDOT:PSS/small molecule/LiF/Al) and their EQE calculated.

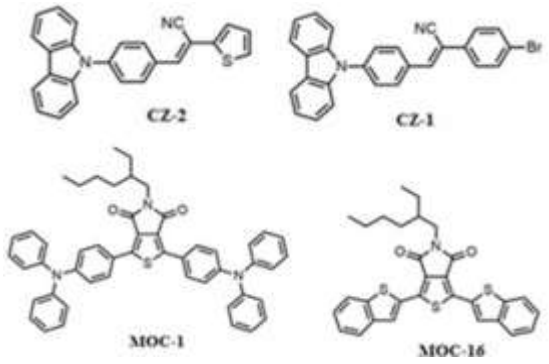

Fig. 28. Molecular structure of the small molecules **CZ-2**, **CZ-1**, **MOC-1** and **MOC-16**.

Two of this small molecules are carbazole derivatives: (E)-3-(4-(9H-carbazol-9-yl)phenyl)-2-(thiophen-2-yl)acrylonitrile (**CZ-2**) and (Z)-3-(4-(9H-carbazol-9-yl)phenyl)-2-(4-bromophenyl)acrylonitrile (**CZ-1**). The other two materials are thienopyrroledine (TPD) derivatives: 1,3-bis(4 (diphenylamino)phenyl-5-(2-ethylhexyl)-4H-thieno[3,4-c]pyrrole-4,6 (5H)-dione (**MOC-1**) and 1,3 bis(benzo[b]thiophen-2-yl)-5-(2-ethylhexyl)-4H-thieno[3,4-c]pyrrole-4,6(5H)-dione (**MOC-16**). Such compounds have good solubility in chlorobenzene, good film formation by solution process, as well as they are of an easy, economical and fast synthesis[45].

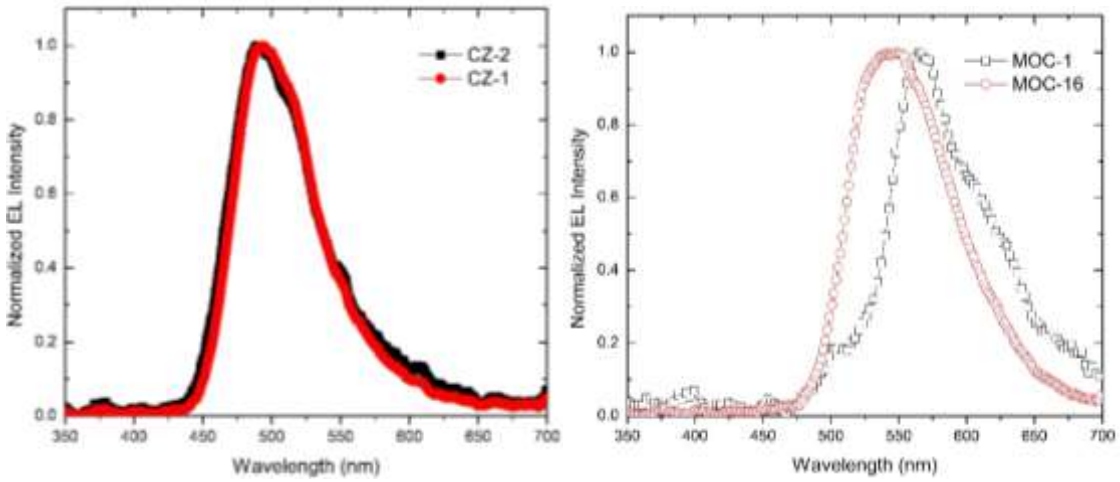

(a) (b)

Fig. 29. Electroluminiscence spectra of OLEDs based on (**a**) carbazole compounds (CZ-1 and CZ-2) and (**b**) TPD derivatives (MOC-1 and MOC-16) as emissive layers.

Electroluminescence peaks for **CZ-1** and **CZ-2** are located at 488 and 492 nm, while for **MOC-1** and **MOC-16** were located at 564 and 567 nm, respectively. **CZ-2** and **CZ-1** OLED based devices, shown in both cases luminances higher than 4000 cd/m^2 and maximum current efficiencies around 20 cd/A. On the other hand, **MOC-1** and **MOC-16** reached a maximum luminance of 651 and 1729 cd/m^2, and a maximum current effiency of 4.5 and 0.6 cd/A respectively. From the J-V-L characteristics and the emission spectrum, EQE efficiencies were estimated. For **CZ-1** and **CZ-2** the estimated EQEs were 8.6 and 9.5 % respectively. On the other hand, **MOC-1** and **MOC-16** shown a low EQEs of 1.5 and 0.1 % respectively (Fig. 30). From the energy levels shown in Fig. 30, it is observed that electrons are injected tunneling because LiF creates a potential barrier between the cathode and the EMLs, leading to an increased population of electrons and then an increased luminous density.

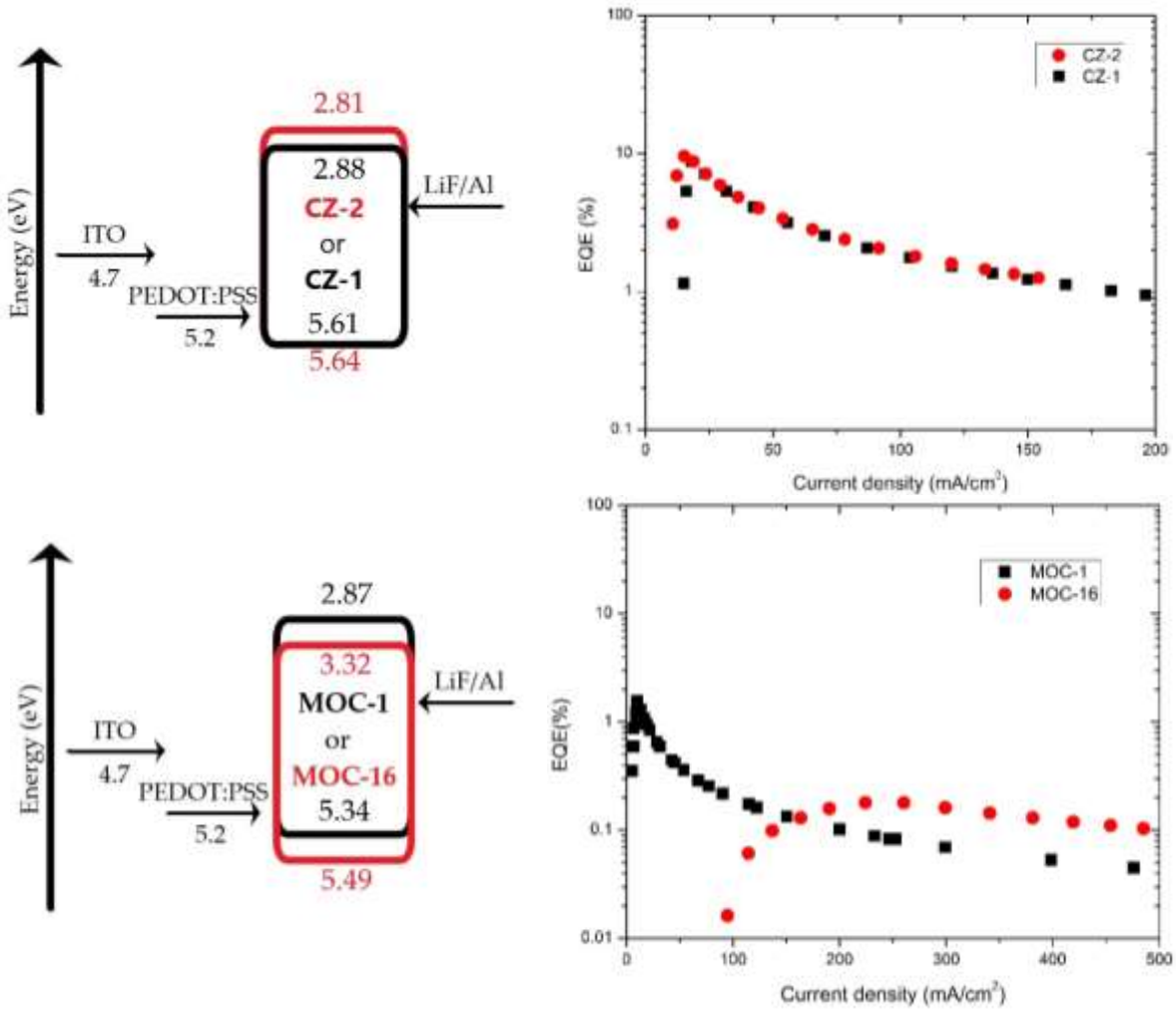

Fig. 30. Schematic energy diagram and external quantum efficiencies (vs current density) for OLEDs based on carbazole derivatives **CZ-1**, **CZ-2** and based on TPD derivatives **MOC-1**, **MOC-16**.

From the analysis of the energy diagram showed in Fig. 30, there exist a better energy level alignment of **CZ-2** and **CZ-1** with the HOMO-LUMO levels of the other compounds than for the case of **MOC-1** and **MOC-16**.

The optimized configuration used for both molecules, **CZ-1** and **CZ-2**, based OLEDs was ITO/PEDOT:PSS(40nm)/CZ-1 or CZ-2(70 nm)/LiF(1 nm)/Al(150 nm) and their principal characteristics are shown in Table 2.

Table 2. Device performance of the four kinds of OLEDs based on carbazole and TPD derivatives as EML. Several other devices from the literature are also mentioned.

EML	$V_{on}(V)$	$L_{max}(\frac{cd}{m^2})$	$V_{L_{max}}(V)$	$\eta_{L_{max}}(\frac{cd}{A})$	$\eta_{max}(\frac{cd}{A})$	$L_{\eta_{max}}(\frac{cd}{m^2})$	EQE_{max} (%)	$\lambda_{EL}(nm)$	Ref.
CZ-2	5.2	4104	7.2	2.6	20.2	3062	9.5	488	**This work**
CZ-1	6.5	4130	8.7	2.1	19.3	3476	8.6	492	"
MOC-1	6.2	651	10.6	0.07	4.5	467	1.5	564	"
MOC-16	7.7	1729	7.9	0.34	0.61	1388	0.1	547	"
CP3[a c]	3	8235	8.8	---	2.53	---	---	474	[84]
CP3*[a c]	2.7	24442	9	---	6.9	---	---	501	[84]
TCBzC[a]	2.5	9226	---	---	31.6	---	---	534	[85]
Blue − 1[b]	3.6	19283	---	---	10.8	---	---	~460	[86]
G3MP(A3)[b]	5.3	9823	---	---	28.2	---	12.8	~480	[87]
G3MP(B3)[b]	4.5	2227	---	---	18.2	---	10.3	~480	[87]
M2[a]	3.4	4543	---	---	1.53	---	3.0	428	[88]
B[a]	3.8	2267	---	---	1.8	---	3.6	436	[88]
Dev.III no.2[a c]	4.6	4390	---	---	1.0	---	0.4	492	[89]
TPE-DFCz[a c]	5.4	3200	---	---	1.16	---	0.4	500	[90]
DCZ-TTR[b]	3.2	~5000	---	---	59.6	---	20.1	512	[91]
CZ-TTR[b c]	3.1	~1000	---	---	32.5	---	14.4	492	[91]

EML=Emissive Layer, a) carbazole emitter (EML),b) carbazole host/guest, c) wavelength similar to our devices, *devices fabricated by evaporation . V_{on}= turn on voltage, L_{max}= maximum luminance, V_{Lmax}= voltage for L_{max}, η_{Lmax}= current efficiency at L_{max}, η_{max}= maximum current efficiency, $L\eta_{max}$= luminance at η_{max}, EQE_{max}= maximum external quantum efficiency, λ_{EL}= peak of electroluminescence.

When comparing results reached for our OLEDs devices based on **CZ-2** and **CZ-1** as EML with those reported in the literature, it can be observed that these measured current efficiencies (around 20 cd/A) as well as their EQE values (8.6 - 9.5 %) are in general larger than those for other OLEDs using also compounds derived from carbazole as emitter material (Table 2). For instance: M2[88], B[86] and CP3[84] (by spin coating as well as by evaporation), have current efficiencies of 1.53 cd/A at 4543 cd/m^2, 1.8 cd/A (and maximum luminance up to 2267 cd/m^2) and 2.53 cd/A (with maximum luminance up to 8235 cd/m^2), respectively. This could be because these OLEDs had larger current densities compared to those for our devices. Also, these previous reported OLEDs showed similar turn on voltages; furthermore, under more robust architectures than those for our devices, larger luminescent values are reached, such is the case of the OLEDs based on Blue-1[86] (host approach) that has two layer buffer and excellent coupling of energy levels, what favors their emission and thus reaching 19 283 cd/m^2. However, the most efficient devices are those based on TCBzC[85] (as EML), DCz-TTR (as host)[91] and CZ-TTR (as host)[91], which presents a

very high current efficiencies (31.6, 59.6 and 32.5 cd/A, respectively), low turn on voltages (2.5, 3.2 and 3.1 V, respectively) very acceptable luminance values (9226, ~5000 and ~1000 cd/m^2, respectively) and high EQE values up to 20.1 % and 14.4 % for DCZ-TTR and CZ-TTR respectively. Recently, carbazole derivatives based OLED devices "Dev. III no. 2"[89] and TPE-DFCz[90] were reported with emission wavelengths (492 and 500 nm, respectively) similar to those for our OLEDs based on **CZ-2** and **CZ-1**. These devices shown maximum luminance within the range 4390-3200 cd/m^2 and current efficiencies of 1 and 1.16 cd/A versus 20.2 and 19.3 cd/A for **CZ-2** and **CZ-1**, respectively. It should be noticed that devices with the highest efficiency are usually those that use carbazole derivatives in their active films under the host/guest approach. For example, OLEDs based on Blue-1[86] and G3MP (A3 and B3 devices)[87] whose luminances are 19 283 cd/m^2 and 9 823 cd/m^2, respectively; with current efficiencies from 10.8 cd/A until 28.2 cd/A, i.e., similar to those values for our OLEDs. Also, devices based on G3MP(A3)[87] and G3MP(B3)[87] as emissive layer, presented similar EQE values (12.8 % and 10.3 %, respectively) to ours (9.5 % and 8.6 %, for **CZ-2** and **CZ-1**), however, we are using a simple EML (deposited by spin coating) not a host/guest type emission layer.

6.1.1 Conclusions

From the chemical structure point of view, for these studied small molecules, some factors that may influence the described behavior (better electroluminescence properties and EQE for **CZ-2** and **CZ-1** compounds than for **MOC-1** and **MOC-16**) could be: electronic dipolar structure for the case of **CZ-2** and **CZ-1** (carbazole derivatives) and quadrupolar for **MOC-1** and **MOC-16.** Furthermore, as the carbazole fragment could impact the molecular packing, thus, enhancing better crystallinity (and probably the charge carrier transport) than with the diphenyl part of the quadrupolar compounds.

In comparison with previous similar OLED devices (either under the EML or the host/guest approach), our results for OLEDs based on carbazole derivatives had very acceptable current efficiencies (19.3 - 20.2 cd/A) and very high and competitive external quantum efficiencies (8.6 - 9.5 %) due to a low generated current density value (<200 mA/cm^2). On the other hand, devices manufactured with TPD derivatives (with quadrupolar structure) showed luminances

up to 1729 cd/m^2 in the case of MOC-16. Nevertheless, current efficiencies are just 4.5 cd/A for the case of MOC-1.

6.2 Efficient OLED devices with polymer PF-2F as EML

Fluorescent OLED devices based on the new polymer (Fig. 31); Poly[(Benzo[*c*][1,2,5]thiadiazole-4,7-diylbis(9,9-dimethyl-9H-fluorene-7,2-diyl))-3,3-diyl(1-(3-(trifluoromethyl)phenyl)-2-oxindole)] (**PF-2F**), were fabricated. **PF-2F** was used as EML in a structurally simple architecture ITO/PEDOT:PSS/polymer/(LiF or PFN)/Al.

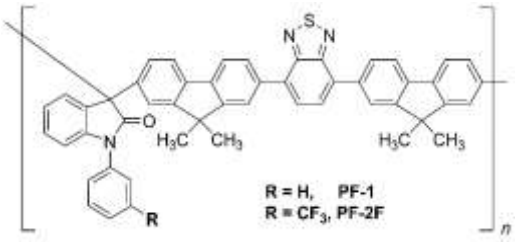

Fig. 31. Molecular structure of the **PF-2F** and PF-1 polymers.

It is worth to mention that this **PF-2F** polymer was chosen among another polymers because their excellent properties as high PLQY, great processability by wet techniques, good EL properties, etc. Other results with molecules synthesized in the research Group of Optical Properties of Materials at the Optical Research Center (GPOM-CIO) group are shown briefly in the Apendix.

PF-2F is a molecular modified version of the previously reported PF-1: Poly[(Benzo[*c*][1,2,5]thiadiazole-4,7-diylbis(9,9-dimethyl-9*H*-fluorene-7,2-diyl(1-phenyl-2-oxindole)], which was applied in OLED and lasing devices[6]. PF-2F has as addition the trifluoromethyl (CF_3) group. This kind of π-conjugated polymers known as fluorinated aromatic have been widely studied because of their excellent properties as improved stability, enhanced intermolecular interactions to improve the supramolecular structure and their performance at high temperatures[92]. Some of the most used are the groups trifluoromethyl ($-CF_3$) (3F) and hexafluoroisopropylidene [$-C(CF_3)_2$] (6F), which besides the mentioned before, leads to improve the resistance to oxidation, glass transition temperature, environmental stability and optical transparency[93]. Also, this groups can reduce crystallinity, dielectric constant and water absorption[94,95]

The inclusion of this CF_3 group for the **PF-2F** polymer lead to an improved electroluminescence and higher EQE in OLED devices because this CF_3 group in the polymer improves mechanical properties, the solubility and the FLQY. **PF-2F** is highly soluble in

organic solvents as chlorobenzene, chloroform, methylene chloride, tetrahydrofuran, etc. The films formed by spin coating technique for this new polymer are transparent, strong and flexible.

As can be seen in the Fig. 32 the maximum absorption wavelength λ_{max}^{abs}, for PF-2F in solid state film, is located at 318 nm with a secondary peak at 400-420 nm. The principal peak located at 318 nm is due to the $\pi \rightarrow \pi^*$ transition of the conjugated system. On the other hand, the shoulder at 400-420 nm is associated with the $\pi \rightarrow \pi^*$ transition of the benzothiadiazole, and the CF_3 group and corresponds to a low-lying energy band which is the probably the mainly excited region in the EL. Then, the fact that the principal peak and the shoulder are generated by different electronic transitions, even when they are emitting at similar wavelengths, implies that they have different decay processes.

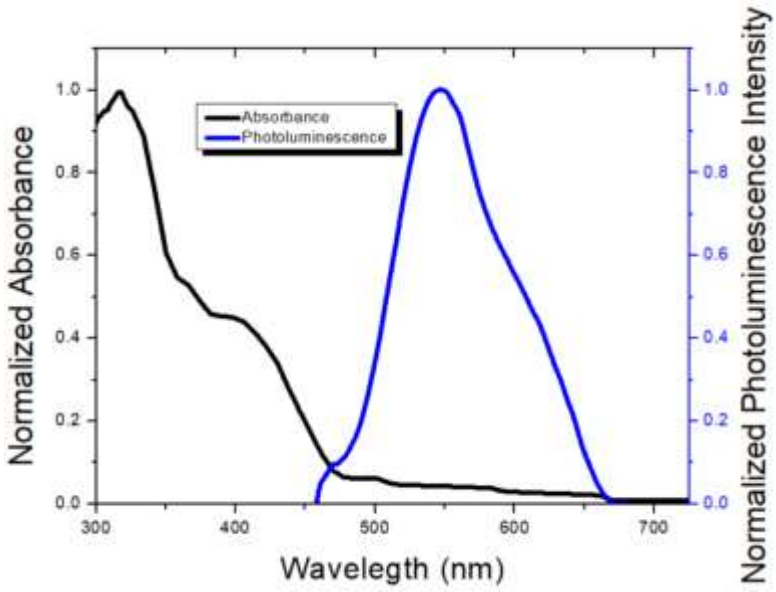

Fig. 32. Absorption and photoluminescence spectra of a solid state film, of **PF-2F** polymer.

Also, in Fig. 32 the photoluminescence spectrum in solid state film is shown, with its maximum peak at 546 nm. It is worth to mention, that the **PF-2F** polymer in solid state film has an excellent fluorescence quantum yield (FLQY) of almost 1 (0.9)[39].

The photoluminescence spectra for PF-1 and **PF-2F** polymers in solid state film (both made and measured at the same experimental conditions) are shown in Fig. 33. The excitation source was at 365 nm(UV lamp), and at 533 nm the maximum peak of photoluminescence

for both, PF-1 and **PF-2F**. The spectra for both polymers is basically the same, then, the inclusion of the CF_3 group does not influence the photoluminescence property.

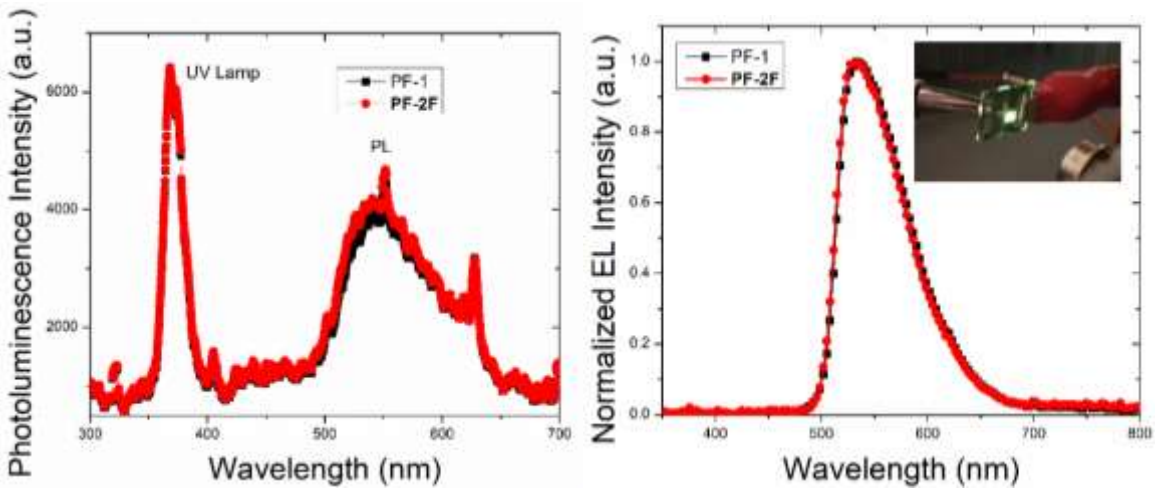

Fig. 33. (a) Relative comparison of photoluminescence spectra for PF-1 and PF-2F films being excited by an UV lamp (peak around 365 nm) and (b) electroluminescence spectra emission with photograph (under room light on) of one OLED based on PF-2F and other based on PF-1.

In Table 3 the principal electrochemical, thermal and photophysical properties are shown. The HOMO/LUMO levels, obtained from cyclic voltammetry(CV), were -5.8 and -4.0 eV respectively, which gives a band gap of 1.8 eV.

Table 3. Electrochemical, Thermal and Photophysical data for **PF-2F** and PF-1 polymers and OLEDs based.

	E_{HOMO}/E_{LUMO}[a] (eV)	Band gap[a] (eV)	T_d[b,c] (°C)	Abs. λ_{max}[d] (nm)	PL λ_{em}[d] (nm)	EL λ_{em} (nm)	Φ[d] (%)
PF-2F	-5.8/-4.0	1.8	502, 485	318	546	533	91
PF-1	-5.7/-4.0	1.7	--	323	544	551	91

The influence of their energy levels were of great importance, because the cathode LiF/Al was choose because its work function is too close of the LUMO level of the **PF-2F**, with a difference of just 0.2 eV. The difference of only 0.2 eV between the work function of the cathode and the LUMO level of the EML is of big importance because the injection of electrons to the EML is efficient and that benefits the performance of the device.

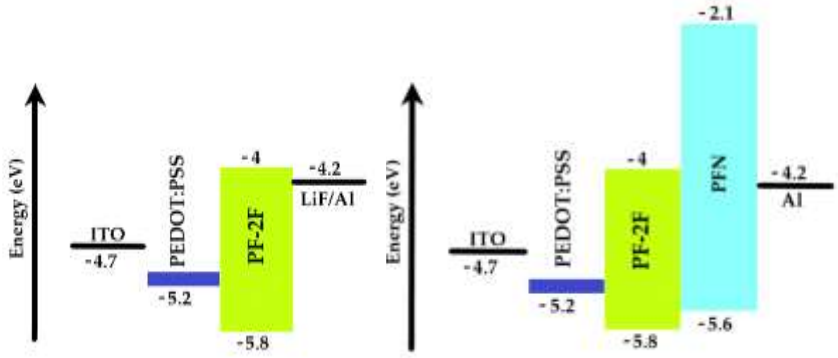

Fig. 34. Schematic energy diagram of the HOMO and LUMO levels for OLEDs based on PF-2F by using (a) LiF and (b) the polymer PFN as EIL.

For these devices, two kind of electron injection layers were used: LiF and PFN. For the first kind, with architecture ITO/PEDOT:PSS/**PF-2F**/LiF/Al the current-luminance-voltage (J-L-V) curves are shown in Fig. 35 (a) while current efficiencies are shown in Fig. 35 (b). The devices with EML thickness of 60-70 nm present a turn on voltage of 3.6 V, a maximum luminance of 1924 cd/m^2 at a current efficiency of 2 cd/A (@6 V). The maximum current efficiency for this device is 14.8 cd/A (@4V) at 1688 cd/m^2. When the thickness of the EML was increased to 80-90 nm, the devices shown a turn on voltage of 3.8 V, this is slightly higher than the previous one, a maximum luminance of 1881 cd/m^2 at a current efficiency of 6.6 cd/A (@6 V) and a maximum current efficiency of 35.3 cd/A (@6 V) at 1638 cd/m^2. The current efficiency is significantly higher (i.e. the current density is lower) in these latter devices due to an equilibrated injection/recombination of electrons and holes with reached through EML thickness optimization[96].

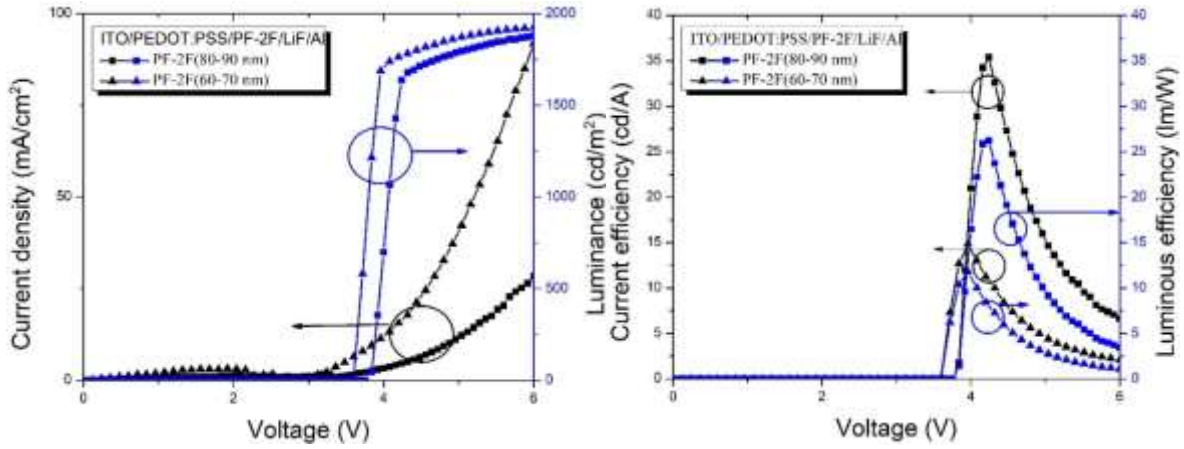

(a) (b)

Fig. 35. (a) J-V plots, luminances, (b) current and luminous efficiency of OLEDs based on **PF-2F** polymer with the simple architecture ITO/PEDOT:PSS/**PF-2F**/LiF/Al.

In Fig. 36 J-L-V curves and current efficiencies for devices with architecture ITO/PEDOT:PSS/**PF-2F**/PFN/Al are shown. Devices with an EML thickness of 60-70 nm present a turn on voltage of 3.8 V and a maximum luminance of 2842 cd/m^2 at a current efficiency of 0.7 cd/A (@5.8 V), with a maximum current efficiency of 10.1 cd/A at 2038 cd/m^2. Also, OLED devices with a thickness of 80-90 nm for the EML had a turn on voltage of 4 V, a maximum luminance of 2451 cd/m^2 at 4.4 cd/A (@5.9 V) and a maximum current efficiency of 17.9 cd/A at 1706 cd/m^2 (@4.7 V).

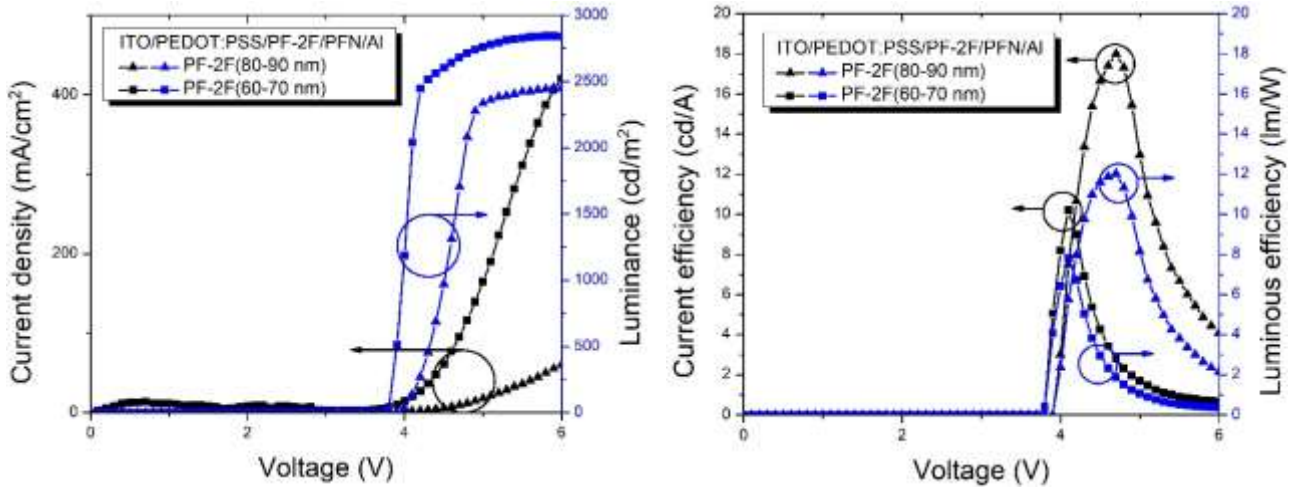

(a) (b)

Fig. 36. (a) J-V curves, luminances, (b) current efficiency and luminous efficiency of OLEDs based on **PF-2F** polymer with the simple architecture ITO/PEDOT:PSS/**PF-2F**/PFN/Al.

In the Fig. 37, external quantum efficiency for the best OLED devices is shown. The devices that used a thickness of 80-90 nm in the EML had the better performance. The one that used LiF as ETL reached an EQE_{max} of 2.6 % and in the other hand, the one with PFN as ETL was just 1.3 %. This remarkable difference between these devices may be a consequence, in addition to the difference of energy levels, of the rinse effect[97], this is when the layer is very sensitive to specific solvents, in this case the EML is too sensitive to solvents where PFN polymer is solubilized (methanol + acetic acid).

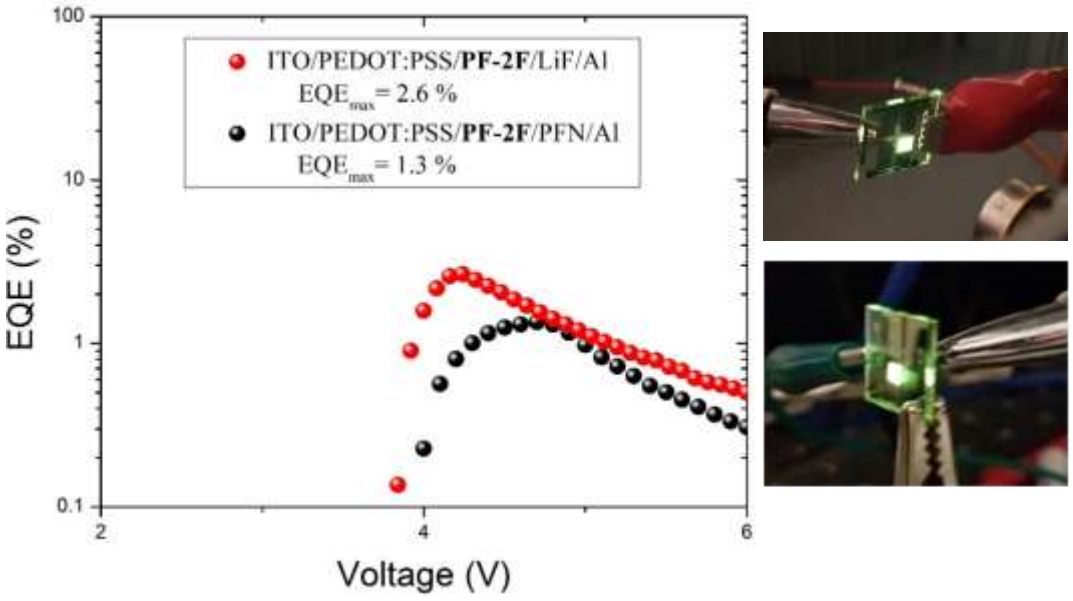

Fig. 37. (a) EQE and (b) photographs of OLEDs based on PF-2F polymer, under room light conditions, using LiF (upper photograph) and PFN (lower photograph).

In Fig. 38 the topography of the interface between the EML and the PFN changed after the deposition of the second one, this is the rinse effect. This change in the morphology (roughness changed from 1-2 nm to 6 nm) can alter the injection/recombination balance of electrons and holes. Anyway, the performance of the devices that used PFN might be

improved by changing the concentration of the PFN polymer solution reducing the amount by volume of methanol or using a water/alcohol solution for PFN[97].

As can be observed in Fig. 38, after the methanol + acetic acid solution was deposited on **PF-2F** film, bigger grains are observed and the film has a lack of planarity because the mentioned rinse effect. The film of **PF-2F** has some grade of solubility in methanol, which induce this kind of changes in the film that can directly influence the overall performance of these OLED devices.

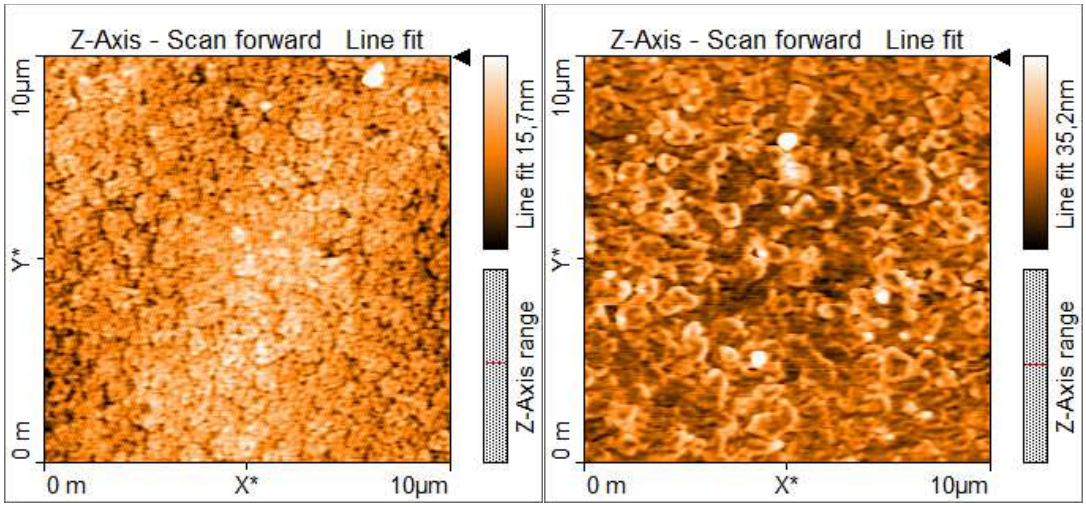

Fig. 38. AFM images of deposited layers by spin coating of (a) **PF-2F** film (EML) with a roughness of 1-2 nm and (b) **PF-2F**/PFN bilayer (PFN was dissolved in a mixture of methanol + acetic acid); film roughness increased up to 6 nm.

In the Table 4 our OLED devices with better performance, by using PF-2F, are compared with other OLEDs with layers based on non-doped emitters. Polymers P1 and P2, reported by Santos *et. al.* [98], shown turn on voltages of 3.7 and 4.2 V, respectively. Even when P1 and P2 had luminances of only 167 and 274 cd/m^2, both of them had an excellent EQE_{max} of 3.3 and 3.9 %, respectively, by using a multilayer architecture ITO/PEDOT:PSS/(P1 or P2)/TPBi/LiF/Al. Also, the well-known Alq_3 is reported, in a multilayer architecture ITO/PTC-U-1hr/NPB/Alq_3/LiF/Al, with an EQE_{max} of 2.6 % and a turn on voltage of 3.6 V, quite similar to our OLEDs with the LiF/Al cathode (EQE_{max} of 2.6 % and turn on voltage of 3.8 V). Also, a series of fluorescent materials reported in 2014[99] showed a turn on voltage of 3.4 V, luminances of 2500 cd/m^2 and an EQE_{max} of 3.2 %, by using a multilayer

architecture ITO/PEDOT:PSS/P5/TPBi/LiF/Al. A turn on voltage of 2.6 V, an EQE_{max} of 3.1 % and a maximum current efficiency of 10.3 cd/A were reported in 2016[100] for OLED devices based on F8BT as EML, with LiF as EIL in a multilayer architecture (ITO/PEDOT:PSS/TFB/F8BT/LiF/Al), and when they used PEI instead of LiF devices reached a turn on voltage of 2.5 V, an EQE_{max} of 3.7 % and a maximum current efficiency of 12.1 cd/A. Also, the well known and reported commercial copolymer "Super Yellow" was used by Yu *et. al.*[101] in almost the same configuration of our PF-2F based devices: ITO/PEDOT:PSS:GO/Super Yellow/LiF/Al (GO = graphene oxide). They reached an excellent EQE_{max} of 3.5 % and a big luminance of 77100 cd/m^2.

Table 4. Performance of OLED devices based on PF-2F polymer as EML, with LiF or PFN as EIL. Several other device performances form literature are also included.

EML	**V_{on} (V)**	**L_{max} (cd/m^2)**	**V_{Lmax} (V)**	**η_{max} (cd/A)**	**EQE_{max} (%)**	**Reference**
PF-2F[a]	3.8	1937	7.8	35.3	2.6	This work
PF-2F[b]	4.0	2452	6.1	17.9	1.3	This work
PF-1[b,d]	4.5	878	--	40.0	2.1	[6]
P1[c]	3.7	167	--	--	3.3	[98]
P2[c]	4.2	274	--	--	3.9	[98]
Alq_3[c]	3.6	--	--	8.9	2.6	[102]
2-DIPO[a,c]	1.5	2636	7.5	1.5	--	[103]
3-DIPO[a,c]	2.5	2228	8.0	0.2	--	[103]
P5[c]	3.4	2500	--	4.4	3.2	[99]
F8BT[a,c]	2.6	--	--	10.3	3.1	[100]
F8BT[c]	2.5	--	--	12.1	3.7	[100]
BP[a,d]	4.5	7544	--	4.2	--	[104]

Compound 4[c]	5.2	849	--	0.08	--	[105]
Device B[b]	3.5	5500	8.7	4.0	--	[106]
Super Yellow[c]	2.0	77100	11.0	10.0	3.5	[101]

EML= Emissive Layer, (a) LiF/Al cathode, (b) PFN/Al cathode, (c) multilayered device, (d) similar architecture than in this work. V_{on}= turn on voltage, L_{max}= maximum luminance, V_{Lmax}= voltage for L_{max}, η_{max}= maximum current efficiency, EQE_{max}= maximum external quantum efficiency.

The last year, 2019, Kaafarani *et. al.*[105] reported OLED devices with an architecture ITO/PEDOT:PSS/Compound 4/Ca/Al with a maximum luminance of 849 cd/m^2 and a maximum current efficiency of 0.08 cd/A. Finally, comparing the devices based on **PF-2F** polymer and the "original" PF-1[6], its maximum current efficiencies are too similar (35.3 an 40 cd/A respectively) but the luminances of the new polymer are higher (2452 and 878 cd/m^2 respectively). Also, a significant improvement on its EQE_{max} from 2.1 % for PF-1 to 2.5 % for **PF-2F** is reached. These improvements could be consequence of the CF_3 group inclusion in the **PF-2F** polymer. This CF_3 group is in the "meta-" position and is an electro-attractor which induce a modified electron density throughout the molecule due to the electronegativity characteristic of the group (F is the most electronegative element). Because of this, it was possible to see a little change from the characterization, the HOMO value was 5.7 eV for PF-1 and 5.8 for **PF-2F** (the LUMO levels have the same value, 4.0 eV). Also, the presence of 3 fluorine atoms, benefits the interaction with the solvent i.e. improves the solubility. So, the deposition of **PF-2F** by spin coating or any other wet method may result in a better packaging of the EML due to this improved processability[107].

6.2.1 Conclusions

OLEDs devices based on the new **PF-2F** polymer showed an acceptable external quantum efficiency (for fluorescent materials) up to 2.6 % and an excellent current efficiency of 35.3 cd/A, even under the simple used architecture: Anode/HIL/EML/EIL/Cathode, which represents an important improvement when is compared with the 2.1 % efficiency reached

with PF-1. By the simple inclusion of the trifluoromethyl group into **PF-2F** polymer, it led to improved processability and an enhancement in the electro-luminescence of the OLED devices, which is a positive influence on the overall device performance. With this **PF-2F** polymer, the solid state thin films with a very good quality (film roughness of only 1-2 nm) were achieved through spin coating and OLEDs luminance value was enhanced. Also, due to its LUMO level, which is at only 0.2 eV from LiF/Al work function level, the efficiency of these simple devices is high.

6.3 Highly luminescent OLED devices based on 3 novel fluorescent oligomers

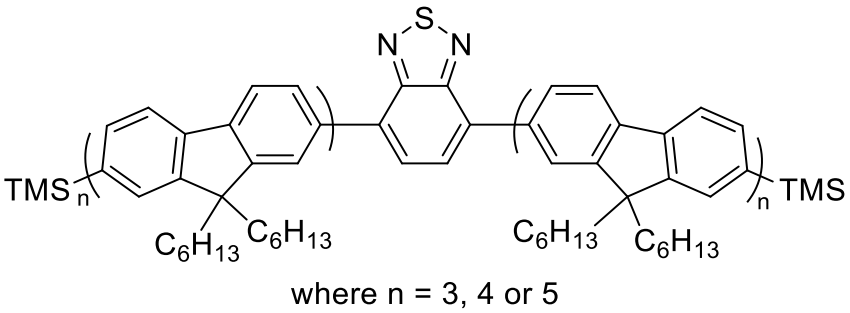

Fig. 39. The structures of **BT-F32**, **BT-F42** and **BT-F52**.

Three new oligomer compounds were used as emissive layer in OLED devices, deposited by spin coating technique. The three materials **BT-F32**, **BT-F42** and **BT-F52** contains a benzothiadiazole core, capped with bifluorene arms attached at the 4- and 7- positions. From the results, it can be seen the number of arms attached (i.e. the length of the molecule) had influence in the luminance, efficiency and lifetime of the OLED devices**.**

Absorbance for the new three compounds is shown in the Fig. 40, with a difference of only 5 nm for the maximum peak of absorption for each material: 360nm, 365nm and 370nm for **BT-F3$_2$**, **BT-F4$_2$** y **BT-F5$_2$** respectively. The three compounds had a good solubility in Toluene, with which was worked to deposit the materials as emissive layers (EMLs) by spin coating technique. Also, the three material present an excellent PLQY of 1 in solid state (also deposited by spin coating).

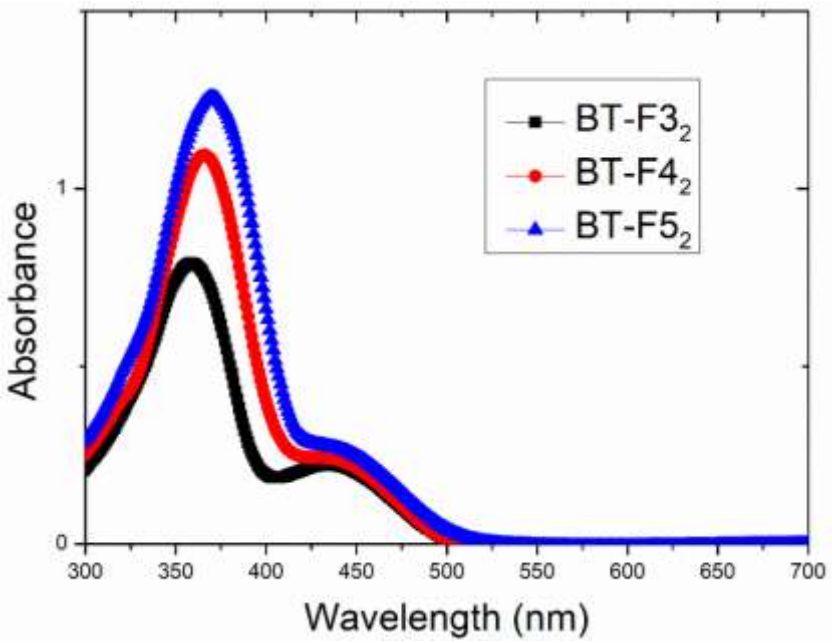

Fig. 40. Absorbance for **BT-F3$_2$**, **BT-F4$_2$** and **BT-F5$_2$** molecules in solid state film.

OLED devices with an architecture ITO/PEDOT:PSS/Molecule/TPBi/Ca (or LiF)/Al were fabricated and optimized to examine the performance of **BT-F3$_2$**, **BT-F4$_2$** and **BT-F5$_2$** molecules. The maximum peak of electroluminescence is basically the same, 543 nm for **BT-F3$_2$** and 541 nm for **BT-F4$_2$** and **BT-F5$_2$** (Fig. 41). Also, the chromaticity coordinates (x,y) in the Commission Internationale d'Eclairage (CIE) 1931 colour space chromaticity diagram were calculated as (0.39,0.60) for the three compounds. This is, because the design of these new materials is based on add additional charge transport units to improve the charge transport characteristics not to change electroluminescent properties[108].

The first architecture used, was ITO/PEDOT:PSS/EML/Ca/Al, this because the LUMO and HOMO levels of the 3 compounds are in 2.8-3.0 and 5.4-5.6 eV approximately. The Ca/Al has a work function of 2.9 eV, a difference of only 0-0.1 eV with the EML. Then, the electron injection from Ca/Al to each compound is efficient. The annealing temperature for the three materials as EMLs was optimized to improve the performance. Devices without annealing treatment and with 40, 60 and 80 °C were fabricated and characterized. In all the cases, annealing treatment at 40 °C shows the better performance.

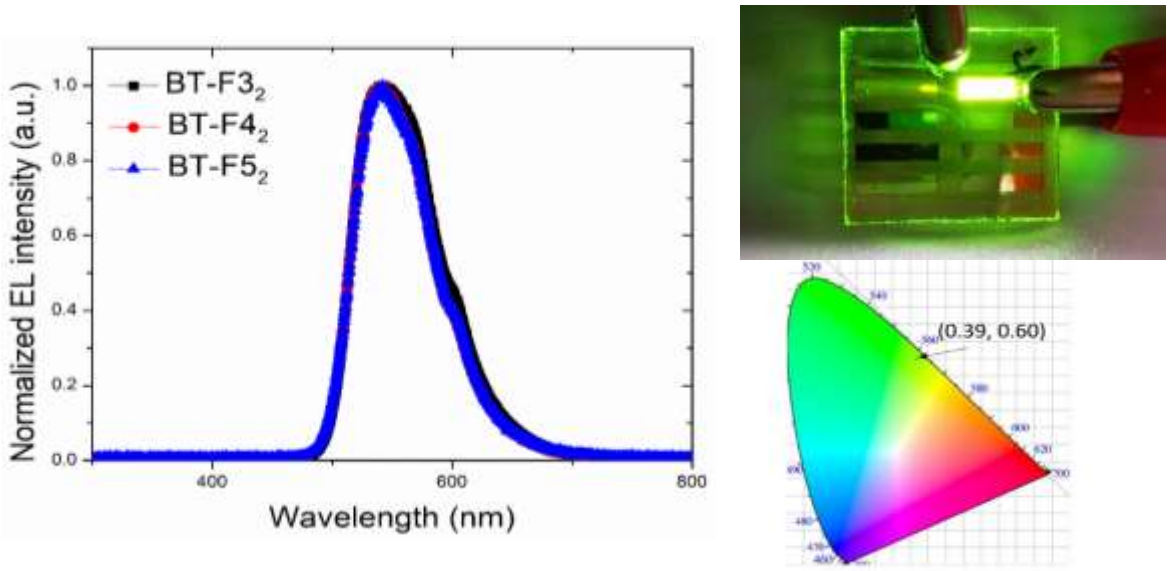

Fig. 41. Electroluminescence (EL) spectra of **BT-F3$_2$**, **BT-F4$_2$** and **BT-F5$_2$**, photograph of one OLED device based on **BT-F4$_2$** and the chromaticity coordinates (0.39,0.60).

From the luminance and current efficiency curves for **BT-F3$_2$** devices unannealed and annealed at 40, 60 and 80 °C, it can be seen that by using 80 °C the turn on voltage was increased (from 3.4 to 4 V), the luminance and the current efficiency are remarkable lower than the other 3 cases (L_{max}= 8 156 cd/m^2 and η_{max}= 1.25 cd/A). Since the best efficiency was

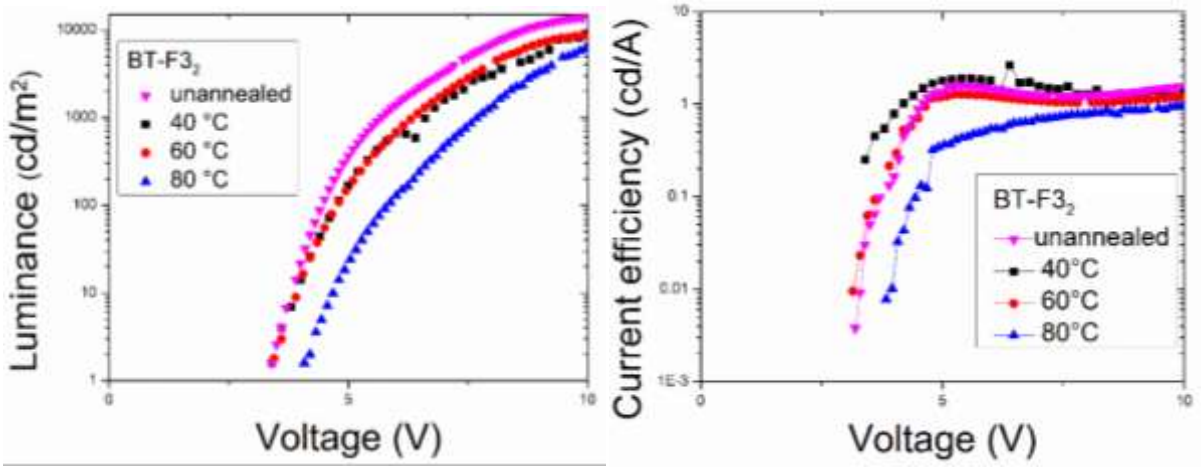

Fig. 42. Luminance and current efficiency of unannealed and annealed OLEDs with architectures of ITO/PEDOT:PSS/**BT-F3$_2$**/Ca/Al.

obtained after annealing the EML at 40 °C, and compared with the device performance

unannealed, this heat treatment may have created a more favourable morphology that benefits the device performance. The devices unannealed and annealed at 40 and 60 °C shown similar values of luminance (higher than 10 000 cd/m^2) and the same turn on voltage. But, devices annealed at 40 °C reached the better and more stable current efficiency (2.6 cd/A).

For annealed devices at 60 and 80 °C based on **BT-F4$_2$**, an increase in the turn on voltage occurred (3.6 and 3.7 V against 3.3 for unannealed and 40°C devices), also the current efficiency (1.7 and 1.5 cd/A respectively) and the luminance (maximum values of 9357 and 3934 cd/m^2 respectively) were lower. The better devices were those unannealed and annealed at 40 °C, with a better luminance (7843 and 8511 cd/m^2) and current efficiency (2.1 in both cases) for the last one.

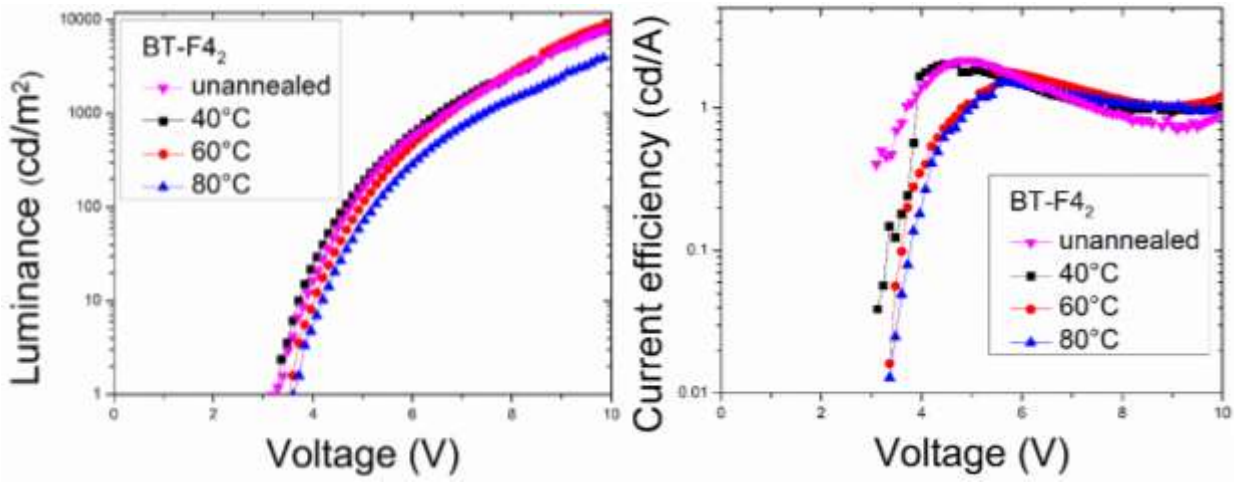

Fig. 43. Luminance and current efficiencies of unannealed and annealed OLEDs with architectures of ITO/PEDOT:PSS/ **BT-F4$_2$**/Ca/Al.

Finally, in the case of the unannealed and annealed devices based on **BT-F5$_2$**, again the devices with 60 and 80 °C presented a lower performance: lower luminances (2116 and 1672 cd/m^2), higher turn on voltage (3.3 and 4.3 V against 3.1 V) and lower current efficiencies. The devices annealed at 40 °C presented better luminances (4918 vs 3287 cd/m^2) and basically the same current efficiency (2.4 cd/A) that the devices unannealed.

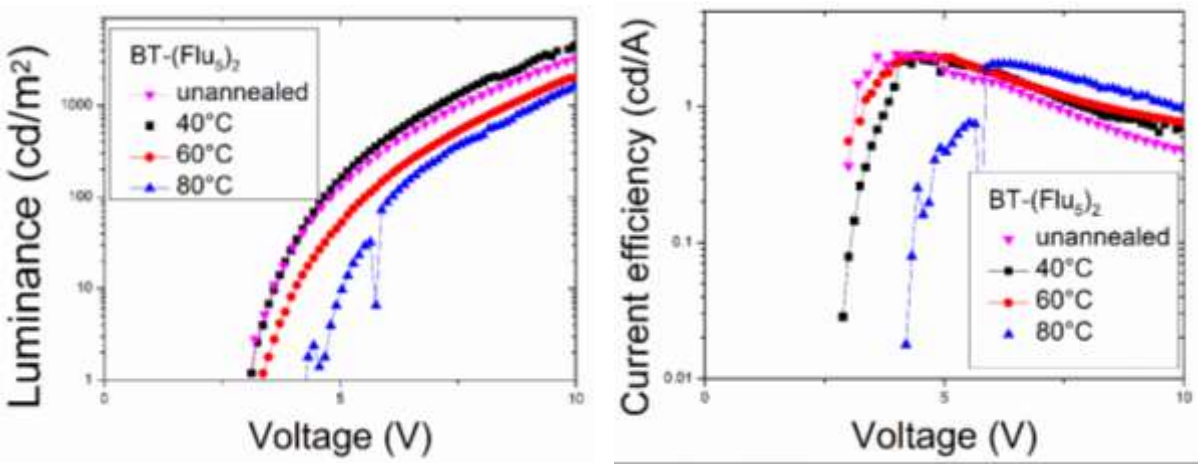

Fig. 44. Luminance and current efficiencies of unannealed and annealed OLEDs with architectures of ITO/PEDOT:PSS/ **BT-F5$_2$**/Ca/Al.

We used the LiF/Al (workfunction~ 4.1 eV) cathode, to see the performance due to the energy difference with the work function and the devices reached luminances lower than 1000 cd/m^2.

The performance of the devices was enhanced, adding an electron transport layer (ETL). TPBi was used as ETL and deposited by spin coating technique, optmizing the thickness for each material and using an architecture multilayer: ITO/PEDOT:PSS/EML/TPBi/Ca/Al. Also, LiF/Al cathode was used in this case, because now we have an specific layer for the transport of electrons. In both kind of devices their luminances, current efficiencies and also the external quantum efficiency (EQE) were improved. In the Table 5 are shown the best OLED devices for both cathodes, LiF/Al and Ca/Al.

Table 5. Performance of the best OLED devices by using the new molecules BT-F3$_2$, BT-F4$_2$ and BT-F5$_2$ as EML, commercial TPBi as ETL, Ca/Al and LiF/Al as cathodes.

Molecule (EML)	**ETL/cathode interface**	V_{on} (V)	L_{max} (cd/m^2)	$\eta_{L_{max}}$ (cd/A)	η_{max} (cd/A)	$L_{\eta_{max}}$ (cd/m^2)	**EQE$_{max}$ (%)**
BT-F3$_3$	TPBi(50 nm)/Ca(40nm)/Al(100nm)	2.8	27266	2.6	4.9	364	1.3
	TPBi(55nm)/LiF(1nm)/Al(100nm)	3.1	29499	3.8	7.1	190	1.9

	TPBi(55nm)/Ca(40nm)/Al(100nm)	3	26701	2.3	4.4	912	1.1
BT-F4$_2$							
	TPBi(55nm)/LiF(1nm)/Al(100nm)	3.1	27274	3.4	8.3	265	2.2
	TPBi(55nm)/Ca(40nm)/Al(100nm)	3	20756	2	6.2	488	1.6
BT-F5$_2$							
	TPBi(55nm)/LiF(1nm)/Al(100nm)	3	20496	2.7	7.4	364	2.0

V_{on}= turn on voltage, L_{max}= maximum luminance, η_{Lmax}= current efficiency at maximum luminance, η_{max}= maximum current efficiency, $L_{\eta max}$= Luminance at maximum current efficiency.

The devices with the interface TPBi/LiF/Al had a better performance than the devices with the TPBi/Ca/Al interface. For **BT-F3$_2$**, the use of LiF instead Ca, increase the luminance from 27266 cd/m^2 to 29499 cd/m^2, current efficiency from 4.9 cd/A to 7.1 cd/A and EQE_{max} from 1.3 % to 1.9 %. Also, the on voltage was improved from 3.1 V to 2.8 V.

For **BT-F4$_2$**, a really good improvement of the EQE_{max} can be seen when LiF is used instead Ca, increasing the double, from 1.1 % to 2.2 %. Also, a decent improvement of the luminance (26701 cd/m^2 to 27274 cd/m^2) and very good increment of the current efficiency (4.4 cd/A to 8.3 cd/A) occurred because the enhanced current density.

Finally for **BT-F5$_2$** the luminance remains similar (20756 cd/m^2 to 20496 cd/m^2), but the current efficiency (6.2 cd/A to 7.4 cd/A) and the EQE_{max} (1.6 % to 2 %) increase. The curves of luminances and current efficiencies for the best OLED device of each molecule are shown in the Fig. 45. In all cases the efficiency of the devices was improved when LiF/Al cathode was used.

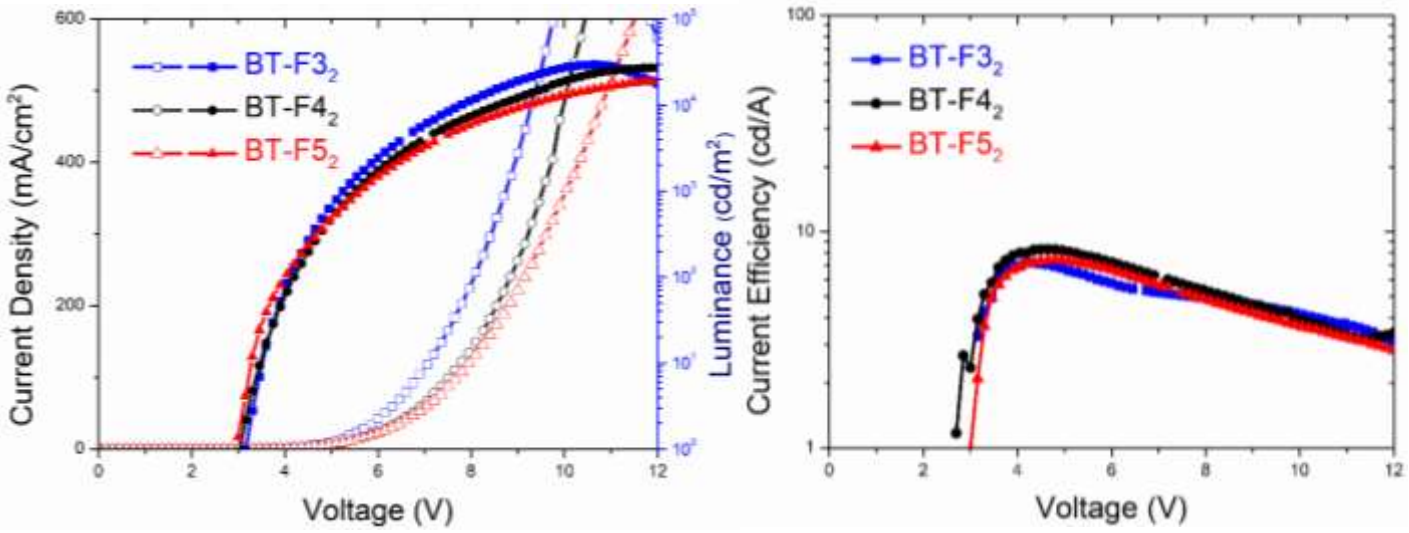

Fig. 45. a) J-V-L curves, b) current efficiency for the OLED devices with architecture ITO/PEDOT:PSS/Molecule/TPBi/LiF/Al for **BT-F3$_2$**, **BT-F4$_2$** and **BT-F5$_2$**.

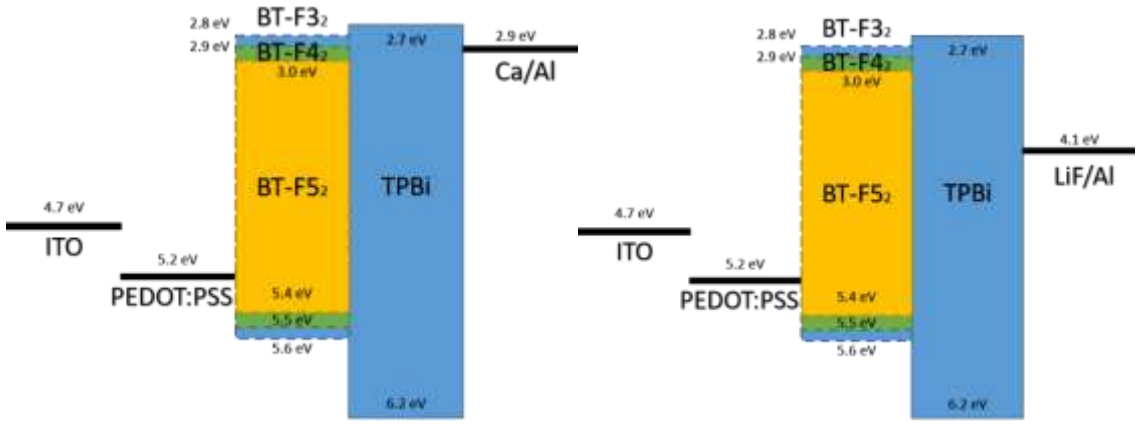

(a) (b)

Fig. 46. Schematic energy levels diagram of **BT-F3$_2$**, **BT-F4$_2$** and **BT-F5$_2$** device architectures, using (a) Ca/Al and (b) LiF/Al cathodes.

Also, lifetime of the devices was measured and calculated by using the stretched exponential decay (SED) model which describe the decay of the luminous flux over the lifetime[64,109]. LT50 (half-life) was calculated fitting the data obtained by applying a constant current of 20 mA/cm^2 and measuring the luminance each minute for a few hours. Devices with Ca/Al cathode shown a significant stability of its luminance compared with those that used LiF/Al.

In all cases the same parameter τ was used (120 000 s^{-1}) and the parameter β for OLEDs based on **BT-F3$_2$**, **BT-F4$_2$** and **BT-F5$_2$** were 0.37682, 0.33769 and 0.26058 respectively.

For the devices with Ca/Al cathode, it was found that the luminance of the devices decay 50% (LT50) after 29398 min (490 h) for **BT-F5$_2$**, 40533 min (675 h) for **BT-F4$_2$** and 45368 min (756 h) for **BT-F3$_2$**. The initial luminance L_0 (@ 20 mA/cm^2) values for the three devices were 982, 869 and 913 cd/m^2 for **BT-F3$_2$**, **BT-F4$_2$** and **BT-F5$_2$** respectively. As we have the same interfaces (ITO/PEDOT:PSS and TPBi/Ca/Al) in the three devices, it can be seen from the LT50 that the length of the molecule has a remarkable influence in the lifetime of the devices, at a major length a lower lifetime is reached. LT50 for **BT-F3$_2$** was 12 % higher than **BT-F4$_2$** and 54 % higher than **BT-F5$_2$**. This could be because at a bigger length of the molecule, exist a higher probability that their energy is spent by de-excitation through vibrational relaxation [110] and then the polymer is heated. This temperature could be inducing a faster degradation of the material that could be one reason that explains why the lifetime is lower for the largest molecule.

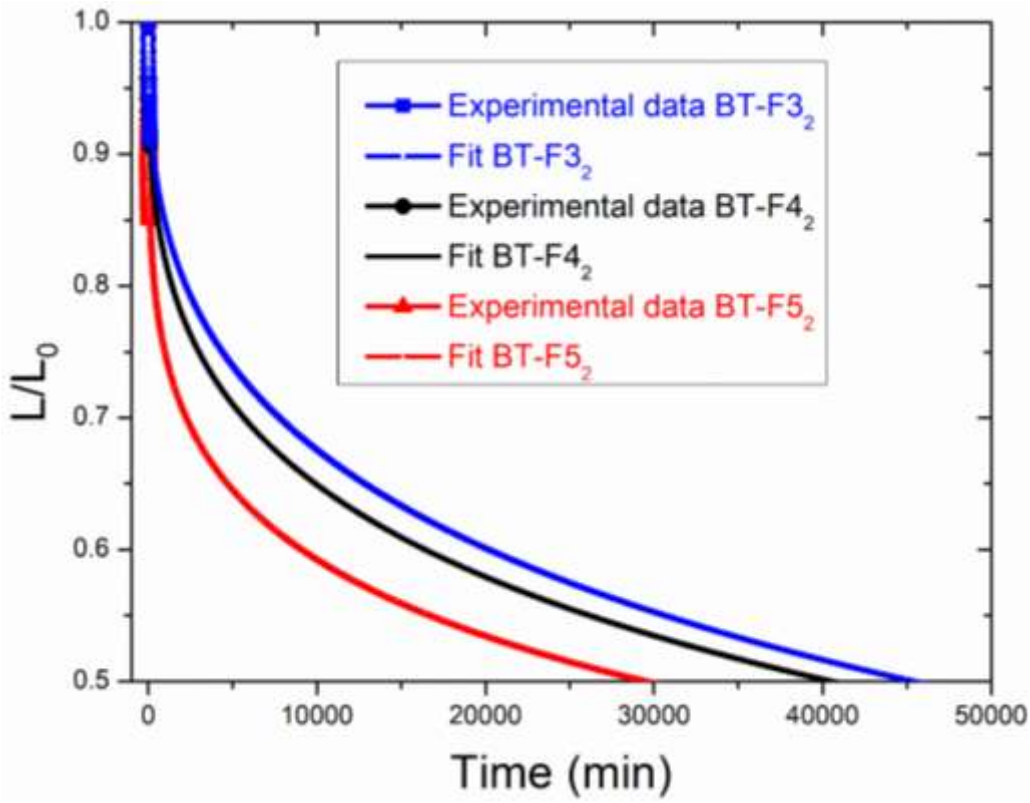

Fig. 47. Relative luminance (L/L_0) decayment over time for OLED devices based on **BT-F3$_2$**, **BT-F4$_2$** and **BT-F5$_2$**. Experimental data and fit by using SED model are shown.

For the efficiency reached with our fluorescent OLED devices, the LT50 obtained is quite acceptable, for example Fu Q. *et. al*.[111] reported for a phosphorescent OLED device an LT50 of 120 h by using $Ir(ppy)_3$ with an architecture ITO/MoO_3/TCTA:$Ir(ppy)_3$/TPBi/LiF/Al (current efficiency of 58.6 cd/A). On the other hand, phosphorescent OLED devices (EQE > 20 %) which are the most used technology in industrial applications (TV, smartphones, displays, etc.) can reach an LT50 (@ 1000 cd/m^2) of about 900 000, 400 000 and 20 000 h for red, green and blue devices respectively[12]. For instance, the best fluorescent OLED devices applied in displays have an LT50 (@ 1000 cd/m^2) of around 10 000 h[12].

For another kind of devices, such as TADF based OLEDs, Adachi C. *et. al*.[112] reported an OLED, with the now commercial, 4CzIPN as EML an LT50 of 184 h by using a bigger architecture than ours: ITO/PEDOT:PSS/CPCB:4CzIPN/T2T/Bpy-TP2/LiF/Al (EQE_{max} = 9%). Also, they were using a similar initial luminance than ours, about 1000 cd/m^2. In 2018, a TADF based OLED with an EQE of 37.8 % and an LT50 (@ 500 cd/m^2) of only 315 h was reported. More recently, Kamata T. *et. al*.[113] reported a TADF based OLED device with a high EQE of 21.6 % and an excellent LT50 of 10 000 h, which is a huge progress compared with the first attempts for this kind of devices. As can be seen, currently TADF based OLEDs have a lower lifetimes than the phosphorescent OLED devices[12].

As can be seen from the literature and from our own results, a bigger efficiency in the devices will not assure a longer lifetime. This lifetime depends of course on the efficiency of the device (at lower current through the device, degradation by this mechanism is lower too), but also from the resistance of the materials to the degradation.

6.3.1 Conclusions

OLED devices based on the family of three new oligomers had a very good luminance values when were fabricated by using a simple architecture, but when the used architecture was multilayer, their performance were significantly improved. The luminance of the better one was almost three times higher (29 499 cd/m^2) and the current efficiency was even 3 times higher (8.3 cd/A and EQE_{max} = 2.2 %). The design of these materials, with more or less "length" (or units), has direct influence on its luminance, efficiency and lifetime. It was shown that when the molecule is longer, the lifetime of the OLED devices is shorter. The shorter material had a lifetime 54 % higher that the longer one, this is 756 h against 490 h,

which is a significant difference. It is worth of mention that from the data obtained and the lifetime model for this family of molecules, for the device in which the bigger luminance was obtained the lifetime was higher too. Because at a bigger length of the molecule, exist a higher probability that their energy is released by de-excitation through vibrational relaxation which is inducing heat i.e. a faster degradation of the material.

6.4 Efficient Phosphorescent OLED devices by optimizing their ETL

Optimized OLED devices with the architecture ITO/PEDOT:PSS/PVK:Ir(ppy)$_3$/TPBi/LiF/Al were made to compare with devices based in the same structure but using new 2,2',2''-(1,3,5-Benzinetriyl)-tris(1-phenyl-1-H-benzimidazole) (TPBi) derivatives: TPBi 3COOK and TPBi OA67 (Fig. 48).

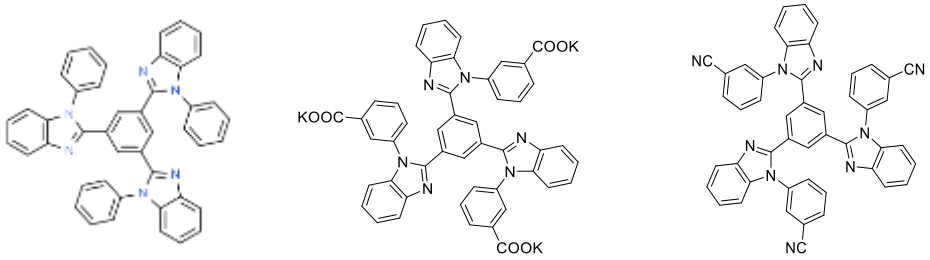

(a) (b) (c)

Fig. 48. (a) Commercial TPBi, and derivatives of TPBi (b) 3-COOK and (c) OA67 synthesized in the Skabara group.

First, the relationship between the Ir(ppy)$_3$ and PVK and the thickness of this EML were optimized. Relations of PVK + 5, 10, 15, 20 % Ir(ppy)$_3$ were used to made OLED devices. The best performance was for devices with PVK + 10 % of Ir(ppy)$_3$ in THF. For 5 % of Ir(ppy)$_3$ the devices shown a poor luminance (about 10 cd/m^2), for 20 % of Ir(ppy)$_3$ shown a luminance of 3000 cd/m^2 and a maximum current efficiency of 3 cd/A. For 15 % of Ir(ppy)$_3$ a luminance of 5000 cd/m^2 and a current efficiency of almost 6 cd/A were reached. Finally, for 10 % of Ir(ppy)$_3$ a maximum luminance of almost 10000 cd/m^2 and a current efficiency of 8 cd/A were reached.

Based in these results, we proceed to optimize the thickness of the EML. The deposit at 5000 RPM (i.e. 30 nm of thickness) had the better performance, more than 10000 cd/m^2 and a current efficiency of 10 cd/A. TPBi commercial and TPBi 3COOK (4 mg/mL) were used as ETL. Also, commercial TPBi and TPBi 3COOK were deposited as ETL by spin coating techinique at different RPM to find the best performance. Annealing was applied to both material at 150 °C 30 min.

Is worth of mention that TPBi OA67 does not made good films by spin coating technique, then its use in OLED devices was discarded.

As can be seen in Fig. 49, the performance for the optimized OLED devices that are using TPBi 3COOK as ETL is low, with luminances of the order of 10 cd/m^2 and maximum current efficiencies lower than 0.2 cd/A. In the other hand, devices that are using commercial TPBi as ETL, shown a very high luminance, up to 18584 cd/m^2, and a very good maximum current efficiency of 10-11 cd/A. In Table 6, the best results for the optimized OLEDs are shown.

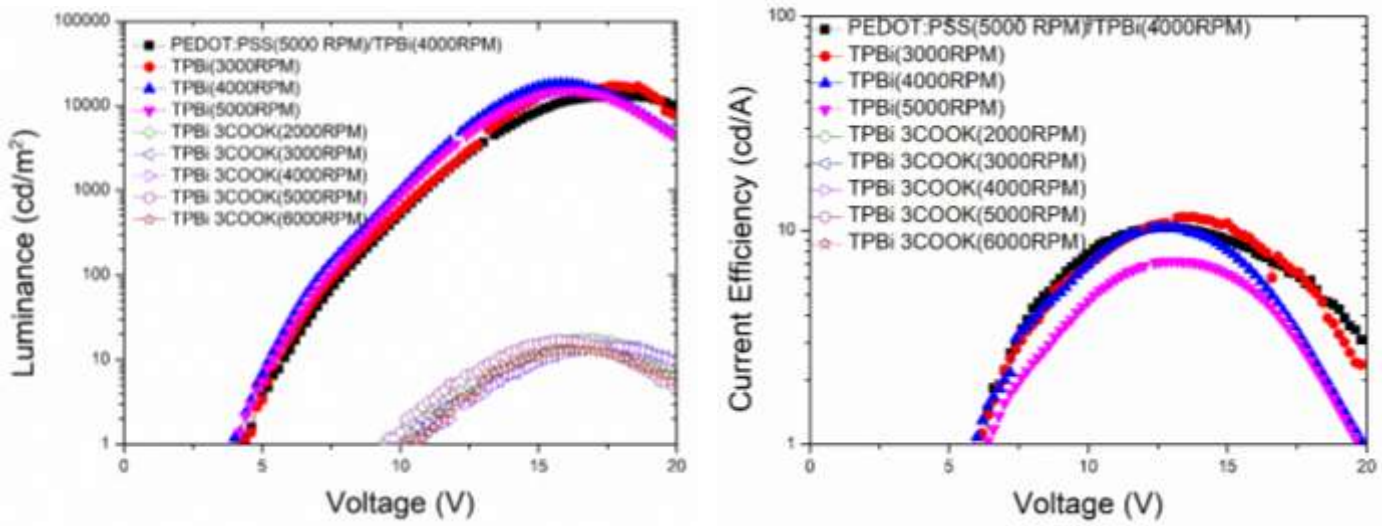

Fig. 49. OLEDs performance for different ETL thickness based on TPBi and TPBi 3COOK (5 mg/mL in both cases).

Due to the lower luminances and current efficiencies we discard the use of TPBi 3COOK as ETL. On the other hand, the use of commercial TPBi and its optimization is of great importance because the change in the performance of the devices is significant.

Table 6. Performance of the best OLED devices using PVK:Ir(ppy)3(+10%) as EML (30 nm), and commercial TPBi as ETL.

Architecture	$\mathbf{V_{on}}$ (V)	$\mathbf{L_{max}}$ (cd/m^2)	$\mathbf{\eta_{L_{max}}}$ (cd/A)	$\mathbf{\eta_{max}}$ (cd/A)	$\mathbf{L_{\eta_{max}}}$ (cd/m^2)
ITO/PEDOT:PSS(35nm)/PVK:Ir(ppy)$_3$ /TPBi(50nm)/LiF/Al	4.6	13870	5.2	10.3	3706

ITO/PEDOT:PSS(40nm)/PVK:Ir(ppy)$_3$ /TPBi(55nm)/LiF/Al	4.2	17145	6.3	11.5	7316
ITO/PEDOT:PSS(40nm)/PVK:Ir(ppy)$_3$ /TPBi(50nm)/LiF/Al	4	18584	6.5	10.3	7831
ITO/PEDOT:PSS(40nm)/PVK:Ir(ppy)$_3$ /TPBi(45nm)/LiF/Al	4.2	15076	4.8	7.1	6834

V_{on}= turn on voltage, L_{max}= maximum luminance, η_{Lmax}= current efficiency at maximum luminance, η_{max}= maximum current efficiency, $L_{\eta max}$= Luminance at maximum current efficiency.

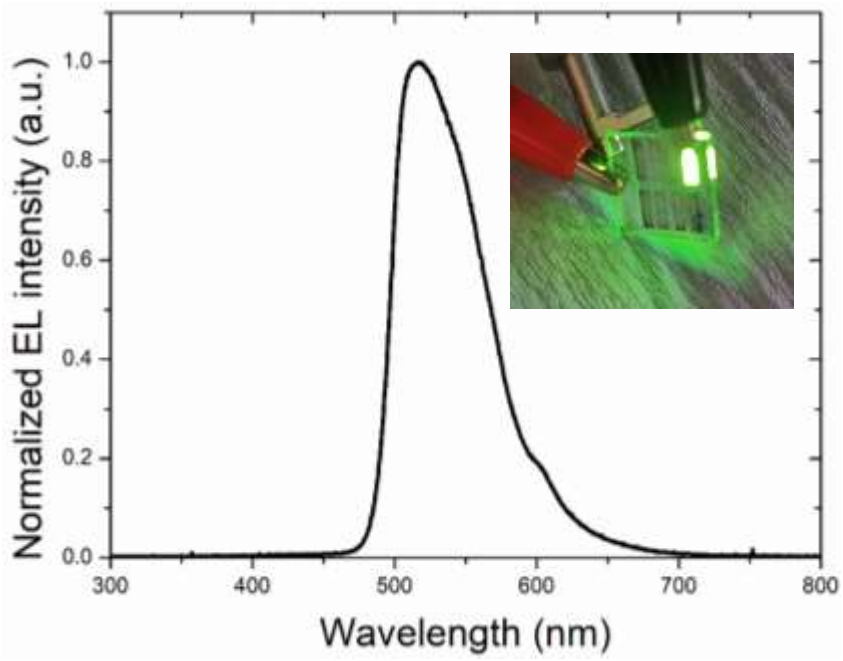

Fig. 50. EL spectrum for OLED based on Ir(ppy)$_3$ and photograph.

As can be seen in Fig. 49 the deposit of commercial TPBi have been varied to 3000, 4000 and 5000 rpm. Recombination zone and charge balance are very sensitive and the most important factors for the improvement and optimization of phosphorescent OLED devices. It is demostrated that the thickness of the ETL,TPBi in our case, has control in the electron transport on the emission layer and in the recombination zone[114]. Then, based in our results

and the current efficiencies of the Fig. 49, TPBi deposited at 3000 rpm optimize the electron/hole ratio at EML.

6.4.1 Conclusions

In the case of these phosphorescent OLEDs the optimization of one simple layer as ETL, TPBi in this case, has a considerable influence in the efficiency and luminance of the devices. This is due the manipulation of the recombination zone i.e. the electron/hole ratio that is injected into the EML.

6.5 Flexible anodes based on conductive PEDOT:PSS and their application in OLED devices

Conductive PEDOT:PSS based anodes were fabricated by spin coating technique on rigid and flexible substrates. Reported anodes based on this polymer[17,82,115] were studied and reproduced to develop a new one alternative. In general, conductive PEDOT:PSS is treated to separate the conductive PEDOT from the non-conductive PSS[116]. The most used treatments to do this are based on addition of one additive (as DMSO, EG, 2-propanol, etc.) in the solution of this conductive PEDOT:PSS or also in post-treatments after the PEDOT:PSS deposition. In the first case, depending of the additive used in the solution, it could help to separate PEDOT from PSS or improve the adhesion (i.e. the static contact angle) of the solution in the substrate. In the second case, generally the post-treatment is used to separate PEDOT from PSS too, and to improve the morphology of the films. In the post-treatment a low amount of solution (DMSO, sulfuric acid, 2-propanol, etc.) is dropped on the film and in general a temperature is applied to evaporate the solution added.

The static contact angle is the characteristic angle made by one liquid droplet on the solid surface. This contact angle depends upon the wettability and tension of the surface [117]. This static angle was corrected for the conductive PEDOT:PSS in order to reach an optimum deposit by spin coating technique. The correction was made applying a plasma treatment in both type of substrates, glass and acetate, by 10 min.

In the Fig. 51 the sheet resistances for PEDOT:PSS anodes fabricated in rigid substrates are shown. All the values of sheet resistance obtained and presented in this work, are average values while transmittance values were obtained at 550 nm.

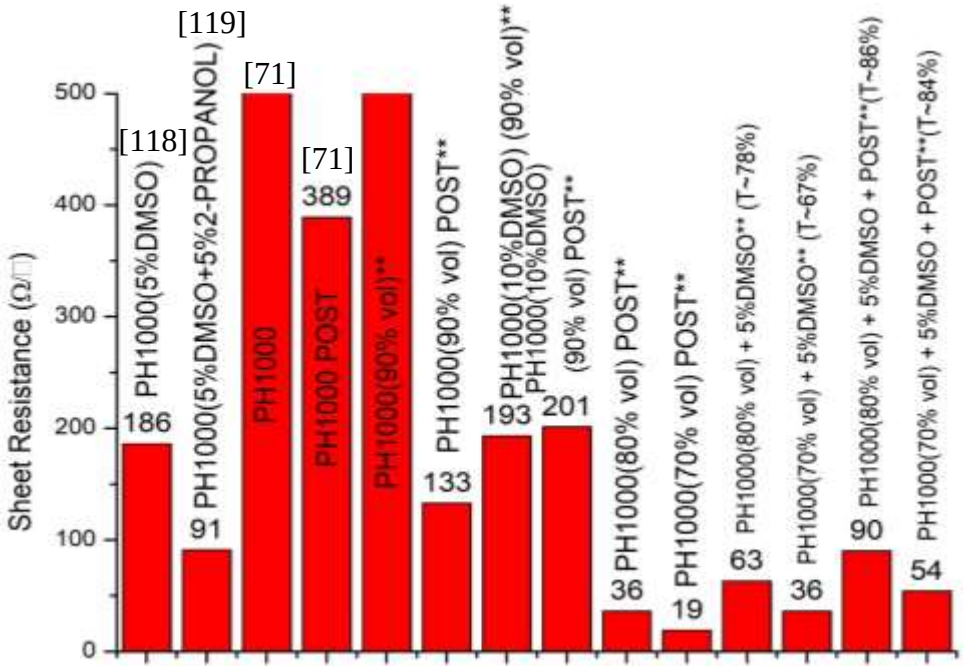

Fig. 51. Anodes fabricated, some of them based on reported ones[71,118,119] and the others based on the new "*volume evaporation"* procedure.

When no treatment or post-treatment was applied in the PEDOT:PSS polymer, the sheet resistance is of the order of even 10^4 Ω/□, and then the conductivity is too low. For example, for ITO which is the most used anode the sheet resistance is of 8-12 Ω/□. But, when some additive, as DMSO (5 %), is added into the solution to separate PEDOT from PSS the sheet resistance is improved to 100-200 Ω/□. Even more, when another additive (2-propanol) was added to improve the adhesion and the package of the PEDOT:PSS, the sheet resistance was 91 Ω/□. It is worth of mention these anodes got two or three layers deposited to reach the mentioned sheet resistances.

Following this idea, separate PEDOT from PSS to induce lower sheet resistance (higher conductivity), we worked evaporating an amount of volume of this conductive PEDOT:PSS, by applying a high temperature in order to modify its microstructure which is reported that can be affected by applying a high temperature or by lack of water[120]. This volume evaporation is basically, removing water from the dispersion of PEDOT:PSS. With this lost of water, the conductive fractions of PEDOT must be closer than before (Fig. 52) and the PSS can be separated by some treatment as mentioned before.

Volume evaporation was tested at different percentages, with final volumes of 90 %, 80 % and 70 %. When we got 90 % of volume, the anodes shown a good transmittance but a high

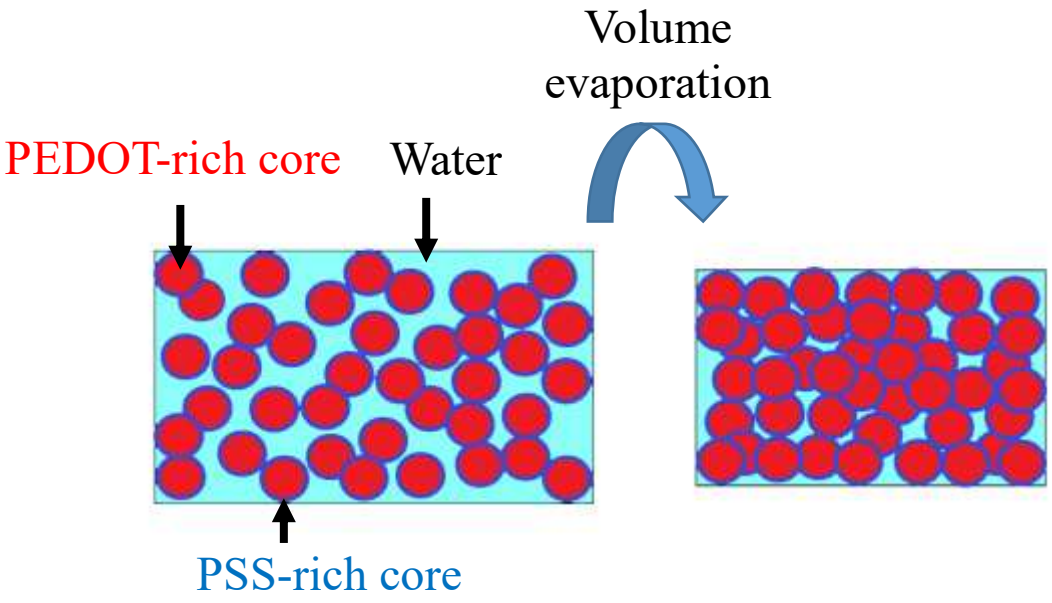

Fig. 52. Volume evaporation induce proximity between conductive fractions (PEDOT).

value of sheet resistance when is compared with the values obtained for 80 % and 70 % of volume, because of this, we choose to work only with 80 and 70 % of volume.

After volume evaporation, DMSO was applied on the films of PEDOT:PSS as post-treatment. DMSO has the function of breaking or the hydrogen bonding between PSS fractions, which leads to separate PSS from PEDOT and then the conductive fractions of PEDOT are even closer than before improving the conductivity of the film as is shown in Fig. 53. This post-treatment with DMSO improve the conductivity of the film up to four orders, and is based on the screening effect caused in the interaction or bond between the fractions of PEDOT and PSS leading to the release of PEDOT from the shell of PSS. This release benefits the connection among PEDOT fractions and then the conductivity.

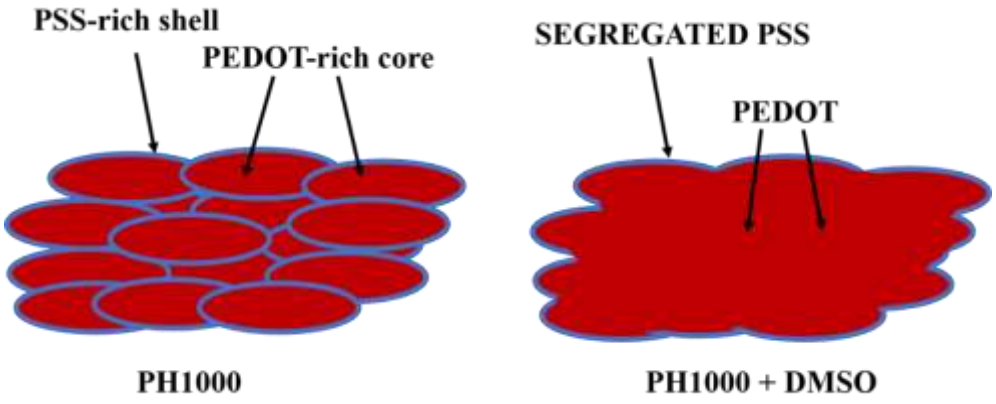

Fig. 53. Schematic diagram of the separation of PEDOT from PSS before and after DMSO addition.

In Fig. 54, morphologies of PEDOT:PSS anodes fabricated on rigid substrates are shown. When 80 % of volume was used, we found that the best results were at 140 and 130 nm of thickness, generated by only one layer of PEDOT:PSS. For 140 nm, the sheet resistance had a value of 57 Ω/□ and a roughness of 3 nm. On the other hand, for 130 nm the sheet resistance was of 73 Ω/□ and a lower roughness of 1-2 nm.

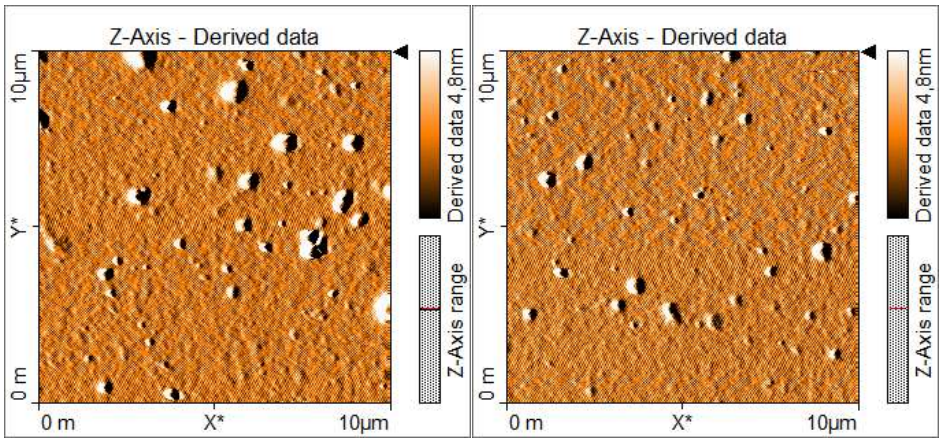

a) b)

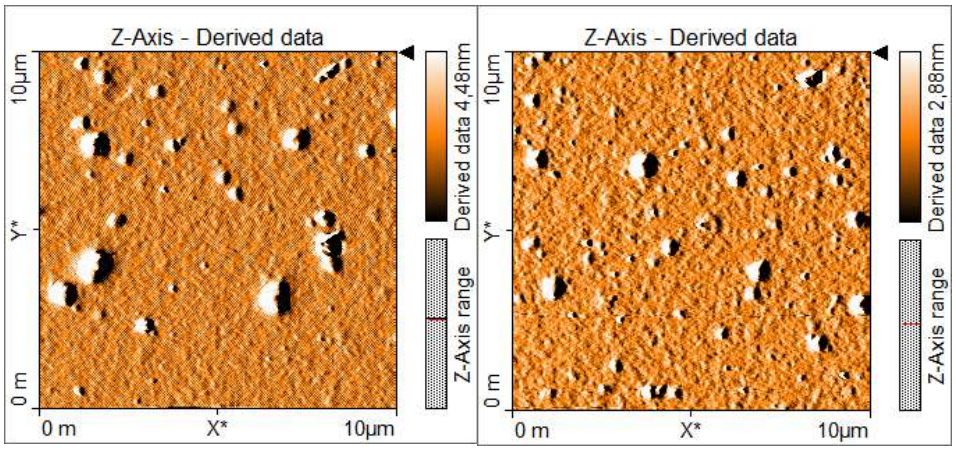

c) d)

Fig. 54. PEDOT:PSS anodes (in glass) morphologies fabricated by volume evaporation, with different thicknesses a)80% vol - 140 nm – Roughness 3 nm – Rs= 57 Ω/□ b)80% vol - 120 nm – Roughness 1-2 nm – Rs= 73 Ω/□ c)70% vol – 460 nm – Roughness 3 nm – Rs= 31 Ω/□ d)70 % vol – 220 nm – Roughness 2 nm – Rs= 50 Ω/□.

When a volume of 70 % was used to produce a film with 460 nm of thickness, the sheet resistance was of only 31 Ω/□ with a roughness of 3 nm. On the other hand, by using the same amount of volume a film with a thickness of 220 nm was produced with a sheet resistance of 50 Ω/□ and a roughness of 2 nm.

In the AFM images, a number of grains about 1 µm or less of diameter are visible. These could be domains of PEDOT that were not completely homogeneous in the deposition and persisted in that way. It is worth of mention that the dispersion of PEDOT:PSS deposited by spin coating was not filtered because its viscosity is high due to volume evaporation which difficult the procedure.

Another important factor together with the sheet resistance is the transmittance. As can be expected, at a bigger thickness lower transmittance. In the case of the anodes fabricated with 80 % of volume, the transmittance was of 85-90 % at 550 nm. After 550 nm, shifted to the infrared, the transmittance decays while in the bandwidth of 350-550 nm the transmittance is even higher than 90 %. Also, in the case of anodes in which 70 % of volume was used, a transmittance of 75-80 % is reached but around of 800 nm decays even down of 60 %. But, around 400 nm, they had a transmittance of around 85 %. Then, if this anodes are used in

OLED devices, the bandwidth around 400-500 nm (violet-blue) will have the better extraction of light, while in the bandwidth between 500-600 nm (green-yellow) will be lower and after 600 nm (orange-red) the extraction will decrease significantly. This actually is not a big problem for OLED devices because in general is precisely the bandwidth of the violet-blue which have the lower efficiency while the bandwidth of 500-800 nm has not this problem.

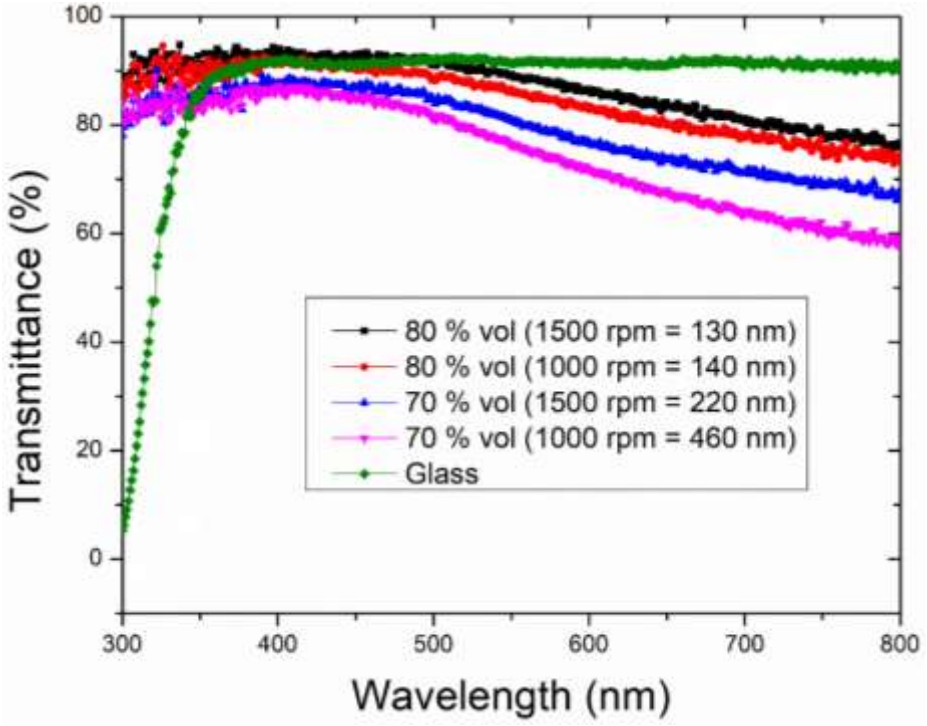

Fig. 55. Transmittances of PEDOT:PSS anodes fabricated by volume evaporation at different rpm and deposited in common glass.

In Fig. 56, morphologies for PEDOT:PSS anodes deposited on flexible substrates of acetate are shown. These flexible substrates were made of common acetate, and the films were deposited by spin coating too. For the specific case of conductive PEDOT:PSS, it was necessary the use of oxygen plasm treatment before the deposition of the film, this is because the adhesion is enhanced by applying this treatment. Again, only 80 and 70 % volumes were used for the PEDOT:PSS anodes fabrication. For 80 % of volume with a thickness of 130 nm a sheet resistance of 40 Ω/□ and a roughness of 6 nm. For 110 nm at the same volume, the sheet resistance was 70 Ω/□ and a roughness of 5 nm. Also, as can be seen in the Fig. 56, the PEDOT:PSS surface deposited in flexible substrates is too different compared with the rigid

ones, this could be because the adhesion is different in the acetate, and the temperature in the annealing treatment is lower (100 °C).

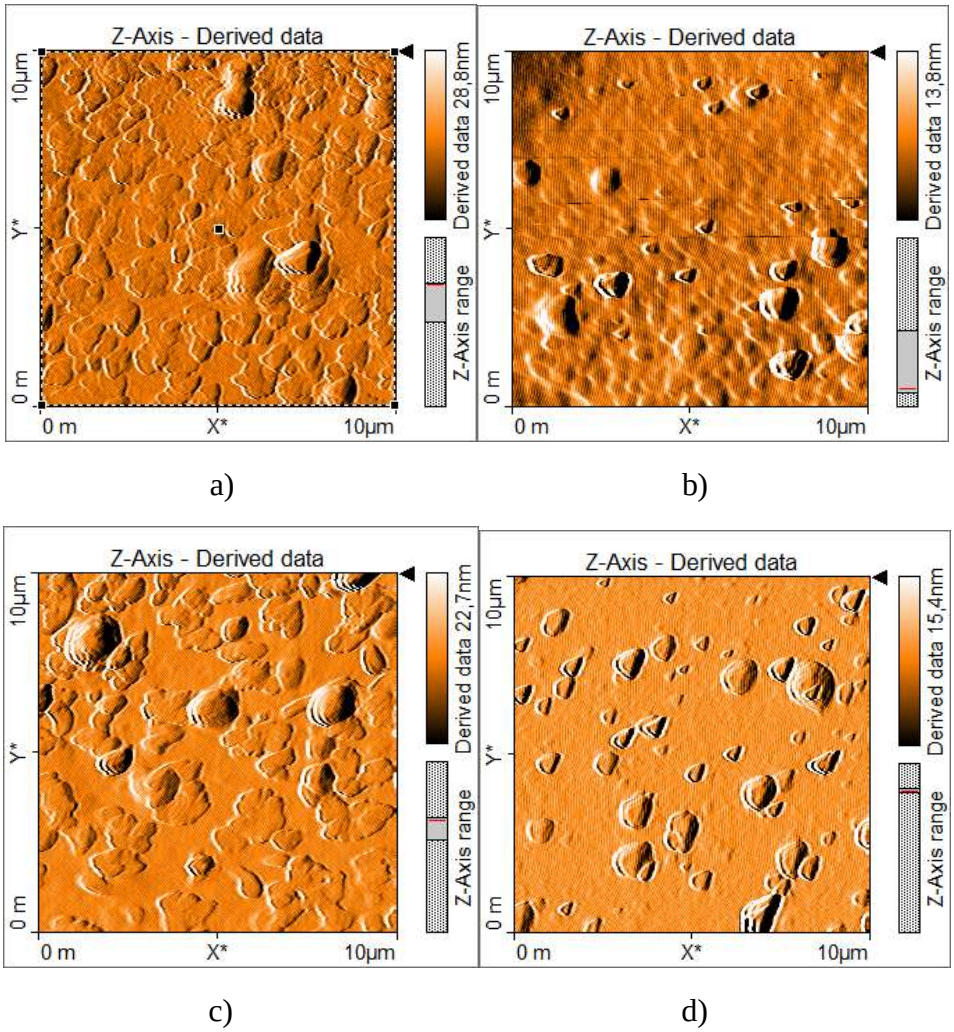

a) b)

c) d)

Fig. 56. PEDOT:PSS anodes (in acetate) morphologies fabricated by volume evaporation, with different thicknesses a)80% vol - 130 nm – Roughness 6 nm – Rs= 40 Ω/□, b)80% vol - 110 nm – Roughness 5 nm – Rs= 70 Ω/□, c)70% vol – 600 nm – Roughness 8 nm – Rs= 15 Ω/□, d)70 % vol – 340 nm – Roughness 8 nm – Rs= 33 Ω/□.

On the other hand, when a volumen of 70 % is used to fabricate flexible PEDOT:PSS anodes the sheet resistance is even lower, even almost the same value that the commercial ITO, but the thickness is too high. For example, depositing at the same rpm used for 80 % of volume @ 130 nm, the thickness obtained by using 70 % of volume was 600 nm and the sheet

resistance of only 15 Ω/□. Adding only 500 rpm more, the sheet resistance changes to 33 Ω/□. This is because the high viscosity obtained at 70 % of volume.

When the AFM images for PEDOT:PSS anodes deposited in acetate are compared with the deposited in glass, a huge difference can be seen. The adhesion is really different among them. If the anode is fabricated in acetate, bigger grains of similar dimensions can be seen while in glass just a few and smaller grains are present. These grains must big domains of PEDOT, because the sheet resistance in anodes fabricated in acetate is lower, in general, than their similar deposited in glass. For example, the flexible anode of 130 nm presented a sheet resistance of 40 Ω/□ and the rigid anode of 140 nm was 57 Ω/□, both at a similar transmittance, even when the roughness value in the second one is the half of the first one.

As can be seen in Fig. 57, when acetate is used as substrate, the difference between use 80 or 70 % of volume has great influence in transmittance. When 80 % of volume was used, the transmittance was about 85 % (40 Ω/□) at 550 nm while when 70 % of volume was used (both deposited at the same rpm) the transmittance decays to 55 % (15 Ω/□) at 550 nm.

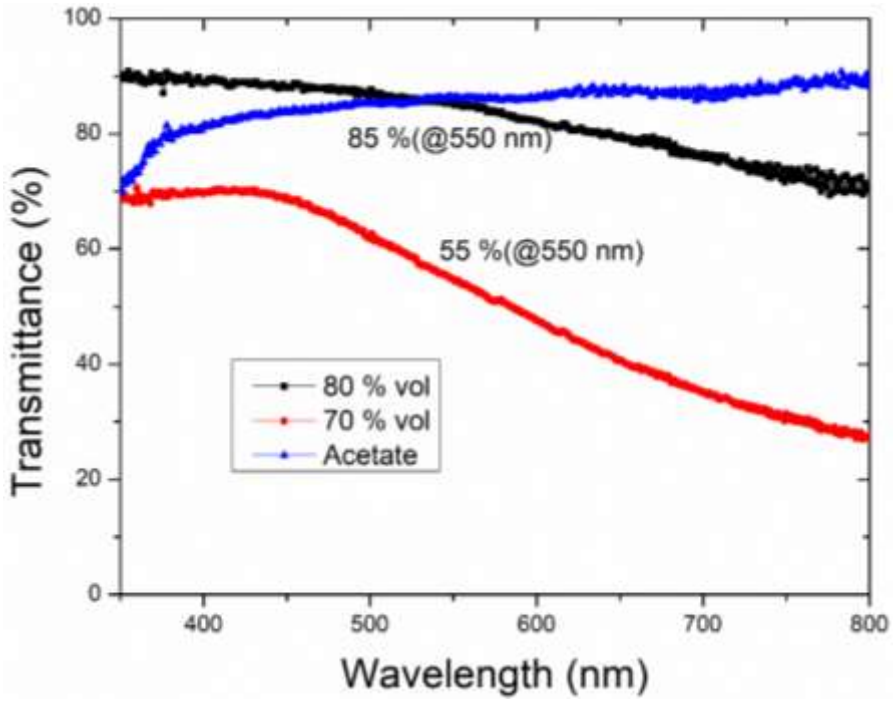

Fig. 57. Transmittances of flexible PEDOT:PSS anodes fabricated by spin coating with volume evaporation of 80 and 70 % with the same rpm and deposited in acetate.

In the case of the PEDOT:PSS anode with higher transmittance, this last remains between 85 % and 70 % after 550 nm, but in the case of the second one the transmittance decays even lower than 30 % because the higher thickness of the film. Between 350 and 550 nm the transmittance of PEDOT:PSS anode that used 80 % of volume remains really stable in 85-90 %, while the one that used 70 % of volume change from 55 % to 70 %. Again, this transmittances are beneficial for the bandwidth with lower performance in OLEDs, which is the violet-blue (400-500 nm).

In Fig. 58 PEDOT:PSS anodes fabricated on acetate are shown, the one with higher transmittance (85 %) had a sheet resistance value of 40 Ω/□ while the one with lower transmittance (55 %) had a value of 15 Ω/□.

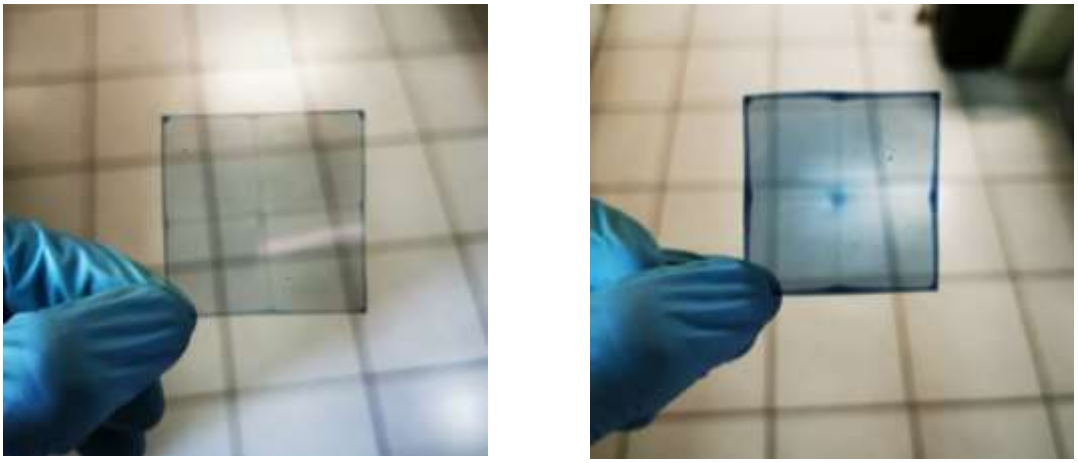

(a) (b)

Fig. 58. PEDOT:PSS anodes deposited in acetate by using (a) 80 % and (b) 70 % of volume and deposited at the same rpm. Area of 4.5 × 4.5 cm.

In Fig. 59 some values of reported PEDOT:PSS anodes are shown and compared with our obtained values. For example, Liu *et. al.*[115] reported a sheet resistance of 70.36 Ω/□ and a high transmittance of 90 % (@550 nm) for PEDOT:PSS based anode, treated with sulfuric acid (H_2SO_4), which are similar values to ours, but we are not using hazardous materials as sulfuric acid.

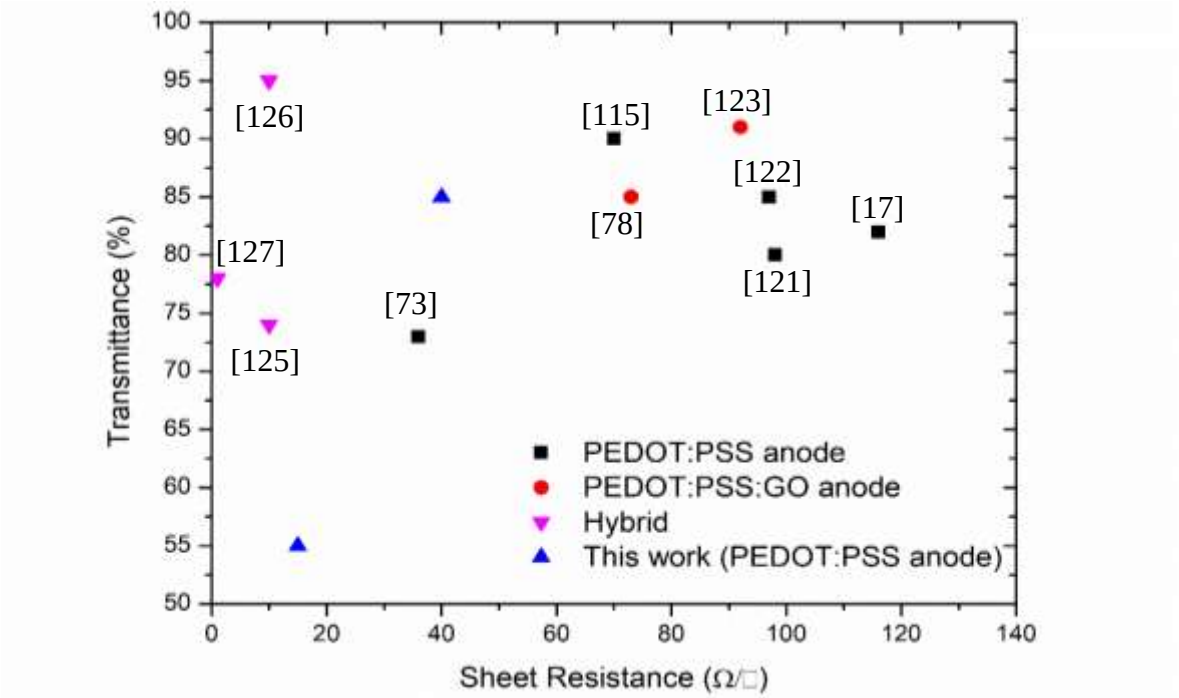

Fig. 59. Transmittance versus sheet resistance values of PEDOT:PSS, PEDOT:PSS:GO and hybrid anodes reported in literature and made in this work (PEDOT:PSS).

Zhao *et. al.*[121] applied 3-Hydroxy-1-propanesulfonic acid (HPSA) as a modification layer on PEDOT:PSS film via spin coating. The sheet resistance of the PEDOT:PSS/HPSA bilayer film was 98 Ω/□, and its transmittance at 550 nm was around 80 %. In 2017, Bjorn *et. al.*[73] reported an anode based on four layers of PEDOT:PSS (total thickness of 133 nm) with an excellent sheet resistance of 36 Ω/□ and a transmittance of 73 % by using a light oxygen plasm treatment in addition to solvent blend additives and post treatments. Anodes (for OLEDs) based on PEDOT:PSS, with a sheet resistance of 97 Ω/□ and transmittance of 85 % trough modifying the surface of PEDOT:PSS films by using ethanol vapor were obtained by Mohammad *et. al.*[122].

Also, Seo *et. al.*[17] reported an anode based also on PEDOT:PSS (solution mixed with 2-ethoxyethanol) and by using methanol based post treatment with a sheet resistance of 116 Ω/□ and a transmittance of 82 %, this was obtained by using solvent post treatment with 2-ethoxyethanol.

Another type of ITO-free anodes reported in literature, based not only on PEDOT:PSS polymer, as the reported by Liu *et. al*.[78] consists in a PEDOT:PSS/graphene oxide composite anode with a sheet resistance of 73 Ω/□ and a transmittance of 85 %, which is reached by optimization of the volume ratio of PEDOT:PSS and GO. Wu *et. al*.[123] reported a sheet resistance of 92 Ω/□ and a high transmittance of 91 % with an hybrid anode of PEDOT:PSS and graphene oxide. They developed this anode by using a low temperature dipping treatment of the bilayer anode in hydriodic acid solution to remove the non-conductive parts (PSS chains of PEDOT:PSS and functional groups on GO).

In 2019, Diker *et. al*.[124] reported a PEDOT:PSS:mGO anode with sheet resistance of 177 Ω/□ and high transmittance of 90 % by applying a sulfuric acid post treatmet and then an O_2 plasma treatment on the film by 3 minutes (@70 W).

On the other hand, the hybrid anodes are another type, which have in general best values of transmittances and sheet resistances, but also their fabrication is not simple and present a significant higher cost. For example, a hybrid anode by using Ag mesh and PEDOT:PSS (Ag mesh/PEDOT:PSS) with a sheet resistance of 10 Ω/□ and a transmittance of 74 % was reported by Park *et. al*.[125]. Kang *et. al*.[126] reported a hybrid electrode with structure PEI/Ag/PEDOT:PSS, with a sheet resistance value lower than 10 Ω/□ and a high transmittance of 95 %. Finally. Chen *et. al*.[127] reported an innovative hybrid anode by using high-resolution Ag grids and PEDOT:PSS, with an excellent low sheet resistance of only 1 Ω/□ and a transmittance of 78 %.

Our PEDOT:PSS anode was applied in the OLED shown in Fig. 60 by using a multilayer architecture PEDOT:PSS anode/PEDOT:PSS/**PF-2F**/TPBi/LiF/Al and reached a maximum luminance of almost 4000 cd/m^2 with a turn on voltage of 7 V. Likewise, J-V-L curves for the best OLED device fabricated for the same EML, PF-2F, is shown. The turn on voltage of the OLED using ITO as anode is about 2 V lower than the device using PEDOT:PSS anode. Also, current densities are quite similar in both devices but the luminance is higher in the one with PEDOT:PSS anode. Anyway, this luminance could be associated with the use of TBPi

in that specific device. As can be seen, this anode can be used in optoelectronic devices, even to fabricate flexible devices.

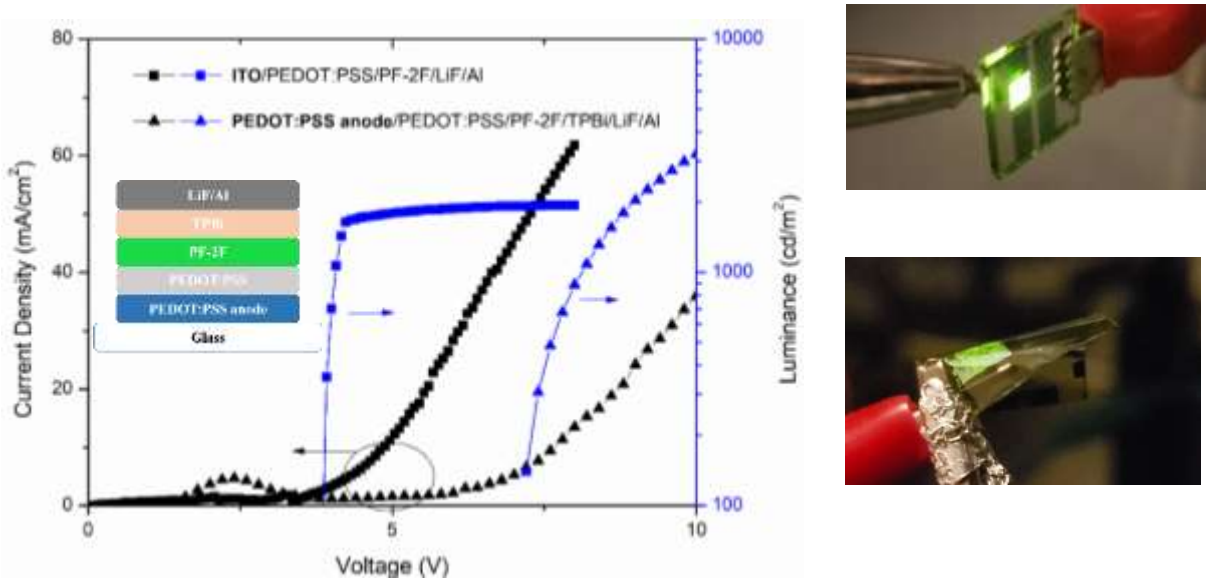

Fig. 60. J-V-L curves for an OLED by using a PEDOT:PSS (in glass) anode with an architecture multilayer PEDOT:PSS anode/PEDOT:PSS/**PF-2F**/TPBi/LiF/Al and its comparison with one using ITO anode. Also, photograph of one rigid and one flexible OLED devices, using this PEDOT:PSS anode, are shown.

6.5.1 Conclusions

In conclusion, the volume evaporation method is a simple way to obtain anodes with good values of transmittance and sheet resistance. The use of only PEDOT:PSS and DMSO, benefits the cost of fabrication when is compared with another PEDOT:PSS anodes that use a wide variety of additives and even dangerous substances as sulfuric acid. Furthermore, even when hybrid anodes in general are better than PEDOT:PSS anodes, its fabrication is too difficult and expensive compared with the method presented here.

7 CONCLUSIONS

It is evident that the field of research in OLED devices is still under development such as the synthesis of new materials, that can be applied in different EML systems (single emissor or host/guest) and the functionalization of specific layers in order to obtain the best electron/hole balance i.e. the best performance. We are reporting fluorescent and phosphorescent OLED devices by using new and also reported materials which can contribute in specific and simple changes that could be beneficial to the performance of OLED devices. For example, the addition of groups that benefit the processability of the materials (as the CF_3 group) and the charge transport (as bifluorene), the adequate use of the HOMO-LUMO levels and the work function, the correct optimization of the EMLs and the buffer layers (ETL, EIL, etc.). Herein the most important conclusions of this thesis are summarized.

- Our results for OLEDs based on carbazole derivatives (**CZ-1** and **CZ-2**) had very acceptable current efficiencies (19.3 - 20.2 cd/A) and very high and competitive external quantum efficiencies (8.6 - 9.5 %) due to a low generated current density value (<200 mA/cm^2). These values are significantly higher than the values obtained with the TPD derivatives (luminances up to 1729 cd/m^2, current efficiencies up to 4.5 cd/A).
- OLEDs devices based on the new **PF-2F** polymer showed an acceptable external quantum efficiency (for fluorescent materials) up to 2.6 % and an excellent current efficiency of 35.3 cd/A, even under a simple used architecture. By the inclusion of the trifluoromethyl group into **PF-2F** polymer, it led to improved processability and an enhancement in the electro-luminescence of the OLED devices, which is a positive influence on the overall device performance. Also, the enhanced performance is due to its LUMO level, which is at only 0.2 eV from LiF/Al work function level, the efficiency of these simple devices is high.
- OLED devices based on the family of three new oligomers had a very high luminance values when were fabricated by using a simple architecture which was significantly improved by using a multilayer architecture. The luminance of the better one was almost three times higher (29 499 cd/m^2) and the current efficiency was even 3 times

higher (8.3 cd/A and EQE_{max} = 2.2 %). The design of these materials, with more or less "length" (or units), has direct influence on its luminance, efficiency and lifetime. The shorter material had a lifetime 54 % higher that the longer one, this is 756 h against 490 h, which is a significant difference. It is worth to mention that from the obtained data and the lifetime model for this specific family of molecules, when bigger luminance was reached in devices, the lifetime was higher too. Because at a bigger length of the molecule, exist a higher probability that their energy is released by de-excitation through vibrational relaxation which is inducing heat i.e. a faster degradation of the material.

- For phosphorescent OLEDs the optimization of one simple layer as ETL, TPBi in this case, has a considerable influence in the efficiency and luminance of the devices. This is due the manipulation of the recombination zone i.e. the electron/hole ratio that is injected into the EML.

Finally, the proposed fabrication method for PEDOT:PSS anode has shown very good results with a really simple, cost-effective and fast fabrication. Most of the literature for PEDOT:PSS anodes in general report values of sheet resistance of 10^2 Ω/□, but this anode fabricated with a dispersion of PEDOT:PSS concentrated at 80 % and deposited in acetate has values of one order of magnitude smaller (40 Ω/□**)** and an acceptable transmittance (> 85%) with only one deposited layer. This is due to the induced closeness among the conductive fractions (PEDOT) by the loss of water and the subsequent DMSO post-treatment applied. PEDOT:PSS dispersion increased its viscosity and then only one deposit was necessary. As was expected, the use of the post-treatment helped to enhance the conductivity taking off the non-conductive fractions (PSS). For these good values of sheet resistance and transmittance obtained, in both rigid and flexible substrates, this PEDOT:PSS anode could be applied not only on OLED devices but in a variety of optoelectronic devices such as organic photovoltaic cells and perovskite solar cells.

8 Perspectives

OLED devices could have a higher lifetime and better performance by using at least one more layer and if they are encapsulated too. Also, phosphorescent OLED devices based on $Ir(ppy)_3$ could have a better performance by using a different host material, as CBP or m-CBP. Could be an interesting study the use of a TADF material as host for the phosphorescent guest, which has recently shown that could improve significantly the OLED performance. Even we could try by combining our fluorescent materials with TADF materials in a hyper-fluorescence emitter system (now called the 4^{th} generation OLED emitters) in order to obtain a higher efficiency, luminance and color purity.

This conductive PEDOT:PSS polymer based anode could be used in different devices and also deposited in glass or plastic substrate as common as acetate. The sheet resistance should be slightly better adding more post-treatments or even by using a plasma treatment directly in the layer. Even when the cost/time would be higher, it will remain being cheaper than another kind of anodes. Also, slot die coating could be used to deposit this anode in bigger areas and in both kind of substrates: rigid and flexible. In the case of the flexible ones, from only one anode of large area deposited, could be extracted (cut) a “massive” quantity of anodes. Of course, this anode could be used for a wide variety of rigid and flexible optoelectronic devices as OLEDs, OPVs, and PSCs.

Scientific publications

1. **Luis-Abraham Lozano-Hernández**, J.L. Maldonado, O. Hernández-Cruz, J. Nicasio-Collazo, M. Rodríguez, O. Barbosa-García, G. Ramos-Ortíz, M. G. Zolotukhin, U. Scherf, *"Structurally simple OLEDs based on a new fluorinated poly(oxindolylidenearylene)"*, Dyes and Pigments **2020**, 173; DOI: https://doi.org/10.1016/j.dyepig.2019.107989
2. **Luis-Abraham Lozano-Hernández**, J.L. Maldonado, Cesar Garcias-Morales, Arian Espinosa Roa, Oracio Barbosa-García, Mario Rodríguez, Enrique Pérez-Gutierrez, *"Efficient OLEDs fabricated by solution process based on carbazole and thienopyrrolediones derivatives"*, Molecules **2018**, 23, 280; DOI: https://doi.org/10.3390/molecules23020280
3. Sergio Romero-Servin, **Luis-Abraham Lozano-Hernández**, J.L. Maldonado, Ramón Carriles, Gabriel Ramos-Ortíz, Enrique Pérez-Gutiérrez, Ullrich Scherf, Mikhail G. Zolotukhin, *"Light emission properties of a cross-conjugated fluorene polymer: demonstration of its use in electro-luminiscence and lasing devices"*, Polymers **2016**, 8, 43; DOI: https://doi.org/10.3390/polym8020043
4. **Luis-Abraham Lozano-Hernández**, M. Rodríguez, O. Barbosa-García, J.L. Maldonado, "Conductive PEDOT:PSS based anode deposited by one-step and its application in rigid and flexible optolectronic devices". Under preparation.
5. Joseph Cameron, **Luis-Abraham Lozano-Hernandez**, Peter J. Skabara, "Highly luminescent OLED devices based on three novel linear, small molecule emitters". Under preparation.

9 References

[1] Tang CW, VanSlyke SA. Organic electroluminescent diodes. Appl Phys Lett 1987;51:913–5. doi:10.1063/1.98799.

[2] Jang JG, Kim WK. High-efficiency red-phosphorescent organic light-emitting diode with the organic structure of 2-TNATA⁄Bebq2:SFC-411⁄SFC-137. J Soc Inf Disp 2010;18:92. doi:10.1889/JSID18.1.92.

[3] Jou J-H, Kumar S, Agrawal A, Li T-H, Sahoo S. Approaches for fabricating high efficiency organic light emitting diodes. J Mater Chem C 2015;3:2974–3002. doi:10.1039/C4TC02495H.

[4] Zhao X, Wang S, You J, Zhang Y, Li X. Solution-processed thermally stable amorphous films of small molecular hole injection/transport bi-functional materials and their application in high efficiency OLEDs. J Mater Chem C 2015;3:11377–84. doi:10.1039/C5TC02559A.

[5] Du X, Yang X, Zhao J, Lin H, Zheng C, Tao S. Highly efficient solution-processed small-molecule white organic light-emitting diodes. Org Electron 2016;38:344–9. doi:10.1016/J.ORGEL.2016.09.016.

[6] Romero-Servin S, Lozano-Hernández LA, Maldonado JL, Carriles R, Ramos-Ortíz G, Pérez-Gutiérrez E, et al. Light emission properties of a cross-conjugated fluorene polymer: Demonstration of its use in electro-luminescence and lasing devices. Polymers 2016;8:43. doi:10.3390/polym8020043.

[7] Huang T, Jiang W, Duan L. Recent progress in solution processable TADF materials for organic light-emitting diodes. J Mater Chem C 2018;6:5577–96. doi:10.1039/C8TC01139G.

[8] Kotadiya NB, Blom PWM, Wetzelaer GJAH. Efficient and stable single-layer organic light-emitting diodes based on thermally activated delayed fluorescence. Nat Photonics 2019;13:765–9. doi:10.1038/s41566-019-0488-1.

[9] Kamata T, Sasabe H, Ito N, Sukegawa Y, Arai A, Chiba T, et al. Simultaneous

realization of high-efficiency, low-drive voltage, and long lifetime TADF OLEDs by multifunctional hole-transporters. J Mater Chem C 2020;8:7200–10. doi:10.1039/d0tc00330a.

[10] Cai M, Zhang D, Duan L. High Performance Thermally Activated Delayed Fluorescence Sensitized Organic Light-Emitting Diodes. Chem Rec 2019;19:1611–23. doi:10.1002/tcr.201800148.

[11] Bernal W, Barbosa-García O, Aguilar-Granda A, Pérez-Gutiérrez E, Maldonado JL, Percino MJ, et al. White Organic Light emitting diodes based On exciplex states by using a new carbazole derivative as single emitter Layer. Dye Pigment 2019;163:754–60. doi:10.1016/j.dyepig.2018.12.052.

[12] Jang HJ, Lee JY, Kwak J, Lee D, Park JH, Lee B, et al. Progress of display performances: AR, VR, QLED, OLED, and TFT. J Inf Disp 2019;20:1–8. doi:10.1080/15980316.2019.1572662.

[13] Reineke S, Lindner F, Schwartz G, Seidler N, Walzer K, Lüssem B, et al. White organic light-emitting diodes with fluorescent tube efficiency. Nature 2009;459:234–8. doi:10.1038/nature08003.

[14] Ashok Kumar S, Shankar JS, K Periyasamy B, Nayak SK. Device engineering aspects of Organic Light-Emitting Diodes (OLEDs). Polym Technol Mater 2019;58:1597–624. doi:10.1080/25740881.2018.1563133.

[15] Bae WJ, Kovalev MK, Kalinina F, Kim M, Cho C. Towards colorless polyimide/silica hybrids for flexible substrates. Polymer (Guildf) 2016;105:124–32. doi:10.1016/J.POLYMER.2016.10.023.

[16] Cao W, Li J, Chen H, Xue J. Transparent electrodes for organic optoelectronic devices: a review. J Photonics Energy 2014;4:040990. doi:10.1117/1.JPE.4.040990.

[17] Seo YK, Han JW, Lim KT, Kim YH, Joo CW, Lee J, et al. Efficient ITO-free organic light-emitting diodes comprising PEDOT:PSS transparent electrodes optimized with 2-ethoxyethanol and post treatment. Org Electron 2017;42:348–54. doi:10.1016/j.orgel.2016.12.059.

[18] Ma Y, Zhi L. Graphene-Based Transparent Conductive Films: Material Systems, Preparation and Applications. Small Methods 2019;3:1800199. doi:10.1002/smtd.201800199.

[19] Chen Y, Yue Y, Wang S-R, Zhang N, Feng J, Sun H-B. Thermally-induced wrinkles on PH1000/graphene composite electrode for enhanced efficiency of organic solar cells. Sol Energy Mater Sol Cells 2019;201:110075. doi:10.1016/J.SOLMAT.2019.110075.

[20] Yang Y, Ding S, Araki T, Jiu J, Sugahara T, Wang J, et al. Facile fabrication of stretchable Ag nanowire/polyurethane electrodes using high intensity pulsed light. Nano Res 2016;9:401–14. doi:10.1007/s12274-015-0921-9.

[21] Huang J-H, Fang J-H, Liu C-C, Chu C-W. Effective Work Function Modulation of Graphene/Carbon Nanotube Composite Films As Transparent Cathodes for Organic Optoelectronics. ACS Nano 2011;5:6262–71. doi:10.1021/nn201253w.

[22] Zhu H, Shen Y, Li Y, Tang J. Recent advances in flexible and wearable organic optoelectronic devices. J Semicond 2018;39:011011. doi:10.1088/1674-4926/39/1/011011.

[23] Display Market by Source, Type, Application & Geography| COVID-19 Impact Analysis|MarketsandMarkets™ n.d. https://www.marketsandmarkets.com/Market-Reports/display-market-925.html (accessed April 26, 2020).

[24] Tyagi P, Srivastava R, Giri LI, Tuli S, Lee C. Degradation of organic light emitting diode: Heat related issues and solutions. Synth Met 2016;216:40–50. doi:10.1016/j.synthmet.2015.10.016.

[25] LG B9 OLED Review (OLED55B9PUA, OLED65B9PUA, OLED77B9PUA) - RTINGS.com n.d. https://www.rtings.com/tv/reviews/lg/b9-oled (accessed May 11, 2020).

[26] Galaxy S20 Ultra OLED Display Technology Shoot-Out n.d. http://www.displaymate.com/Galaxy_S20_ShootOut_1U.htm (accessed May 17, 2020).

[27] OLED TV Reliability: Burn-In & Lifespan – Get The Facts | LG USA n.d. https://www.lg.com/us/experience-tvs/oled-tv/reliability (accessed May 11, 2020).

[28] Society for Information Display Unveils 2020 Display Industry Award Winners n.d. https://www.prnewswire.com/news-releases/society-for-information-display-unveils-2020-display-industry-award-winners-301064640.html (accessed June 7, 2020).

[29] (No Title) n.d. http://www.lgdisplay.com/eng/product/oled_light.jsp (accessed June 7, 2020).

[30] Coca Cola is using flexible OLED lighting in its Star Wars Singapore promotion campaign | OLED-Info n.d. https://www.oled-info.com/coca-cola-using-flexible-oled-lighting-its-star-wars-singapore-promotion (accessed June 7, 2020).

[31] Yin D, Feng J, Ma R, Liu Y-F, Zhang Y-L, Zhang X-L, et al. Efficient and mechanically robust stretchable organic light-emitting devices by a laser-programmable buckling process. Nat Commun 2016;7:11573. doi:10.1038/ncomms11573.

[32] Li F, Shen J, Liu X, Cao Z, Cai X, Li J, et al. Flexible QLED and OPV based on transparent polyimide substrate with rigid alicyclic asymmetric isomer. Org Electron 2017;51:54–61. doi:10.1016/J.ORGEL.2017.09.010.

[33] Lin Q, Huang H, Jing Y, Fu H, Chang P, Li D, et al. Flexible photovoltaic technologies. J Mater Chem C 2014;2:1233. doi:10.1039/c3tc32197e.

[34] Sakamoto K, Kuwae H, Kobayashi N, Nobori A, Shoji S, Mizuno J. Highly flexible transparent electrodes based on mesh-patterned rigid indium tin oxide. Sci Rep 2018;8:2825. doi:10.1038/s41598-018-20978-x.

[35] Samsung: we fixed all the Galaxy Fold issues, will start shipping it in September | OLED-Info 2019. https://www.oled-info.com/samsung-we-fixed-all-galaxy-fold-issues-will-start-shipping-it-september (accessed August 13, 2019).

[36] Huawei launches its foldable Mate X 5G smartphone | OLED-Info 2019. https://www.oled-info.com/huawei-launches-its-foldable-mate-x-5g-smartphone (accessed August 13, 2019).

[37] LG brings a rollable 65" OLED TV to CES 2018 | OLED-Info 2018. https://www.oled-info.com/lgd-brings-rollable-65-oled-tv-ces-2018 (accessed August 13, 2019).

[38] Lozano-Hernández L-A. Development of efficient OLEDs based on low molecular weight molecules by using evaporated cathodes under N2 atmosphere. Optical Research Center (CIO), Master Thesis, 2016.

[39] Lozano-Hernández LA, Maldonado JL, Hernández-Cruz O, Nicasio-Collazo J, Rodríguez M, Barbosa-García O, et al. Structurally simple OLEDs based on a new fluorinated poly(oxindolylidenearylene). Dye Pigment 2020;173. doi:10.1016/j.dyepig.2019.107989.

[40] Kim KP, Hussain AM, Hwang DK, Woo SH, Lyu HK, Baek SH, et al. Work function modification of indium-tin oxide by surface plasma treatments using different gases. Jpn J Appl Phys 2009;48:021601. doi:10.1143/JJAP.48.021601.

[41] Hung LS, Tang CW, Mason MG. Enhanced electron injection in organic electroluminescence devices using an Al/LiF electrode. Appl Phys Lett 1997;70:152–4. doi:10.1063/1.118344.

[42] Hsiao YS, Whang WT, Chen CP, Chen YC. High-conductivity poly(3,4-ethylenedioxythiophene):poly(styrene sulfonate) film for use in ITO-free polymer solar cells. J Mater Chem 2008;18:5948–55. doi:10.1039/b813079e.

[43] Shahnawaz S, Sudheendran Swayamprabha S, Nagar MR, Yadav RAK, Gull S, Dubey DK, et al. Hole-transporting materials for organic light-emitting diodes: An overview. J Mater Chem C 2019;7:7144–58. doi:10.1039/c9tc01712g.

[44] Rhee SH, Nam KB, Kim CS, Song M, Cho M, Jin SH, et al. Effect of electron mobility of the electron transport layer on fluorescent organic light-emitting diodes. ECS Solid State Lett 2014;3:R19. doi:10.1149/2.011404ssl.

[45] Lozano-Hernández L-A, Maldonado J-L, Garcias-Morales C, Espinosa Roa A, Barbosa-García O, Rodríguez M, et al. Efficient OLEDs Fabricated by Solution Process Based on Carbazole and Thienopyrrolediones Derivatives. Molecules

2018;23:280. doi:10.3390/molecules23020280.

[46] Liu L, Liu X, Wu K, Ding J, Zhang B, Xie Z, et al. Efficient solution-processed blue phosphorescent organic light-emitting diodes with halogen-free solvent to optimize the emissive layer morphology. Org Electron 2014;15:1401–6. doi:10.1016/J.ORGEL.2014.04.005.

[47] Sekine C, Tsubata Y, Yamada T, Kitano M, Doi S. Recent progress of high performance polymer OLED and OPV materials for organic printed electronics. Sci Technol Adv Mater 2014;15:034203. doi:10.1088/1468-6996/15/3/034203.

[48] Findlay NJ, Breig B, Forbes C, Inigo AR, Kanibolotsky AL, Skabara PJ. High brightness solution-processed OLEDs employing linear, small molecule emitters. J Mater Chem C 2016;4:3774–80. doi:10.1039/c5tc03579a.

[49] Bui T-T, Goubard F, Ibrahim-Ouali M, Gigmes D, Dumur F, Bui T-T, et al. Thermally Activated Delayed Fluorescence Emitters for Deep Blue Organic Light Emitting Diodes: A Review of Recent Advances. Appl Sci 2018;8:494. doi:10.3390/app8040494.

[50] Shizu K, Tanaka H, Uejima M, Sato T, Tanaka K, Kaji H, et al. Strategy for Designing Electron Donors for Thermally Activated Delayed Fluorescence Emitters. J Phys Chem C 2015;119:1291–7. doi:10.1021/jp511061t.

[51] Diouf B, Jeon WS, Pode R, Kwon JH. Efficiency Control in Iridium Complex-Based Phosphorescent Light-Emitting Diodes. Adv Mater Sci Eng 2012;2012:14. doi:10.1155/2012/794674.

[52] Watanabe Y, Sasabe H, Kido J. Account/Review for Materials Innovation Review of Molecular Engineering for Horizontal Molecular Orientation in Organic Light-Emitting Devices 2019. doi:10.1246/bcsj.20180336.

[53] Tyona MD. A theoritical study on spin coating technique. Adv Mater Res 2013;2:195–208. doi:10.12989/amr.2013.2.4.195.

[54] Thin Film Coating Solution-Processing Techniques Compared | Ossila n.d. https://www.ossila.com/pages/solution-processing-techniques-comparison (accessed

June 8, 2020).

[55] Choi KJ, Lee JY, Park J, Seo YS. Multilayer slot-die coating of large-area organic light-emitting diodes. Org Electron 2015;26:66–74. doi:10.1016/j.orgel.2015.07.025.

[56] Hong S, Lee J, Kang H, Lee K. Slot-die coating parameters of the low-viscosity bulk-heterojunction materials used for polymer solarcells. Sol Energy Mater Sol Cells 2013;112:27–35. doi:10.1016/j.solmat.2013.01.006.

[57] Yokoyama D. Molecular orientation in small-molecule organic light-emitting diodes. J Mater Chem 2011;21:19187–202. doi:10.1039/c1jm13417e.

[58] Shibata M, Sakai Y, Yokoyama D. Advantages and disadvantages of vacuum-deposited and spin-coated amorphous organic semiconductor films for organic light-emitting diodes. J Mater Chem C 2015;3:11178–91. doi:10.1039/c5tc01911g.

[59] CIE | International Commission on Illumination / Comission internationale de l'Eclairage / Internationale Beleuchtungskommission n.d. http://cie.co.at/ (accessed May 10, 2020).

[60] Vázquez-Córdova S, Ramos-Ortiz G, Maldonado JL, Meneses-Nava MA, Barbosa-García O. Simple assembling of organic light-emitting diodes for teaching purposes in undergraduate labs. Rev Mex Fis E 2008;54:146–52.

[61] Chamorro Posada P, Martín-Gil J, Martín Ramos P, Navas García LM, Universidad de Valladolid. Departamento de Teoría de la Señal e Ingeniería Telemática., Universidad de Valladolid. Departamento de Ingeniería Agrícola y Forestal. Fundamentos de la tecnología OLED. Los autores; 2008.

[62] So F, Kondakov D. Degradation Mechanisms in Small-Molecule and Polymer Organic Light-Emitting Diodes. Adv Mater 2010;22:3762–77. doi:10.1002/adma.200902624.

[63] Azrain MM, Mansor MR, Fadzullah SHSM, Omar G, Sivakumar D, Lim LM, et al. Analysis of mechanisms responsible for the formation of dark spots in organic light emitting diodes (OLEDs): A review. Synth Met 2018;235:160–75. doi:10.1016/j.synthmet.2017.12.011.

[64] Fŕy C, Racine B, Vaufrey D, Doyeux H, Cin̓ S. Physical mechanism responsible for the stretched exponential decay behavior of aging organic light-emitting diodes. Appl Phys Lett 2005;87:1–3. doi:10.1063/1.2133922.

[65] Kristukat C, Gerloff T, Hoffmann M, Diekmann K. Lifetime determination procedure for OLED lighting panels and proposal for standardisation. Org. Light. Diodes Mater. Devices Appl., Elsevier Ltd.; 2013, p. 601–34. doi:10.1533/9780857098948.3.601.

[66] Lee HB, Jin W-Y, Ovhal MM, Kumar N, Kang J-W. Flexible transparent conducting electrodes based on metal meshes for organic optoelectronic device applications: a review. J Mater Chem C 2019;7:1087–110. doi:10.1039/C8TC04423F.

[67] Woo YS. Transparent conductive electrodes based on graphene-related materials. Micromachines 2018;10. doi:10.3390/mi10010013.

[68] Nuramdhani I, Jose M, Samyn P, Adriaensens P, Malengier B, Deferme W, et al. Charge-Discharge Characteristics of Textile Energy Storage Devices Having Different PEDOT:PSS Ratios and Conductive Yarns Configuration. Polymers (Basel) 2019;11:345. doi:10.3390/polym11020345.

[69] Ibanez JG, Rincón ME, Gutierrez-Granados S, Chahma M, Jaramillo-Quintero OA, Frontana-Uribe BA. Conducting Polymers in the Fields of Energy, Environmental Remediation, and Chemical-Chiral Sensors. Chem Rev 2018;118:4731–816. doi:10.1021/acs.chemrev.7b00482.

[70] Ouyang L, Musumeci C, Jafari MJ, Ederth T, Inganäs O. Imaging the Phase Separation between PEDOT and Polyelectrolytes during Processing of Highly Conductive PEDOT:PSS Films. ACS Appl Mater Interfaces 2015;7:19764–73. doi:10.1021/acsami.5b05439.

[71] Shi H, Liu C, Jiang Q, Xu J. Effective Approaches to Improve the Electrical Conductivity of PEDOT:PSS: A Review. Adv Electron Mater 2015;1:1500017. doi:10.1002/aelm.201500017.

[72] Kim N, Kee S, Lee SH, Lee BH, Kahng YH, Jo Y-R, et al. Highly Conductive

PEDOT:PSS Nanofibrils Induced by Solution-Processed Crystallization. Adv Mater 2014;26:2268–72. doi:10.1002/adma.201304611.

[73] Vaagensmith B, Reza KM, Hasan MDN, Elbohy H, Adhikari N, Dubey A, et al. Environmentally Friendly Plasma-Treated PEDOT:PSS as Electrodes for ITO-Free Perovskite Solar Cells. ACS Appl Mater Interfaces 2017;9:35861–70. doi:10.1021/acsami.7b10987.

[74] Cho DY, Eun K, Choa SH, Kim HK. Highly flexible and stretchable carbon nanotube network electrodes prepared by simple brush painting for cost-effective flexible organic solar cells. Carbon N Y 2014;66:530–8. doi:10.1016/j.carbon.2013.09.035.

[75] Novoselov KS, Geim AK, Morozov S V., Jiang D, Zhang Y, Dubonos S V., et al. Electric field in atomically thin carbon films. Science (80-) 2004;306:666–9. doi:10.1126/science.1102896.

[76] Jia S, Sun HD, Du JH, Zhang ZK, Zhang DD, Ma LP, et al. Graphene oxide/graphene vertical heterostructure electrodes for highly efficient and flexible organic light emitting diodes. Nanoscale 2016;8:10714–23. doi:10.1039/c6nr01649a.

[77] An CJ, Jang S, Kang KM, Kim SJ, Jin ML, Jung HT. A combined graphene and periodic Au nanograte structure: Fundamentals and application as a flexible transparent conducting film in a flexible organic photovoltaic cell. Carbon N Y 2016;103:488–96. doi:10.1016/j.carbon.2016.03.035.

[78] Liu YF, Feng J, Zhang YF, Cui HF, Yin D, Bi YG, et al. Improved efficiency of indium-tin-oxide-free organic light-emitting devices using PEDOT:PSS/graphene oxide composite anode. Org Electron 2015;26:81–5. doi:10.1016/j.orgel.2015.06.031.

[79] Khan A, Lee S, Jang T, Xiong Z, Zhang C, Tang J, et al. High-Performance Flexible Transparent Electrode with an Embedded Metal Mesh Fabricated by Cost-Effective Solution Process. Small 2016;12:3021–30. doi:10.1002/smll.201600309.

[80] Kim G, Ryu I, Yim S. Retarded saturation of the areal capacitance using 3D-Aligned

MnO2 thin film nanostructures as a supercapacitor electrode. Sci Rep 2017;7. doi:10.1038/s41598-017-09039-x.

[81] Novarials - Silver Nanowires A70 n.d. http://novarials.com/ProductsAgNWsA70.html (accessed May 3, 2020).

[82] Lu S, Sun Y, Ren K, Liu K, Wang Z, Qu S. Recent development in ITO-free flexible polymer solar cells. Polymers (Basel) 2017;10:5. doi:10.3390/polym10010005.

[83] Yun HJ, Kim SJ, Hwang JH, Shim YS, Jung SG, Park YW, et al. Silver nanowire-IZO-conducting polymer hybrids for flexible and transparent conductive electrodes for organic light-emitting diodes. Sci Rep 2016;6:34150–34150. doi:10.1038/srep34150.

[84] Kotchapradist P, Prachumrak N, Tarsang R, Jungsuttiwong S, Keawin T, Sudyoadsuk T, et al. Pyrene-functionalized carbazole derivatives as non-doped blue emitters for highly efficient blue organic light-emitting diodes. J Mater Chem C 2013;1:4916–24. doi:10.1039/c3tc30719k.

[85] Zhang M, Xue S, Dong W, Wang Q, Fei T, Gu C, et al. Highly-efficient solution-processed OLEDs based on new bipolar emitters. Chem Commun 2010;46:3923–5. doi:10.1039/c001170c.

[86] Huang Y, Du X, Tao S, Yang X, Zheng CJ, Zhang X, et al. High efficiency non-doped deep-blue and fluorescent/phosphorescent white organic light-emitting diodes based on an anthracene derivative. Synth Met 2015;203:49–53. doi:10.1016/j.synthmet.2014.10.019.

[87] Wang X, Wang S, Ma Z, Ding J, Wang L, Jing X, et al. Solution-Processible 2,2′-Dimethyl-biphenyl Cored Carbazole Dendrimers as Universal Hosts for Efficient Blue, Green, and Red Phosphorescent OLEDs. Adv Funct Mater 2014;24:3413–21. doi:10.1002/adfm.201302849.

[88] Gao Z, Wang Z, Shan T, Liu Y, Shen F, Pan Y, et al. High-efficiency deep blue fluorescent emitters based on phenanthro[9,10-d]imidazole substituted carbazole and their applications in organic light emitting diodes. Org Electron 2014;15:2667–76.

doi:10.1016/j.orgel.2014.07.019.

[89] Chan CYK, Lam JWY, Zhao Z, Chen S, Lu P, Sung HHY, et al. Aggregation-induced emission, mechanochromism and blue electroluminescence of carbazole and triphenylamine-substituted ethenes. J Mater Chem C 2014;2:4320–7. doi:10.1039/c4tc00097h.

[90] Li J, Han X, Bai Q, Shan T, Lu P, Ma Y. Electropolymerized AIE-active polymer film with high quantum efficiency and its application in OLED. J Polym Sci Part A Polym Chem 2017;55:707–15. doi:10.1002/pola.28414.

[91] Wang K, Liu W, Zheng CJ, Shi YZ, Liang K, Zhang M, et al. A comparative study of carbazole-based thermally activated delayed fluorescence emitters with different steric hindrance. J Mater Chem C 2017;5:4797–803. doi:10.1039/c7tc00681k.

[92] Zhang Q, Kelly MA, Bauer N, You W. The Curious Case of Fluorination of Conjugated Polymers for Solar Cells. Acc Chem Res 2017;50:2401–9. doi:10.1021/acs.accounts.7b00326.

[93] Bong S, Yeo H, Ku B-C, Goh M, You N-H. Highly soluble polyimide based on asymmetric diamines containing trifluoromethyl group for high performance dielectric material. Macromol Res 2018;26:85–91. doi:10.1007/s13233-018-6010-7.

[94] Wu T, Dong J, Gan F, Fang Y, Zhao X, Zhang Q. Low dielectric constant and moisture-resistant polyimide aerogels containing trifluoromethyl pendent groups. Appl Surf Sci 2018;440:595–605. doi:10.1016/j.apsusc.2018.01.132.

[95] Ghosh A, Banerjee S. Sulfonated fluorinated-aromatic polymers as proton exchange membranes. E-Polymers 2014;14:227–57. doi:10.1515/epoly-2014-0049.

[96] Wang Y, Wang W, Huang Z, Wang H, Zhao J, Yu J, et al. High-efficiency red organic light-emitting diodes based on a double-emissive layer with an external quantum efficiency over 30%. J Mater Chem C 2018;6:7042–5. doi:10.1039/C8TC01639A.

[97] An D, Zou J, Wu H, Peng J, Yang W, Cao Y. White emission polymer light-emitting devices with efficient electron injection from alcohol/water-soluble polymer/Al

bilayer cathode. Org Electron 2009;10:299–304. doi:10.1016/J.ORGEL.2008.11.016.

[98] Santos J, Cook JH, Al-Attar HA, Monkman AP, Bryce MR. Fluorene co-polymers with high efficiency deep-blue electroluminescence. J Mater Chem C 2015;3:2479–83. doi:10.1039/C4TC02766C.

[99] Cook JH, Santos J, Li H, Al-Attar HA, Bryce MR, Monkman AP. Efficient deep blue fluorescent polymer light-emitting diodes (PLEDs). J Mater Chem C 2014;2:5587–92. doi:10.1039/C4TC00896K.

[100] Itoh E, Kurami K. Influence of polymeric electron injection layers on the electrical properties of solution-processed multilayered polymer light-emitting diodes. Jpn J Appl Phys 2016;55:02BB16. doi:10.7567/JJAP.55.02BB16.

[101] Yu JC, Jang JI, Lee BR, Lee G-W, Han JT, Song MH. Highly Efficient Polymer-Based Optoelectronic Devices Using PEDOT:PSS and a GO Composite Layer as a Hole Transport Layer. ACS Appl Mater Interfaces 2014;6:2067–73. doi:10.1021/am4051487.

[102] Shih H-K, Chen Y-H, Chu Y-L, Cheng C-C, Chang F-C, Zhu C-Y, et al. Photo-Crosslinking of Pendent Uracil Units Provides Supramolecular Hole Injection/Transport Conducting Polymers for Highly Efficient Light-Emitting Diodes. Polymers (Basel) 2015;7:804–18. doi:10.3390/polym7050804.

[103] Gong P, Ye K, Sun J, Chen P, Xue P, Yang H, et al. Electroluminescence and fluorescence response towards acid vapors depending on the structures of indole-fused phospholes. RSC Adv 2015;5:94990–6. doi:10.1039/C5RA19867D.

[104] Gopal R, Huang Y-C, Lee H-F, Chang M-S, Huang W-Y. Synthesis, characterization and properties of novel blue light emitting discrete π-functional polymer consisting of carbazole and anthracene units and their applications in polymer light emitting diodes. Electron Mater Lett 2017;13:240–8. doi:10.1007/s13391-017-6276-5.

[105] Kaafarani BR, El-Assaad TH, Smith WA, Ryno S, Hermerschmidt F, Lyons J, et al. Bis(Tercarbazole) Pyrene and Tetrahydropyrene Derivatives: Photophysical and

Electrochemical Properties, Theoretical Modeling, and OLEDs. J Mater Chem C 2019. doi:10.1039/C8TC06266H.

[106] Xue S, Qiu X, Yao L, Wang L, Yao M, Gu C, et al. Fully solution-processed and multilayer blue organic light-emitting diodes based on efficient small molecule emissive layer and intergrated interlayer optimization. Org Electron 2015;27:35–40. doi:10.1016/j.orgel.2015.08.026.

[107] Li Z, Liu W, Yu Y, Lv X, Si C, Wu Z, et al. Effect of fluorocarbon (trifluoromethyl groups) substitution on blue electroluminescent properties of 9,9′-bianthracene derivatives with twisted intramolecular charge-transfer excited states 2015. doi:10.1016/j.dyepig.2015.06.034.

[108] Findlay NJ, Breig B, Forbes C, Inigo AR, Kanibolotsky AL, Skabara PJ. High brightness solution-processed OLEDs employing linear, small molecule emitters. J Mater Chem C 2016;4:3774–80. doi:10.1039/c5tc03579a.

[109] Oh K, Hong SK, Kwon OK. Lifetime extension method for active matrix organic light-emitting diode displays using a modified stretched exponential decay model. IEEE Electron Device Lett 2015;36:277–9. doi:10.1109/LED.2015.2394451.

[110] Zhu M, Yang C. Blue fluorescent emitters: Design tactics and applications in organic light-emitting diodes. Chem Soc Rev 2013;42:4963–76. doi:10.1039/c3cs35440g.

[111] Fu Q, Chen J, Shi C, Ma D. Room-temperature sol-gel derived molybdenum oxide thin films for efficient and stable solution-processed organic light-emitting diodes. ACS Appl Mater Interfaces 2013;5:6024–9. doi:10.1021/am4007319.

[112] Suzuki Y, Zhang Q, Adachi C. A solution-processable host material of 1,3-bis{3-[3-(9-carbazolyl)phenyl]-9-carbazolyl}benzene and its application in organic light-emitting diodes employing thermally activated delayed fluorescence. J Mater Chem C 2015;3:1700–6. doi:10.1039/c4tc02211d.

[113] Kamata T, Sasabe H, Igarashi M, Kido J. A Novel Sterically Bulky Hole Transporter to Remarkably Improve the Lifetime of Thermally Activated Delayed Fluorescent OLEDs at High Brightness. Chem - A Eur J 2018;24:4590–6.

doi:10.1002/chem.201705262.

[114] Lee WH, Kim DH, Justin Jesuraj P, Hafeez H, Lee JC, Choi DK, et al. Improvement of charge balance, recombination zone confinement, and low efficiency roll-off in green phosphorescent OLEDs by altering electron transport layer thickness. Mater Res Express 2018;5. doi:10.1088/2053-1591/aacec6.

[115] Liu YF, Feng J, Zhang YF, Cui HF, Yin D, Bi YG, et al. Improved efficiency of indium-tin-oxide-free flexible organic light-emitting devices. Org Electron 2014;15:478–83. doi:10.1016/j.orgel.2013.11.035.

[116] Fan X, Nie W, Tsai H, Wang N, Huang H, Cheng Y, et al. PEDOT:PSS for Flexible and Stretchable Electronics: Modifications, Strategies, and Applications. Adv Sci 2019;6:1900813. doi:10.1002/advs.201900813.

[117] Mishra A, Bhatt N, Bajpai AK. Nanostructured superhydrophobic coatings for solar panel applications. Nanomater. Coatings, Elsevier; 2019, p. 397–424. doi:10.1016/b978-0-12-815884-5.00012-0.

[118] Lee I, Kim GW, Yang M, Kim TS. Simultaneously Enhancing the Cohesion and Electrical Conductivity of PEDOT:PSS Conductive Polymer Films using DMSO Additives. ACS Appl Mater Interfaces 2016;8:302–10. doi:10.1021/acsami.5b08753.

[119] Choi EY, Seo JH, Kim HM, Kim JH, Je JT, Kim YK. Improved efficiency and adhesion property between the PEDOT: PSS and ITO in solution-processed organic light-emitting diodes. INEC 2010 - 2010 3rd Int. Nanoelectron. Conf. Proc., 2010, p. 921–2. doi:10.1109/INEC.2010.5425127.

[120] Zhou J, Anjum DH, Chen L, Xu X, Ventura IA, Jiang L, et al. The temperature-dependent microstructure of PEDOT/PSS films: Insights from morphological, mechanical and electrical analyses. J Mater Chem C 2014;2:9903–10. doi:10.1039/c4tc01593b.

[121] Zhao Z, Liu Q, Zhang W, Yang S. Conductivity enhancement of PEDOT:PSS film via sulfonic acid modification: application as transparent electrode for ITO-free polymer solar cells. Sci China Chem 2018;61:1179–86. doi:10.1007/s11426-017-

9205-x.

[122] Yousefi MH, Fallahzadeh A, Saghaei J, Darareh MD. Fabrication of flexible ITO-Free OLED using vapor-treated PEDOT:PSS thin film as anode. J Disp Technol 2016;12:1647–51. doi:10.1109/JDT.2016.2624341.

[123] Wu X, Lian L, Yang S, He G. Highly conductive PEDOT:PSS and graphene oxide hybrid film from a dipping treatment with hydroiodic acid for organic light emitting diodes. J Mater Chem C 2016;4:8528–34. doi:10.1039/c6tc02424f.

[124] Diker H, Yesil F, Varlikli C. Contribution of O2 plasma treatment and amine modified GOs on film properties of conductive PEDOT:PSS: Application in indium tin oxide free solution processed blue OLED. Curr Appl Phys 2019;19:910–6. doi:10.1016/j.cap.2019.04.018.

[125] Kim W, Kim S, Kang I, Jung MS, Kim SJ, Kim JK, et al. Hybrid Silver Mesh Electrode for ITO-Free Flexible Polymer Solar Cells with Good Mechanical Stability. ChemSusChem 2016;9:1042–9. doi:10.1002/cssc.201600070.

[126] Kang H, Jung S, Jeong S, Kim G, Lee K. Polymer-metal hybrid transparent electrodes for flexible electronics. Nat Commun 2015;6:1–7. doi:10.1038/ncomms7503.

[127] Mao L, Chen Q, Li Y, Li Y, Cai J, Su W, et al. Flexible silver grid/PEDOT: PSS hybrid electrodes for large area inverted polymer solar cells. Nano Energy 2014;10:259–67. doi:10.1016/j.nanoen.2014.09.007.

10 APPENDIX. Additional OLED devices

OLED devices with different materials were made in order to obtain efficient devices. The devices shown in this appendix were not extensively described above because their performance was not so high as the ones reported before.

The polymers shown in the Fig. A1 were used as EML in OLED devices, with an architecture: ITO/PEDOT:PSS/polymer/LiF/Al. OLED devices were fabricated with the same method used for PF-2F polymer.

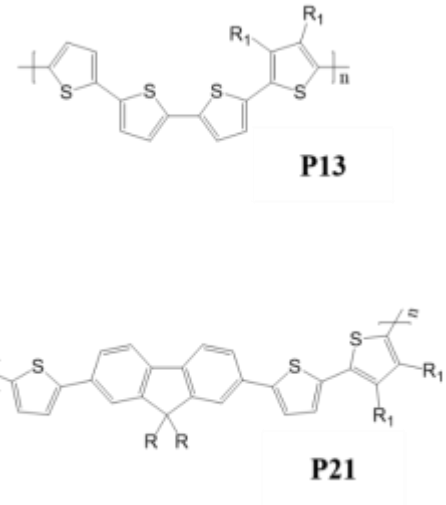

Fig. A1. P13 and P21 polymers used as EML for OLED devices

P13 based OLED devices, with different thicknesses of EML, shown luminances quite similar but with different turn on voltages (4.3 and 4.9 V) as can be seen in Fig. A2. Current efficiency for the device with the thicker EML was 0.1, On the other hand, for the EML deposited at 2000 rpm, the current efficiency was of only 0.06 cd/A.

J-V-L curves for P21 based OLEDs are shown in Fig. A3, with maximum luminances of around 1800 cd/m^2 for two different thicknesses but with turn on voltages of almost 1 V of difference (4.4 and 5.3 V). Maximum current efficiency for both devices was the same (0.55 cd/A).

As can be seen, both kind of OLED devices shown relatively good turn on voltages, low-medium luminances but they have very low efficiencies because their really high current of densities.

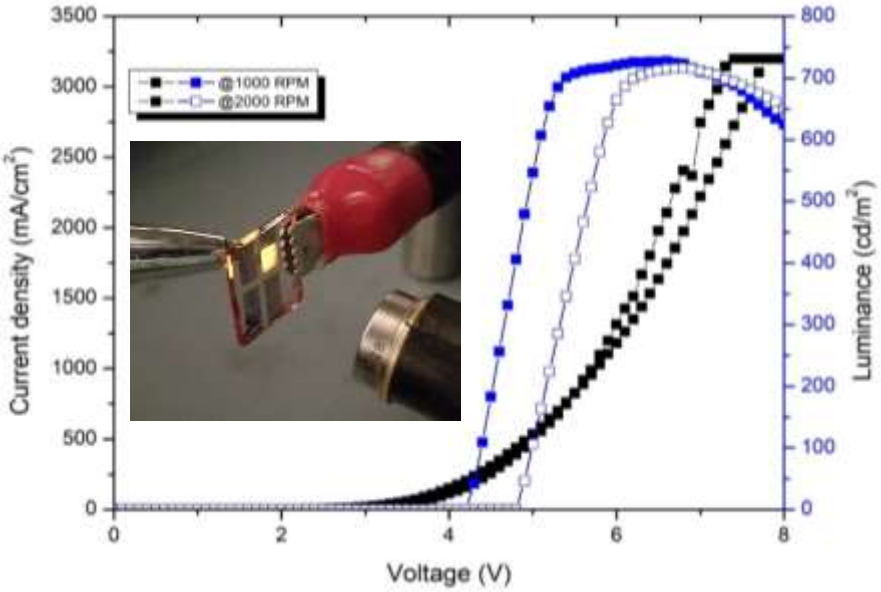

Fig. A2. J-V-L curves for P13 polymer based OLED devices.

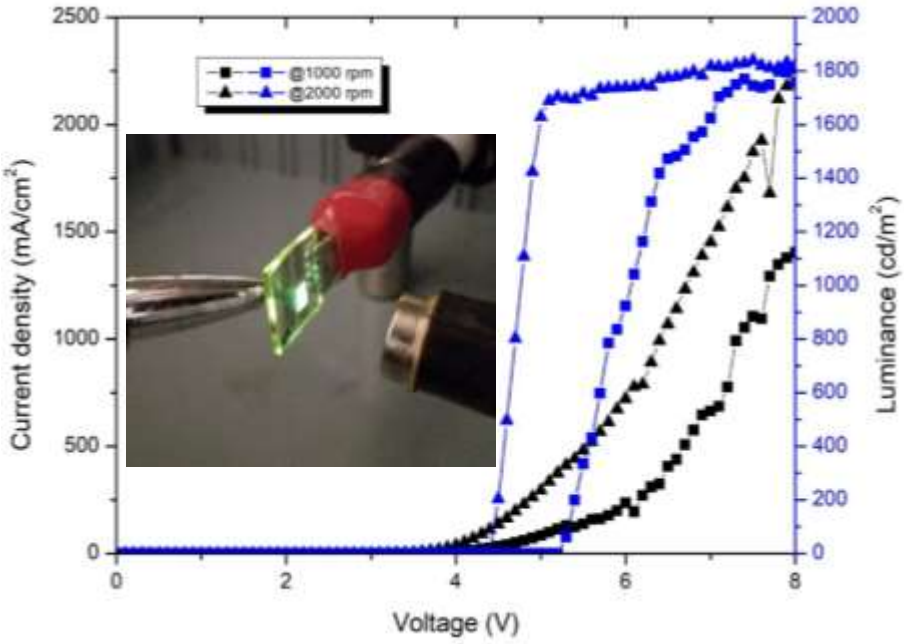

Fig. A3. J-V-L curve for P21 polymer based OLED devices.